THE APPLICATION OF ELECTROANALYTICAL TECHNIQUES TO THE STUDY OF COATING SYSTEMS

A Thesis
Submitted to the Graduate Faculty
of the
North Dakota State University
of Agriculture and Applied Science

By

Kenneth James Croes

In Partial Fulfillment of the Requirements
for the Degree of
MASTER OF SCIENCE

Major Department:
Coatings and Polymeric Materials

December 2014

Fargo, North Dakota

North Dakota State University
Graduate School

Title

THE APPLICATION OF ELECTROANALYTICAL TECHNIQUES TO THE STUDY OF COATING SYSTEMS

By

Kenneth James Croes

The Supervisory Committee certifies that this ***disquisition*** complies with North Dakota State University's regulations and meets the accepted standards for the degree of

MASTER OF SCIENCE

SUPERVISORY COMMITTEE:

Dr. Victoria J. Gelling
Co-Chair

Dr. Andriy Voronov
Co-Chair

Dr. Dante Battocchi

Dr. Chad Ulven

Approved:

4/17/2015
Date

Dr. Dean Webster
Department Chair

ABSTRACT

Electroanalytical techniques are often employed to augment standard practices utilized to study and characterize coating performance on metal substrates, yielding information that is not provided by standard coating analysis methods.

Electrochemical impedance spectroscopy (EIS) was utilized to study epoxy-amine coatings incorporating oligomers and monomers of phenylenediamine in the coating structure; these results were compared to unusual EIS results obtained in previous studies of organic-inorganic hybrid sol-gel coatings attributed to the sol-gel structure. With a different coating structure, the unusual results were replicated in coatings containing phenylenediamine oligomers but not monomer. The results suggested the oligomers caused the coatings to act as osmotic membranes.

Potentiodynamic polarization studies were utilized to study a highly alkaline chemical bath used for the deposition of magnetite on steel. The results were used to develop a working model of how the bath functions and explain the high temperature and pH required for proper bath function.

ACKNOWLEDGEMENTS

I would like to thank Dr. Victoria Johnston Gelling for employing me in her lab full-time on a number of interesting projects while encouraging me to pursue my Master's degree on a part-time basis. Several projects were among the most enjoyable work I have ever performed.

I would like to thank my other committee members, Dr. Andriy Voronov, Dr. Dante Battocchi, and Dr. Chad Ulven for their time involved in meetings and review of this thesis.

I would like to acknowledge the financial support of the various clients on whose projects I worked over the years, most notably one client who allowed me to include part of the studies I performed for them as part of this thesis; due to the proprietary nature of the work and their ongoing patent, they have asked to remain anonymous. I would like to acknowledge the support of the U.S. Army Research Laboratory for a portion of my employment and part of this thesis under grants W911NF-09-2-0014, W911NF-10-2-0082, and W911NF-11-2-0027. I am also grateful to the students, staff, and faculty of the Department of Coatings and Polymeric Materials at NDSU, most notably Dr. Niteen Jadhav for many helpful discussions related to my work and review of this manuscript.

TABLE OF CONTENTS

LIST OF TABLES

LIST OF FIGURES

LIST OF SCHEMES

CHAPTER 1. INTRODUCTION

Traditional methods of analyzing coating systems are numerous and varied. The traditional methods include thermal analysis techniques such as differential scanning calorimetry (DSC), dynamic mechanical analysis (DMA), and thermal gravimetric analysis (TGA). DSC can reveal a coating's glass transition temperature, melting point, and effects of pigmentation. DMA can reveal the glass transition temperature and give a measure of the cross-link density of a coating achieved in the curing process. TGA can reveal the presence of unreacted materials in the coating, leftover solvents, byproducts of reactants that may remain in the coatings, and temperatures at which the coatings may begin to degrade, therefore establishing an upper limit temperature for curing [1].

Other methods include methyl ethyl ketone (MEK) double rubs which can give a measure of solvent resistance. Pencil hardness testing gives a measure of abrasion resistance while cross-hatch adhesion testing provides a measure of adhesion to the substrate. In conical mandrel bend testing, a coated metal panel is bent at a controlled curvature to stress the coating around the bend to test for flexibility or brittleness. However, the results of some of these measurements can be somewhat subjective, depending on the observer, or the technique can vary from person to person; ASTM standards have been published to attempt to remove some of the subjectivity from these measurements [2-5]. These tests are also destructive in nature so each individual sample can be measured only once.

Coatings are usually expected to last long periods of time but it is impractical to test coatings for such long periods. Therefore, accelerated weathering techniques have been developed to speed the process of studying the stability, wear, and breakdown of coatings. These methods include ultraviolet (UV) exposure and salt spray testing methods [6-7]. The ensuing

coating degradation can be measured by nondestructive methods to give measurements of the rates of degradation. These methods include gloss, color, and water contact angle measurements, with the obtained values compared to values measured prior to accelerated exposure methods [1]. However, these techniques generally yield information for only the surface of the coating, not at depth into the bulk of the coating. Defects are often introduced through the coating to allow the study of the interface between the substrate (wood, metal, other materials) and the coating in response to attack by the elements of the chosen method, such as salts, water, oxygen, or UV light. In the case of metal substrates, the advance of corrosion and the effects of corrosion products on the adhesion of the coating can be visually studied by the formation of cathodic blisters or filiform structures by the introduced defects.

Many of the aforementioned techniques can provide values for physical properties of coatings. The information can be used to predict how a given coating may perform under certain conditions (such as coastal environments versus desert environments) or to compare coatings; but, they give little mechanistic information about how the coatings may function such as do they simply serve as moisture barriers, incorporate something in the coating to scavenge oxygen, or act as a corrosion inhibitor for an underlying metal. Numerous electroanalytical techniques can study these properties and have found use in the study of coating systems for metals and metal alloys to complement the information obtained from the aforementioned techniques. More complex instruments such as scanning Kelvin probe (SKP) can be used to measure the advancing front of corrosion processes beneath a coating on steel even before it is detected visually [8-10]. Scanning electrochemical microscopy (SECM) can be used to detect and map heterogeneity in metal alloys caused by the alloying elements and intermetallic particles formed during processing, their activity relative to the surrounding matrix, and the effects coatings may have on

those activities [11-13]. Scanning vibrating electrode technique (SVET) is used to measure current flow to and from anodic and cathodic sites on the underlying metal in a defect introduced through a coating on a metal substrate; a well adhered coating will confine corrosion processes to the defect or the presence of corrosion inhibition by the coating will be detected by reduced current flow in the defect [14-16].

Other methods of analysis involve the use of a potentiostat connected to a metal substrate as the working electrode with a counter electrode and reference electrode, in the basic arrangement, with other more complex arrangements utilized depending upon the experiment. The metal may be coated to study the response of coatings in an electrolyte solution; simple measurements can give an indication of how long it takes water and salts to diffuse and penetrate the coating to the metal surface [17-19] while more complex analysis can yield mechanistic information as the electrolyte penetrates the coating [20-22]. This can also be combined with accelerated weathering methods because the electrolyte can penetrate into the bulk of the coating to the advancing front of degradation and yield information that surface techniques cannot. A metal may also be uncoated to study the response of the metal to a specific reagent added to the electrolyte solution, such as whether the reagent might act as a corrosion inhibitor and how it performs that function [23-25].

1.1. References

[1] Z.W. Wicks Jr., F.N. Jones, S.P. Pappas, D.A. Wicks, Organic Coatings Science and Technology, John Wiley & Sons, Hoboken, NJ, 2007.

[2] ASTM D3359-09e2, Standard Test Methods for Measuring Adhesion by Tape Test, ASTM International, West Conshohocken, PA, 2009, www.astm.org.

[3] ASTM D3363-05e2, Standard Test Method for Film Hardness by Pencil Test, ASTM International, West Conshohocken, PA, 2011, www.astm.org.

[4] ASTM D5402-06e2, Standard Practice for Assessing the Solvent Resistance of Organic Coatings Using Solvent Rubs, ASTM International, West Conshohocken, PA, 2011, www.astm.org.

[5] ASTM D522 / D522M, Standard Test Methods for Mandrel Bend Test of Attached Organic Coatings, ASTM International, West Conshohocken, PA, 2013, www.astm.org.

[6] ASTM 4587-11, Standard Practice for Fluorescent UV-Condensation Exposures of Paint and Related Coatings, ASTM International, West Conshohocken, PA, 2011, www.astm.org.

[7] ASTM G85-11, Standard Practice for Modified Salt Spray (Fog) Testing, ASTM International, West Conshohocken, PA, 2011, www.astm.org.

[8] A. Vimalanandan, L.-P. Lv, T.H. Tran, K. Landfester, D. Crespy, M. Rohwerder, Advanced Materials, 25 (2013) 6980-6984.

[9] I. Mabbett, J. Elvins, C. Gowenlock, C. Glover, P. Jones, G. Williams, D. Worsley, Progress in Organic Coatings, 77 (2014) 494-501.

[10] D. Mizuno, R.G. Kelly, Corrosion, 69 (2013) 580-592.

[11] A. Davoodi, J. Pan, C. Leygraf, R. Parvizi, S. Norgren, Materials and Corrosion, 64 (2013) 195-198.

[12] K. Fushimi, Y. Takabatake, T. Nakanishi, Y. Hasegawa, Electrochimica Acta, 113 (2013) 741-747.

[13] M.B. Jensen, D.E. Tallman, Electroanalytical Chemistry: A Series of Advances, 24 (2012) 171-286, CRC Press-Taylor & Francis Group.

[14] D. Snihirova, L. Liphardt, G. Grundmeier, F. Montemor, Journal of Solid State Electrochemistry, 17 (2013) 2183-2192.

[15] D. Borisova, H. Möhwald, D.G. Shchukin, ACS Nano, 5 (2011) 1939-1946.

[16] N. Jadhav, C.A. Vetter, V.J. Gelling, Electrochimica Acta, 102 (2013) 28-43.

[17] B. Liu, Y. Li, C.H. Lin, C.N. Cao, Corrosion Science, 44 (2002) 2657-2664.

[18] B. Liu, Y. Li, C.H. Lin, C.N. Cao, Corrosion, 59 (2003) 817-820.

[19] F.C. Liu, L.H. Yang, E.H. Ha, Journal of Coatings Technology and Research, 7 (2010) 301-313.

[20] H. Xu, D. Battocchi, D.E. Tallman, G.P. Bierwagen, Corrosion, 65 (2009) 318-325.

[21] M. Mahdavian, M.M. Attar, Electrochimica Acta, 50 (2005) 4645-4648.

[22] R. Naderi, M.M. Attar, Progress in Organic Coatings, 66 (2009) 314-320

[23] I.B. Obot, N.O. Obi-Egbedi, Journal of Applied Electrochemistry, 40 (2010) 1977-1984.

[24] S.J. Garcia, T.A. Markley, J.M.C. Mol, A.E. Hughes, Corrosion Science, 69 (2013) 346-358.

[25] H. Guan, R.G. Buchheit, Corrosion, 60 (2004) 284-296.

CHAPTER 2. OBJECTIVES

The objectives of this thesis research were to provide better understanding of two coating systems by utilizing electroanalytical methods to obtain mechanistic information for the two systems which was unobtainable by the standard measurements described in the introduction.

For one system, sol-gel coatings were synthesized and applied to aluminum alloy substrates as primer layers. The sol-gels were organic-inorganic silane hybrids with epoxide functionality incorporated that was further cross-linked by amine reagents. Two coating systems were synthesized in an identical manner with the only difference being that one incorporated aliphatic amines as the organic cross-linking agents while the other incorporated the isomers of phenylenediamine as the cross-linking agents. The standard testing methods described earlier revealed remarkable performance differences, with much better corrosion inhibition provided by the coating incorporating phenylenediamine. However, the standard methods of analysis could not explain this performance difference and further analysis with different methods was required. Earlier work utilizing an electroanalytical method revealed dramatic differences in the results yielding a possible explanation; this thesis expands on the theory presented in that work.

For the second coating system, steel was introduced to a commercially available highly alkaline chemical bath yielding a layer of black magnetite on the metal; this was the desired end product that was then further treated with a sealant. This process is used in lieu of painting the metal black. The coating was developed through much trial and error over several months to years but without much understanding how the bath functioned. It was determined that proper bath temperature and pH are very important but not why. Additionally, a critical feature is the bath will reach a point at which it no longer functions properly; the bath components can be replenished before reaching that point and the bath will continue to function but not if the

chemicals are added at or beyond that point. The company that developed the bath performed various analyses on the bath to determine pH and concentrations of components at different points of the bath's life and the byproducts generated, but none of those analyses explained the necessary bath pH and temperature nor were they useful in determining the critical point at which the chemicals needed to be replenished in the bath, thus requiring a different approach to analyze the bath.

CHAPTER 3. BACKGROUND OF THE TWO COATING SYSTEMS

3.1. Introduction to the first coating system: the study of phenylenediamine cross-linked sol-gel and epoxy coatings

Previous work performed with organic-inorganic hybrid sol-gel systems by NDSU in collaboration with researchers at Trent University, Ontario, Canada, led to the study of the first coating system in this thesis [1-2]. In sol-gel systems, organometallic molecules with metal centers (M) (typically silicon) and alkoxyl groups (alkane groups attached to an oxygen atom) are hydrolyzed in water yielding $M(OH)_4$ structure and small alcohol molecules as byproducts (typically methanol, ethanol, and isopropanol, R-OH, where R represents methyl, ethyl, isopropyl) (the "sol" step). These hydrolyzed structures then react to one another by water condensation, leaving one oxygen (O) yielding M-O-M-O-M bonding and water molecules as byproduct (the "gel" step); these steps are displayed in Scheme 3.1. As the system dries, the water and alcohol molecules evaporate, leading to even greater cross-linking [3]. While silicon is very commonly the metal center, other common metals include titanium and zirconium, while vanadium, aluminum, cerium, and tin also display similar chemistry.

$$M(OR)_4 + H_2O \rightarrow M(OR)_3OH + R\text{-}OH \text{ (“sol”)}$$

$$M(OR)OH + H_2O \rightarrow \rightarrow \rightarrow M(OH)_4 + R\text{-}OH \text{ (“sol”)}$$

$$M(OH)_4 + M(OH)_4 \rightarrow (OH)_3M\text{-}O\text{-}M(OH)_3 + H_2O \rightarrow \rightarrow \rightarrow M\text{-}O\text{-}M\text{-}O\text{-}M + xH_2O \text{ (“gel”)}$$

Scheme 3.1. Generalized reaction for sol-gel systems.

As far as anticorrosion coatings are concerned, a straight inorganic sol-gel system is often not useful. Once cured, the high level of cross-linking obtained in the sol-gel through the metal-oxygen-metal bonding creates too much strain in the necessarily thin layer of coating and cracking results [4]. Thus, organic-inorganic sol-gel systems began to be studied. In these

systems, one of the alkoxyl groups is replaced by a reactive group such as epoxide or methacrylate [5-7]. Replacing one of the alkoxyl groups with a non-hydrolysable moiety accomplishes two feats: first, with one of the alkoxyl groups removed the level of M-O-M cross-linking is reduced throughout the material leaving the material more flexible; and second, the reactive group can be reacted to another cross-linking agent that imparts additional flexibility without actually sacrificing the total amount of cross-linking that was lost due to the simple presence of the reactive moiety. Or, the level of M-O-M bonding in these coatings can be adjusted simply by replacing a certain portion of the alkoxyl groups with an inert group such as methyl if no additional cross-linker is desired. As a bonus, if used as a primer layer, the next layer of coating applied can incorporate reactive groups that can form covalent bonds with any remaining reactive groups of the sol-gel layer, thus improving adhesion. The other attraction to this chemistry is the sol-gel can also form M-O-M bonding to the metal substrate thereby, potentially, yielding a coating system with covalent bonding from the substrate to pretreatment to primer to topcoat for excellent adhesion of the entire coating system [8-12]. Figure 3.1 displays a representative schematic for this mechanism.

In a typical sol-gel application, the components are simply mixed with water and/or solvent (which is used to control the rate of the hydrolysis reaction) and a small amount of acid or base is added to catalyze the hydrolysis [13-17]. The solution is allowed to stir for approximately 30 minutes to a few hours which allows time for hydrolysis of the alkoxides and for the first stages of cross-linking to occur. The solution is then normally dip-coated or spin-coated onto a prepared substrate and dried as the procedure calls for. The early work with mixed organic-inorganic hybrids focused on adjusting the ratios of organic to inorganic alkoxides

[14, 17] and incorporating organic cross-linkers to react to the chosen functionalized groups [18-20]. More recent work has focused on incorporating corrosion inhibitors directly into the sol-gel solution or encapsulating the inhibitors into some type of microcapsule and incorporating those into the coatings to respond to corrosion processes as needed [21-26].

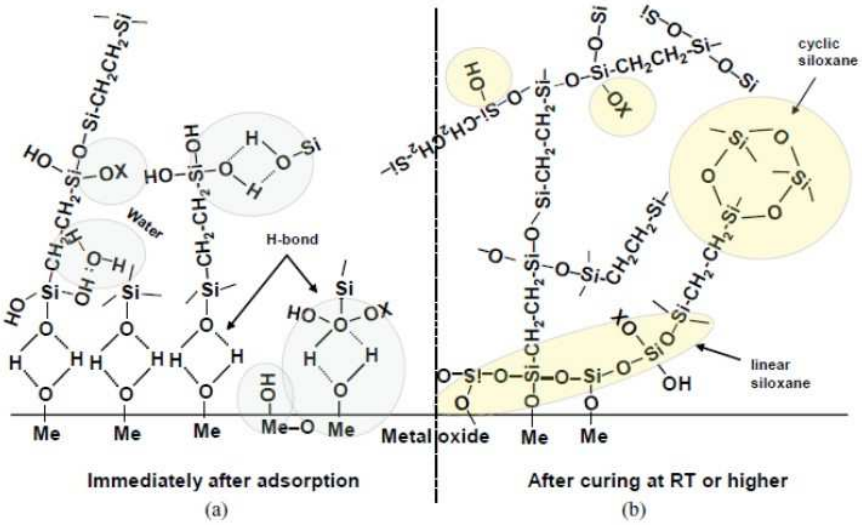

Figure 3.1. A simplified schematic of the bonding mechanism between silane molecules and the metal surface hydroxide layer. OX could refer to reactive functional groups, small inert groups, or the original alkoxyl group. Reprinted from reference [9], with permission from Elsevier.

One often used technique to study these films is electrochemical impedance spectroscopy (EIS); this technique will be discussed in detail in the following chapter but, in brief, coatings on metals with another conductive media on the top of the coating, such as electrolyte, behave as electrical capacitors. When the sol-gel samples are exposed to constant immersion in electrolyte and measured by EIS, many of the samples display what is known as Randle's cell behavior such as observed in Figure 3.2 [16, 21-22, 27-30]. The coatings are thin so they display resistive behavior at high frequencies (although when a coating that is a good barrier is applied thick enough it will display capacitive behavior at high frequency), capacitive behavior in the middle frequencies, and resistive behavior again at low frequencies. In a few instances, however, a more unique behavior was observed in which the coating is capacitive at high frequencies (even

though it is thin) and low frequencies but resistive in the middle frequencies, as observed at 7 hours in Figure 3.3 [26, 31-35]. This behavior was described as the result of a thicker, very porous layer on top of a thinner, more dense layer, where the high frequency capacitance is the coating capacitance of the thick layer, the flat, resistive region is the coating (or pore) resistance of the thick layer, and the low frequency capacitance is due to the thin dense layer at the interface enhancing the oxide layer [31]. Because the first layer of molecules at the substrate is covalently bonded to the substrate, the first few layers of molecules are quite likely to be highly ordered and cross-linked, yielding a dense layer at the interface, and a less ordered and more porous structure with distance from the substrate.

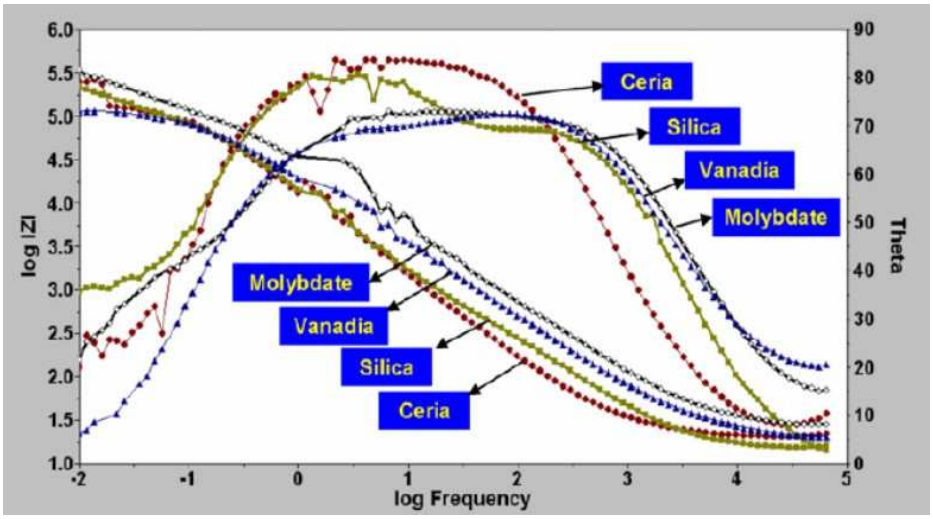

Figure 3.2. EIS results for sol-gel coatings displaying Randle's cell behavior after 30 days of immersion in 3.5% NaCl solution. "Silica" sol-gel was derived from tetraethoxyorthosilicate (TEOS) precursor. When the slope of the line described by the values of log [Z] (impedance) approaches negative 1, the coating is displaying capacitive behavior (note also the θ value approaches 90); when the slope approaches 0, the coating is displaying more resistive behavior (and the θ value approaches 0). Reprinted from reference [27], with permission from Elsevier.

Electrical circuit models can be used to extract a measurement of the coating capacitance and coating (pore) resistance, among other phenomena, and are described in the following chapter. The circuit model depicted in Figure 3.4 was quite reasonable for the behavior observed in the studies cited; indeed, in one instance, a coating containing an aluminum polyphosphate

inhibitor was studied in which the pores of the thick layer (as well as the aluminum oxide layer) became clogged as the inhibitor migrated and reacted, and the impedance measured at the flat, resistive middle frequencies (R_{coat}) actually increased with time [33].

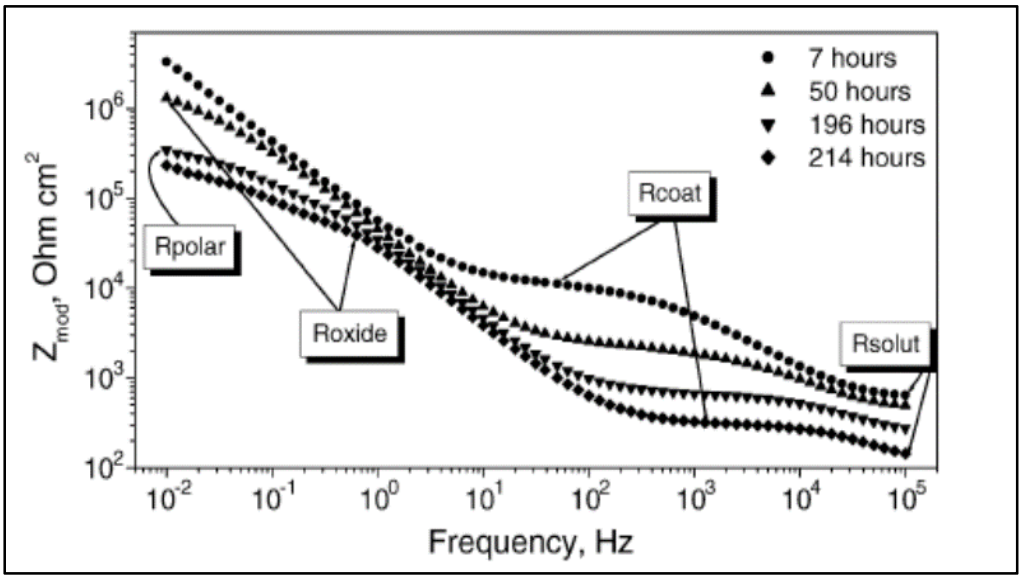

Figure 3.3. EIS results for a sol-gel coating displaying capacitive-resistive-capacitive behavior. Coating resistance (Rcoat) is depicted as the flatter region at 10^1-10^3 Hz. At low and high frequency, the Z mod (impedance) values describe a slope approaching negative 1, especially at 7 hours. Reprinted from reference [31], with permission from Elsevier.

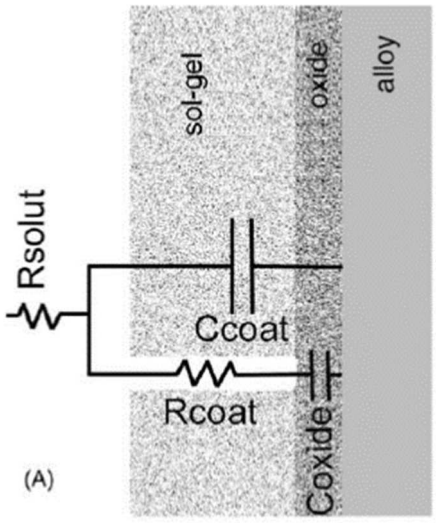

Figure 3.4. Circuit model used to fit the 7 hour graph in Figure 3.3. Ccoat is coating capacitance, Rcoat is coating (pore) resistance, Rsolut is solution resistance, and Coxide is the capacitance of the thin, dense layer, displayed here as the oxide layer. Reprinted from reference [31], with permission from Elsevier.

In the previous NDSU-Trent University collaboration, a different approach to the sol-gel hydrolysis step was utilized. The alkoxysilanes were dissolved in a ratio of water at 15:1 water to siloxane and stirred for 72 hours. This ratio of water to alkoxysilane allows for rapid hydrolysis of the alkoxysilanes but slow condensation and M-O-M cross-linking [36]. The result is most of the M-O-M cross-linking occurs in solution forming colloidal particles of siloxane with the functional groups concentrated around the outside, as depicted in Figure 3.5 [37]. In the previous studies, the functional group incorporated into the siloxane was epoxide, which was further cross-linked with aliphatic amines and the isomers of phenylenediamine (PDA) [1-2]. The cured samples were exposed to constant immersion under dilute Harrison's solution (DHS) (0.35% ammonium sulfate + 0.05% sodium chloride) with periodic EIS measurements. The results were surprisingly different considering the only difference was the amine cross-linker, with those cross-linked by aliphatic amines displaying Randle's cell behavior while those cross-linked with phenylenediamine displayed high and low frequency capacitance with resistive nature in the middle frequencies; Figure 3.6 compares representative results from those studies.

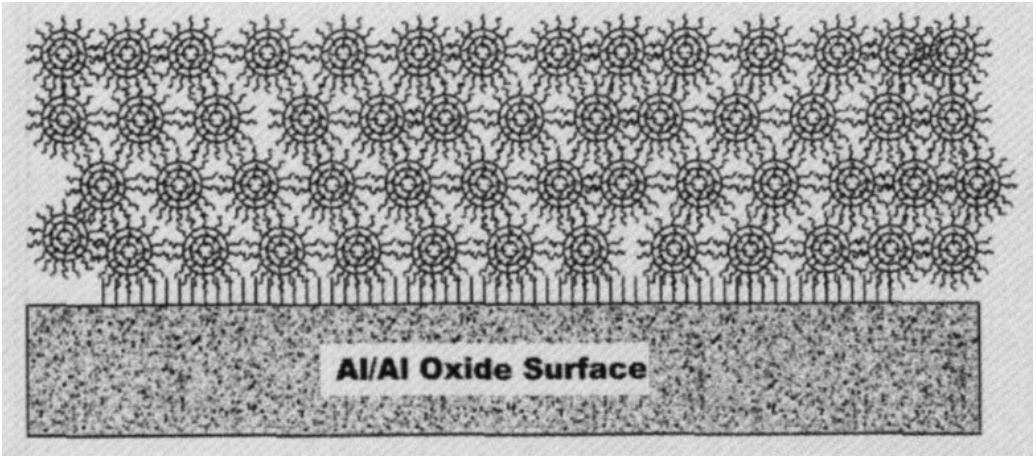

Figure 3.5. Colloidal particles of silane surrounded by epoxide functional groups. The amine cross-linking agents would likely be concentrated in the interstitial spaces between the particles. Reprinted from reference [37], with kind permission from Springer Science and Business Media.

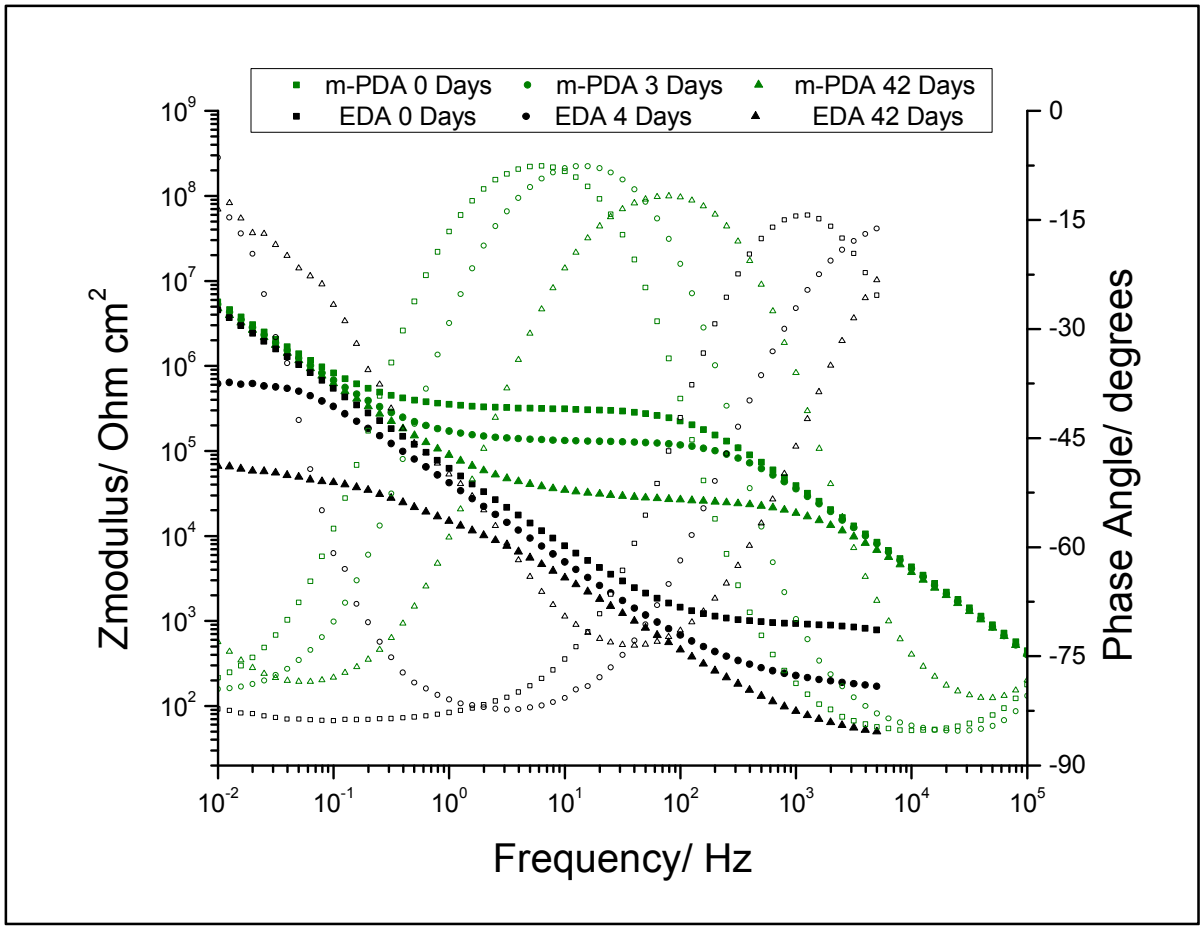

Figure 3.6. Comparison of representative EIS results from previous studies. These coatings were cross-linked with 1,3-phenylenediamine (m-PDA) and ethylenediamine (EDA) [1-2]. EDA cross-linked coatings revealed Randle's cell behavior from the initial measurement and double layer capacitance/charge transfer resistance at low frequencies by Day 4. The m-PDA cross-linked coating revealed continuous decrease in the coating resistance at middle frequencies with little change at high and low frequencies. The hollow symbols represent the phase angle values, with the shape corresponding to the solid Bode symbols.

Even though the EIS behavior of the PDA cross-linked coatings was similar to the behavior of some sol-gel coatings observed in the literature, and essentially the same circuit model was used to model the results (like that observed in Figure 3.4), the interpretation for the EIS behavior was different from the sol-gel coatings previously described for several reasons. First, phenylenediamine can be polymerized, yielding a polymer that is conductive, with structures similar to those observed for poly(aniline), which is also a conductive polymer [38-40]. The interpretation of the results for the PDA cross-linked coatings was conductive

pathways are developed through the coating that change the resistivity of the coating as the electrolyte penetrates the coating; it was postulated the conductivity increases during immersion due to oxidation of the PDA into conductive oligomers in situ, thus, the coating becomes less resistive over time and displayed the observed behavior. The low frequency capacitance is due to pristine coating nearer the interface through which the electrolyte has not yet penetrated. The circuits displayed in Figure 3.4 could be redrawn such that C_{oxide} (in that figure) could be placed in series after R_{coat}, thus in parallel to C_{coat}; the modeling software would model the data equally well and would return nearly identical values for the circuit components, even though the circuits are arranged differently. As noted in [2], this behavior suggests a transmission line model would also be appropriate; a transmission line model is often used with conductive polymers in which the charge transfer through the coating is through both ionic conduction in the pores and electronic conduction through the polymer itself [41].

The interpretation of the EIS results was different, second, because the colloidal structure of the siloxanes with epoxide groups around the perimeter should greatly reduce the amount of M-O-M bonding at the interface with the substrate; the ability to form the thin dense layer would likely be reduced and/or it would not stabilize the oxide layer as well. Third, the colloidal structure of the siloxane particle would likely necessarily push the PDA molecules into the interstitial space between the colloids and into close proximity with each other, where unreacted amine groups could potentially react to the next PDA ring and create conductive oligomeric fragments. Phenylenediamine reacts quite easily to form at least a dimer structure under mildly oxidizing conditions [42-43]. Indeed, mild acetic acid solutions have demonstrated the ability to polymerize PDA [44]; the acetic acid used as the catalyst to hydrolyze the siloxane in this sol-gel system is still present when the PDA is added to the sol and could begin to oxidize PDA

immediately in solution and as the coating cures. It likely remained entrapped in the coating as it dried, leaving it available to further polymerize PDA when exposed in the electrolyte. Additionally, both the coatings that were immersed and dry samples that were stored in a drawer became darker over time as the PDA was oligomerized due to the solution or air oxidation. And finally, fourth, the aliphatic cross-linked system did not display this same behavior; if the formation of a thin, dense layer and/or the aluminum oxide layer is the sole reason for the low frequency capacitance for the coating cross-linked with PDA, it would not seem unreasonable to assume the coatings cross-linked with aliphatic amines should also have formed a thin, dense layer and displayed this EIS behavior, which the coatings did not.

This interpretation of the sol-gel results was met with great resistance at the time the paper was submitted for publication. The reviewers felt the model describing the EIS behavior already presented in the literature was adequate and seemed reticent to consider a different possibility, even though the PDA cross-linked coatings were synthesized in a much different fashion than those described in the literature. The paper was finally accepted for publication, for the reviewers could not explain why the simple change of amine cross-linking agent would change the structure of the sol-gel itself nor why the aluminum oxide layer should be any different due to a change of amine cross-linker, either.

During the review process it was decided to continue this project by attempting to cross-link non-sol-gel, more standard epoxies with PDA and study the EIS results of the resulting coatings. It was believed this process would remove the thin, dense layer created at the interface by the M-O-M bonding of the sol-gel and also reduce the porosity of the thick layer while still incorporating the conductive nature of the PDA. It was also determined the epoxies should not form colloidal structures and the PDA molecules may not be forced into sufficiently close

proximity to form oligomer structures, as with the sol-gel coatings; thus, the PDA was also pre-oligomerized and then added to the coatings. The synthesis and characterization of these oligomers are also discussed because notable differences were observed depending on the method of synthesis.

3.2. Introduction to the second coating system: the formation of magnetite on steel as a coating system

The second coating in this thesis was studied for an industrial client of NDSU. It is a commercially available chemical bath that forms a black magnetite layer on steel when it is immersed in the bath; this layer is then covered with a clear sealant. This coating system is applied in lieu of painting and is used primarily for coating tools. Figure 3.7 presents a photograph of steel before and after immersion in the bath as well as a scanning electron microscope (SEM) image of the finished product. The client has held the patent for the product for approximately 20 years, with a revision approximately 10 years ago as the formulation was adjusted. The product begins to reach a critical point (termed "souring") at which the quality of the coating developed is less than specifications call for; at that point, a solution to replenish the chemicals can be added and the resulting coating will return to specifications. This addition can be repeated several times, however, with diminishing returns upon each addition; eventually it becomes more cost effective to simply replace the bath. Importantly, if the chemicals to replenish the solution are not added before the critical point, the bath becomes unusable and must be replaced. The client sought the help of NDSU to study the formulation to gain a better understanding of it inner workings, develop a method to test the bath to determine where in its life cycle it is at, and possibly improve its performance.

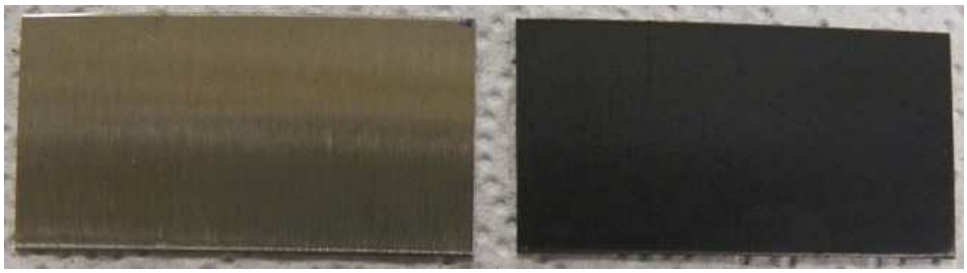

Figure 3.7. Photograph of steel before and after immersion in the bath revealing the black color.

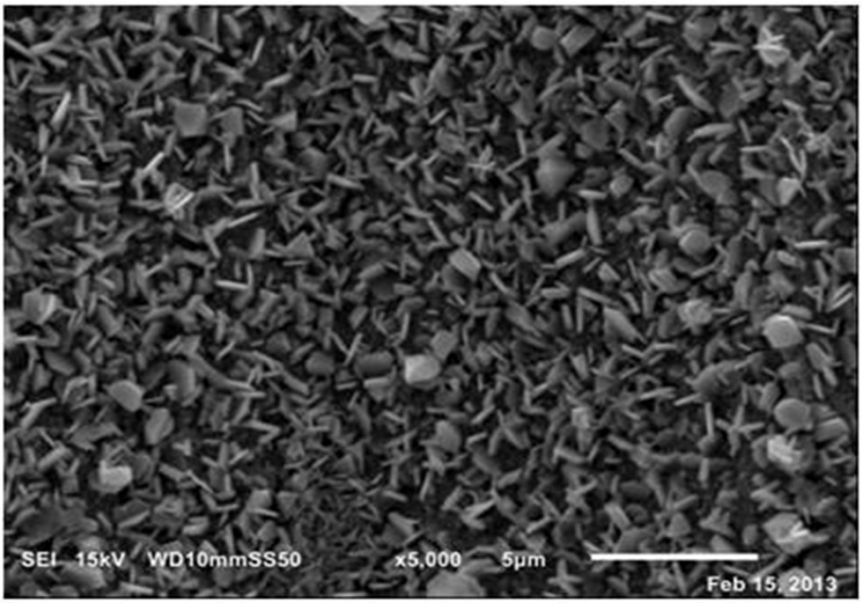

Figure 3.8. SEM image of the finished product revealing platy crystal structure.

The bath is a complex mixture of chemicals, as displayed in Table 3.1; the amounts and identities of all of the chemicals will not be revealed due to the proprietary nature of the bath formulation. Upon immersion into the bath, the reactions occurring at the metal surface complicate the mixture further by generating additional chemical species that migrate into the solution and further react. Complicating the study of the process still further, and thus, the analysis, is the fact the bath is highly alkaline (pH>14) and must be operated at a temperature of approximately 200^{o}F for it to function properly. Indeed, parts of the study focused on reducing the level of sodium hydroxide in the bath to study the effects, as well as studying the complete bath and bath components at reduced temperatures to observe the related changes.

Table 3.1.
Composition of bath used to form a layer of magnetite on steel.

Chemical	Formula	Amount
Sodium Hydroxide	NaOH	> 3M
Sodium Nitrate	$NaNO_3$	~ 0.5M
Tin Compound		
Sodium Thiosulfate	$Na_2S_2O_3$	
Complexing Agent		
Sodium Nitrite	$NaNO_2$	
Charge Transfer Agent		

The client provided NDSU several pieces of information which aided in the analysis of the bath. First, sodium hydroxide, sodium nitrate, sodium nitrite and sodium thiosulfate are the four key ingredients; all are needed or no magnetite is formed. The other three ingredients are not necessary but seem to improve the bath performance. The complexing agent was originally added to attempt to control the level of sludge generated in the bath; however, it was determined the bath also worked "better" when it was added. The charge transfer agent (CTA) and tin compound helped yield a better coating at a faster rate. The client performed many trial and error experiments to perfect the coating and determined several facts. Addition of too much nitrite or tin compound rendered the bath unusable; it simply did not form the coating. The levels of nitrite and nitrate can be reduced but the ratio of the two is rather specific. And although extremely alkaline, the bath needs this level of hydroxide to function correctly. These are some areas the project focused on in the attempt to analyze this formulation.

The high alkalinity, amount of nitrate present, and temperatures are reminiscent of conditions observed in electrical power plants and the corrosion properties observed therein; several published studies discuss the techniques employed to study the corrosion processes under these conditions [45-49]. One often used technique to study these systems is potentiodynamic polarization measurements [50-54]. With the similarity between the studied bath conditions and

those of the conditions in the power plants, it was determined polarization measurements might be a good starting point to study this coating bath. Indeed, a great deal of data was generated with this method and most of the project revolved around analysis of the resulting data and developing a working hypothesis as to the reaction mechanisms involved in the formation of magnetite by this coating bath. Potentiodynamic polarization is discussed in detail in the following chapter.

3.3. References

[1] A.J. Vreugdenhil, V.J. Gelling, M.E. Woods, J.R. Schmelz, B.P. Enderson, Thin Solid Films, 517 (2008) 538-543.

[2] K.J. Croes, A.J. Vreugdenhil, M. Yan, T.A. Singleton, S. Boraas, V.J. Gelling, Electrochimica Acta, 56 (2011) 7796-7804.

[3] C.J. Brinker, G.W. Scherer, Sol-Gel Science: The Physics and Chemistry of Sol-Gel Processing, Academic Press, 1990.

[4] M. Guglielmi, Journal of Sol-Gel Science and Technology, 8 (1997) 443-449.

[5] U. Schubert, N. Hüsing, A. Lorenz, Chemistry of Materials, 7 (1995) 2010-2027.

[6] G. Schottner, Chemistry of Materials, 13 (2001) 3422-3435.

[7] J. Wen, G.L. Wilkes, Chemistry of Materials, 8 (1996) 1667-1681.

[8] T.L. Metroke, R.L. Parkhill, E.T. Knobbe, Progress in Organic Coatings, 41 (2001) 233-238.

[9] Figure 3.1 reprinted from Progress in Organic Coatings, 47 (3.4), V. Palanivel, D. Zhu, W.J. van Ooij, "Nanoparticle-filled silane films as chromate replacements for aluminum alloys," 384-392, 2003, with permission from Elsevier.

[10] M.L. Zheludkevich, I.M. Salvado, M.G.S. Ferreira, Journal of Materials Chemistry, 15 (2005) 5099-5111.

[11] A. Duran, Y. Castro, M. Aparicio, A. Conde, J.J. de Damborenea, International Materials Reviews, 52 (2007) 175-192.

[12] S.-X. Zheng, J.-H. Li, Journal of Sol-Gel Science and Technology, 54 (2010) 174-187.

[13] O. Kachurina, T.L. Metroke, E. Stesikova, E.T. Knobbe, JCT Journal of Coatings Technology, 74 (2002) 43-48.

[14] T.L. Metroke, O. Kachurina, E.T. Knobbe, Progress in Organic Coatings, 44 (2002) 295-305.

[15] R. DiMaggio, L. Fedrizzi, S. Rossi, Journal of Adhesion Science and Technology, 15 (2001) 793-808.

[16] N.N. Voevodin, N.T. Grebasch, W.S. Soto, L.S. Kasten, J.T. Grant, F.E. Arnold, M.S. Donley, Progress in Organic Coatings, 41 (2001) 287-293.

[17] T.P. Chou, C. Chandrasekaran, S.J. Limmer, S. Seraji, Y. Wu, M.J. Forbess, C. Nguyen, G.Z. Cao, Journal of Non-Crystalline Solids, 290 (2001) 153-162.

[18] A.L.K. Tan, A.M. Soutar, I.F. Annergren, Y.N. Liu, Surface and Coatings Technology, 198 (2005) 478-482.

[19] R. Zandi-zand, A. Ershad-langroudi, A. Rahimi, Progress in Organic Coatings, 53 (2005) 286-291.

[20] A.J. Vreugdenhil, M.E. Woods, Progress in Organic Coatings, 53 (2005) 119-125.

[21] N.C. Rosero-Navarro, S.A. Pellice, A. Duran, M. Aparicio, Corrosion Science, 50 (2008) 1283-1291.

[22] H. Wang, R. Akid, Corrosion Science, 50 (2008) 1142-1148.

[23] V. Moutarlier, B. Neveu, M.P. Gigandet, Surface and Coatings Technology, 202 (2008) 2052-2058.

[24] A.N. Khramov, N.N. Voevodin, V.N. Balbyshev, M.S. Donley, Thin Solid Films, 447-448 (2004) 549-557.

[25] D.G. Shchukin, S.V. Lamaka, K.A. Yasakau, M.L. Zheludkevich, M.G.S. Ferreira, H. Möhwald, Journal of Physical Chemistry C, 112 (2008) 958-964.

[26] M.L. Zheludkevich, D.G. Shchukin, K.A. Yasakau, H. Möhwald, M.G.S. Ferreira, Chemistry of Materials, 19 (2007) 402-411.

[27] Figure 3.2 reprinted from Electrochimica Acta, 52 (9) A.S. Hamdy, D.P. Butt, A.A. Ismail, "Electrochemical impedance spectroscopy studies of sol-gel based ceramic coatings systems in 3.5% NaCl solution," 3310-3316, 2007, with permission from Elsevier.

[28] L.M. Palomino, P.H. Suegama, I.V. Aoki, M.F. Montemor, H.G. de Melo, Corrosion Science, 50 (2008) 1258-1266.

[29] A.S. Hamdy, D.P. Butt, Surface and Coatings Technology, 201 (2006) 401-407.

[30] L.E.M. Palomino, P.H. Suegama, I.V. Aoki, Z. Paszti, H.G. de Melo, Electrochimica Acta, 52 (2007) 7496-7505.

[31] Figures 3.3 and 3.4 reprinted from Electrochimica Acta, 51 (2), M.L. Zheludkevich, R. Serra, M.F. Montemor, K.A. Yasakau, I.M. Miranda Salvado, M.G.S. Ferreira, "Nanostructured sol-gel coatings doped with cerium nitrate as pre-treatments for AA2024-T3: Corrosion protection performance," 208-217, 2005, with permission from Elsevier.

[32] M.L. Zheludkevich, R. Serra, M.F. Montemor, I.M. Miranda Salvado, M.G.S. Ferreira, Surface and Coatings Technology, 200 (2006) 3084-3094.

[33] D. Raps, T. Hack, J. Wehr, M.L. Zheludkevich, A.C. Bastos, M.G.S. Ferreira, O. Nuyken, Corrosion Science, 51 (2009) 1012-1021.

[34] M.L. Zheludkevich, K.A. Yasakau, A.C. Bastos, O.V. Karavai, M.G.S. Ferreira, Electrochemistry Communications, 9 (2007) 2622-2628.

[35] A. Conde, A. Duran, J.J. de Damborenea, Progress in Organic Coatings, 46 (2003) 288-296.

[36] T.L. Metroke, O. Kachurina, E.T. Knobbe, Progress in Organic Coatings, 44 (2002) 185-199.

[37] Figure 3.5 reprinted from Journal of Coatings Technology, 73 (915), A.J. Vreugdenhil, V.N. Balbyshev, M.S. Donley, "Nanostructured silicon sol-gel surface treatments for Al 2024-T3 protection," 35-43, 2001, with kind permission from Springer Science and Business Media.

[38] S. Bhadra, D. Khastgir, N.K. Singha, J. H. Lee, Progress in Polymer Science, 34 (2009) 783-810.

[39] R.H. Sestrem, D.C. Ferreira, R. Landers, M.L.A. Temperini, G.M. do Nascimento, European Polymer Journal, 46 (2010) 484-493.

[40] R.H. Sestrem, D.C. Ferreira, R. Landers, M.L.A. Temperini, G.M. do Nascimento, Polymer, 50 (2009) 6043-6048.

[41] J.F. Rubinson, Y.P. Kayinamura, Chemical Society Reviews, 38 (2009) 3339-3347.

[42] F. Cataldo, European Polymer Journal, 32 (1996) 43-50.

[43] D. Ichinohe, T. Muranaka, T. Sasaki, M. Kobayashi, H. Kise, Journal of Polymer Science A, 36 (1998) 2593-2600.

[44] W. Qin, X. Zhao, F. Li, Acta Polymerica Sinica, 4 (1993) 502-505.

[45] G.L. Edgemon, M.J. Danielson, G.E.C. Bell, Journal of Nuclear Materials, 245 (1997) 201-209.

[46] J.D. Genders, D. Hartsough, D.T. Hobbs, Journal of Applied Electrochemistry, 26 (1996) 1-9.

[47] E. Sosa, R. Cabrera-Sierra, M.T. Oropeza, I. Gonzalez, Journal of Applied Electrochemistry, 32 (2002) 905-913.

[48] J. Leifer, P.E. Zapp, J.I. Mickalonis, Corrosion, 55 (1999) 31-37.

[49] X. Li, F. Gui, H. Cong, C.S. Brossia, G.S. Frankel, Journal of the Electrochemical Society, 16 (2013) C521-C530.

[50] K. Subramanian, J. Mickalonis, Electrochimica Acta, 50 (2005) 2685-2691.

[51] K.N. Mohana, A.M. Badiea, Corrosion Science, 50 (2008) 2939-2947.

[52] X. Li, F. Gui, H. Cong, C.S. Brossia, G.S. Frankel, Electrochimica Acta, 117 (2014) 299-309.

[53] G.O.H. Whillock, T.J. Binks, C.J. Donohoe, Corrosion, 68 (2012) 967-981.

[54] G.O.H. Whillock, S.E. Worthington, C.J. Donohoe, Corrosion, 68 (2012) 677-687.

CHAPTER 4. ELECTROANALYTICAL METHODS

4.1. Electrochemical impedance spectroscopy (EIS)

A perfectly coated metal will behave similarly to an electrical capacitor. A capacitor consists of an insulating material (high dielectric) sandwiched between two conductive materials; when current is applied to one of the conductors, the charge will build to the point that it discharges to the other conductor. The coated metal has the same structure as a capacitor where the metal acts as one conductor, the coating as the insulating material, and an electrolyte solution in contact with the other side of the coating as the other conductor (Figure 4.1). Thus, a coated metal will have a similar electrical response to a capacitor when it is pristine; however, as it begins to break down and the electrolyte can penetrate the coating, it will begin to behave similar to a resistive element. These are termed the coating capacitance and coating (or pore) resistance [1-3].

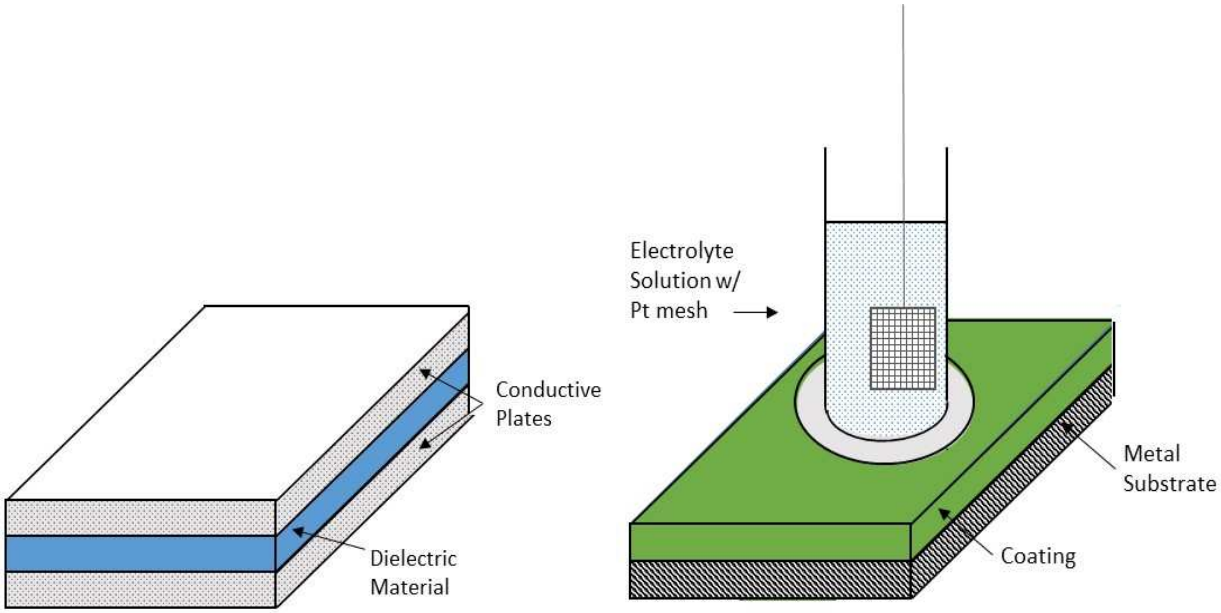

Figure 4.1. Diagrams of a simple parallel plate capacitor and a coated metal substrate. The second conductive plate of the simple capacitor (left) is replaced by electrolyte solution (right) displaying the similarity between the two systems. The platinum (Pt) mesh and substrate serve as connection points to the measuring device, a potentiostat.

The resistance of an element can be determined by the relationship, Ohm's Law:

$$V=IR \tag{4.1}$$

where V is the voltage (volts), I is the current (amps), and R is the resistance (ohms). This relationship applies when the current is direct current, DC. Direct current and resistance have magnitude whereas alternating current has a magnitude and phase. In EIS, an AC perturbation current is applied to the working electrode and instead of resistance, impedance is measured which also has a magnitude and phase. Impedance can be determined through this relationship:

$$V \approx IZ = I\,|Z|\,e^{j\theta} \tag{4.2}$$

where V is again voltage, I current, and Z is the impedance (ohms), or |Z| is the magnitude of the impedance, j is the imaginary unit and θ is the phase angle. Impedance has components of both capacitance (farads) and resistance; the resistance is essentially the part of the impedance that has a phase angle equal to 0. The phase angle is the shift in phase that results from the lag of the current with respect to the applied voltage when the current is passed through a capacitive element. Thus, a phase shift of -90^{o} would indicate pure capacitance. The imaginary term arises from the use of complex numbers necessary to solve the equations created by the lag of the phase of the sinusoidal waves of the current and voltage [4].

EIS results are presented in two ways: the Bode graph and the Nyquist graph. The data used is from the same set of information, it is just presented differently. Figures 4.2 and 4.3 display an example of the results that may be expected from this technique. The sample was a paint system on aluminum alloy that was exposed to 4000 hours of accelerated weathering and measured by EIS at intervals to study whether the coating was exhibiting failure. In Figure 4.2, the Bode graph is presented; in this graph, the impedance (modulus) is graphed against the frequency, in this case, from 0.01Hz to 100,000Hz. Note both axes are logarithmic. Also

graphed is the phase angle observed at each measurement point. The phase axis is on the right and is linear, for the angle will generally vary from 0 to -90° for capacitive and resistive behavior (the value can be larger than -90 or positive if unusual behavior is observed). The 0 hours Bode points are not visible because no notable changes were detected during the first 1000 hours of exposure. However, by 2000 hours, the impedance at the lowest frequencies had begun to decline, indicating penetration of electrolyte partially into the coating. This electrolyte penetration is also detected by the change in the phase angles at the lowest frequencies; the values are much nearer 0 degrees than -90 degrees as the values were during the first two measurements. By 3000 hours the electrolyte had most likely reached the metal-coating interface; that point is reflected by the change in slope of the Bode graph in the mid-frequencies as well as the multiple changes of direction of the slope visible in phase angle. At 4000 hours the impedance had declined further still. Importantly, by visual inspection, this sample did not display any indication of failure of the coating but the EIS results revealed some level of failure.

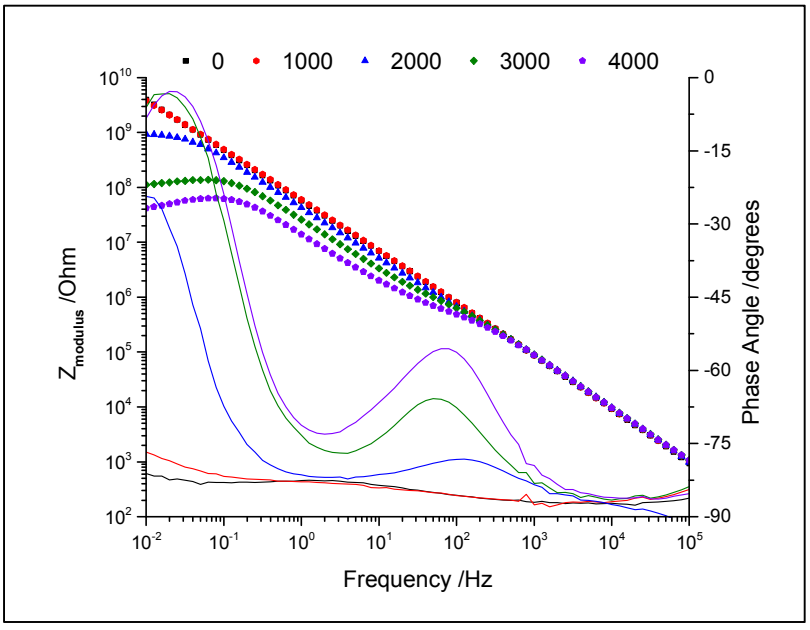

Figure 4.2. Example Bode graph of a coating on aluminum alloy. Dots are the impedance values, solid lines are the phase angles, color matched for each measurement. Values at top are hours of accelerated weathering. Results are from unpublished data.

The Nyquist graph in Figure 4.3 displays the same sample results. Here, the frequency information is not presented. In this graph, the "real" component of the impedance – the resistance or in-phase component – is graphed against the "imaginary" component of the impedance – the capacitance or out-of-phase component. As noted, the imaginary term arises from the use of complex numbers necessary to solve the equations created by the lag of the phase of the sinusoidal waves of the current and voltage; this process necessitates taking the square root of negative values, i.e. a complex, imaginary number [4]. The horizontal axis is reversed from the Bode graph with the lower frequency data graphed to the right and high frequency data graphed to the left. This reversal is because the values of impedance are larger at the lower frequencies, as was observed in the Bode graph. At high frequency, only a small contribution from capacitance is observed, very little contribution from resistance so the value is very low; the resistive contribution would be from the solution resistance and would be detected at still higher frequencies that are above the range of the instrument. As the frequency is reduced, the total impedance value will increase so the contribution from each component becomes larger; the capacitance may contribute all the value to the impedance (as observed by the 0 and 1000 hours graphs which are nearly vertical). Or, it may start to become a mixture of capacitance and resistance; the graph at 2000 hours displays that behavior, with decreased contribution from capacitance at high frequency and more contribution from resistance at low frequency. Thus, the graph slope initially increases as the contribution from capacitance increases, with little contribution from resistance; then, the slope reaches a maximum and turns negative as the contribution from capacitance begins to decrease while the resistance contribution continues to increase. This behavior yields a semi-circular graph; had the phase angle observed in the Bode graph reached 0 at 0.01 Hz, the 2000 hour data in the Nyquist graph would be a complete semi-

circle touching the horizontal axis. The slight hook in the graph observed at low frequency for 3000 and 4000 hours exposure (inset) indicates the system was not at steady state during the course of the measurement, also suggesting the electrolyte solution had reached the substrate.

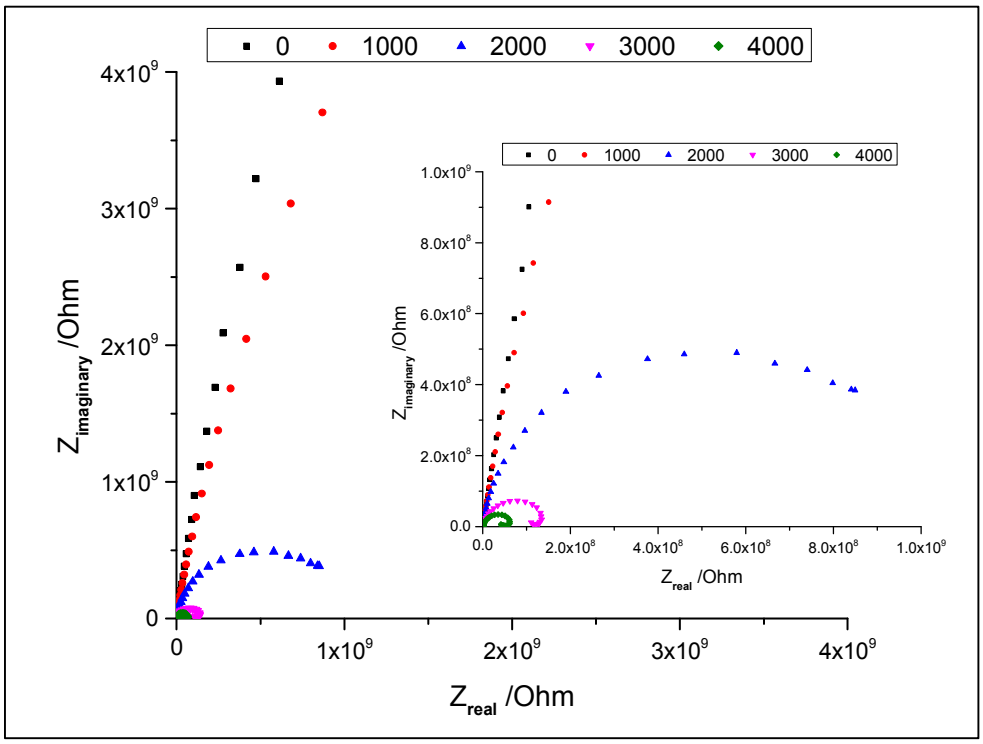

Figure 4.3. Example Nyquist graph of a coating on aluminum alloy. Values at top are hours of accelerated weathering. Inset is the lower left corner of the large graph. Results are from unpublished data.

When the electrolyte has penetrated to the substrate, additional processes begin to occur that are also detected. First, electrolyte in contact with the metal surface will create an electrochemical double layer. Electrons on the metal surface create a net negative charge which attracts a layer of polar water molecules with the positive side of the water molecules aligned with the negative charge of the metal; the cations in the electrolyte are also solvated by water molecules with the negative side of the water molecules aligned to the positive cation. These clusters then have a positive charge around the outside that align to the negative charges of the water molecules at the metal surface; all these are depicted in Figure 4.4 [5].

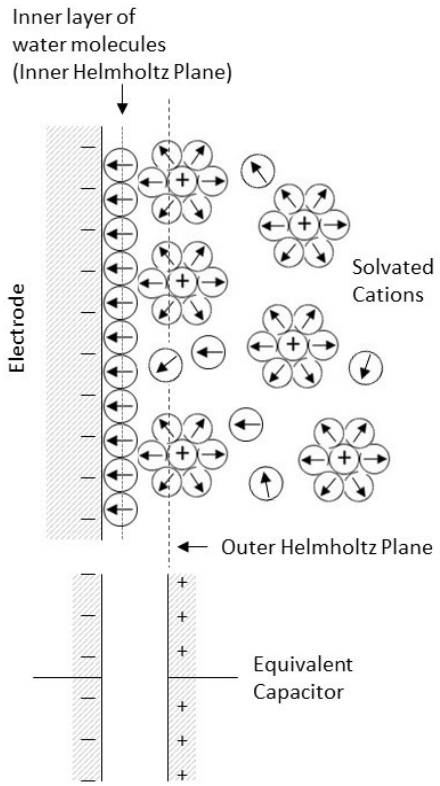

Figure 4.4. Model of the electrical double layer observed at the interface of a metal electrode placed in an electrolyte solution. The inner Helmholtz plane is a layer of water molecules aligned with the positive end of the polar molecule toward electrons at the electrode surface; the outer Helmholtz plane is a layer of solvated cations that are limited in how close the ions may approach the metal surface by the water molecules solvating them. Diagram is redrawn and modified from reference 5.

This "double layer" provides a barrier to current flow in the form of another capacitance (charge builds, then dissipates) which is detected at lower frequencies in coated systems but at middle frequencies on bare metals; this phenomenon is termed the double layer capacitance. Second, when electrolyte contacts metal, the metal is oxidized and another species is reduced; this phenomenon is termed a charge transfer reaction. There is an activation energy that must be overcome by physically transferring electrons, which presents resistive behavior, thus, this behavior is known as the charge transfer resistance [6]. At low frequencies and as the coating degrades, this resistance forms a greater amount of the total impedance when detected.

The example presented in Figures 4.2 and 4.3 displayed double layer capacitance and charge transfer resistance at 3000 and 4000 hours of exposure. In the Bode graph, the phase angle is near -90 at high frequency (revealing the coating capacitance); it reaches approximately -60 at 10^2 Hz (beginning to reveal the coating resistance); then becomes more capacitive until 10^0 Hz (revealing double layer capacitance); and then becomes resistive at lowest frequencies (revealing charge transfer resistance). The two reversals observed in the phase angle graph at 10^2 and 10^0 Hz were reflected in Nyquist graph but the scale was too small to observe clearly. Additionally, the Nyquist graph displayed an inductive loop at the very right of the graphs; this phenomenon is also occasionally observed. This behavior can occur if the system is not at steady state during the course of the measurement and may indicate active corrosion while the measurement is being made or may be due to adsorption of corrosion products on the surface which changes the surface area in contact with electrolyte as the measurement is made.

Circuit modeling provides a means to analyze the data obtained from the EIS measurements. The various resistances and capacitances observed by EIS measurements can be compared to standard electrical circuit elements which can be combined in various configurations to attempt to fit the data obtained. These models can be used to help determine the behaviors and processes which are displayed by the coating as well as the magnitudes of the capacitances and resistances. Example models are displayed in Figure 4.5. The first is the model that would be used for a pristine coating which has displayed no evidence of electrolyte penetration and is acting as perfect capacitor; a resistor is added because the electrolyte solution plus electrodes will add a small resistive component to the total (it is generally termed the solution resistance). This model is representative of the data observed for 0 and 1000 hours for the example above. The second is the Randle's cell which consists of the solution resistance,

coating capacitance, and coating resistance; this model is representative of the 2000 hour data where some level of electrolyte penetration into the coating is observed (and representative of some sol-gel coatings presented in Chapter 3). The third model is the Randle's cell slightly modified; it is rare that the coating will act as a perfect capacitor once electrolyte has begun to penetrate. Therefore, the capacitance is often represented by the constant phase element (CPE) which accounts for and calculates how close the capacitive behavior is to a pure capacitor. The fourth model adds the elements of double layer capacitance and charge transfer resistance. An example of how the data is fit to the model is displayed in Figure 4.6; here, model 3 is fit to the data obtained at 2000 hours for the Bode, phase angle, and Nyquist graphs (modeling software was ZView by Scribner and Associates).

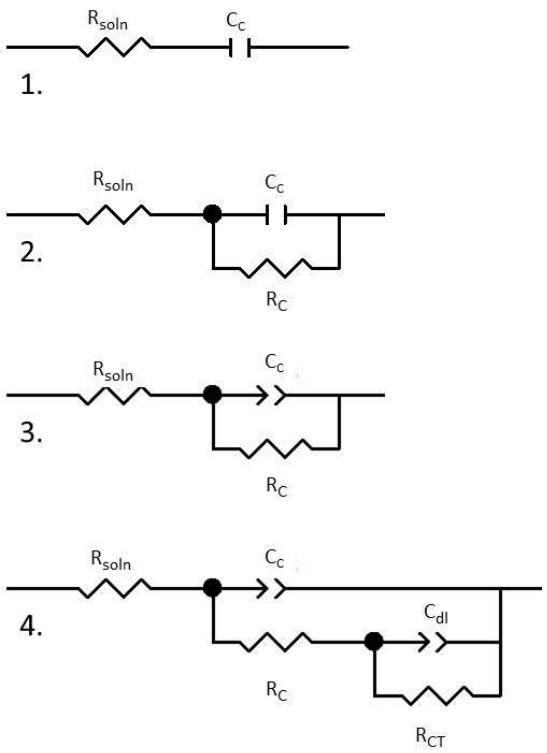

Figure 4.5. Example circuit models that can be used to model the data for the graphs in Figures 4.2 and 4.3. R_{soln} is the solution resistance; C_c is the coating capacitance; R_c is the coating resistance; C_{dl} is the double layer capacitance; and R_{CT} is the charge transfer resistance.

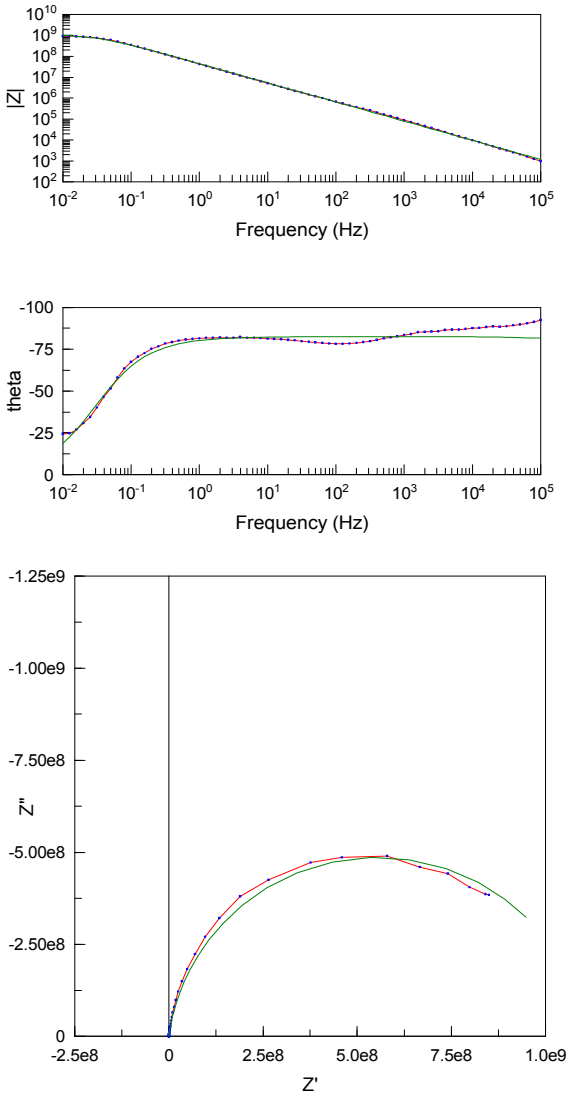

Figure 4.6. Fitting results for the data from 2000 hours in Figures 4.2 and 4.3 using circuit model 3 from Figure 4.5. The pink/blue line is the data, the green line is the fitting result.

4.2. Potentiodynamic polarization

Every metal/electrolyte solution pairing creates a unique system where the water, oxygen (if present), and salts in the solution interact with the metal atoms at the surface of the substrate through oxidation-reduction (redox) reactions. Depending on the system, electrons will flow from the metal to the salts and/or water and/or oxygen, oxidizing the metal atoms at the surface and reducing components in the solution. Additionally, in metal alloys, the alloying elements can create more favorable sites for electron exchange or may be oxidized or reduced relative to

the main metal element through a galvanic couple, thereby increasing the rate of electron exchange versus the pure metal. This electron exchange occurs at a given electrochemical potential and at a given pace based on the particular metal/electrolyte system and other factors such as electrolyte concentration and surface area of metal substrate exposed to the electrolyte.

The process proceeds at a steady state or equilibrium state that is known as the "corrosion" or "open circuit" potential (OCP); the OCP represents a point where all oxidation reactions and all reduction reactions yield a net sum zero current flow. It will remain at that potential unless or until it is affected by an external force or a change in the solution composition or change in the metal surface, such as the buildup of metal oxides. As an example, electron exchange will occur more rapidly initially but will become subdued if corrosion products precipitate in the pores of coatings and prevent the passage of ions that further corrode the surface [7]. A single oxidation and single reduction reaction may occur or multiple redox reactions may occur simultaneously with all contributing to lesser or greater extent to the observed open circuit potential; this phenomenon is known as the mixed potential theory [8].

The potential of the system can be adjusted to potentials other than the OCP by a potentiostat in a potentiodynamic polarization experiment. The response of the system to these different potentials can yield information about the presence of specific reactions that may be occurring that might otherwise be undetected because of the influence of other reactions. The potential is generally applied over a chosen range with increase in the observed current density as the potential reaches a point conducive to a particular reaction and decrease in current density as the potential moves away from a region at which reactions of some kind might easily occur. Typically, the open circuit potential will be observed at the point of least activity because the potential set by the potentiostat matches the natural condition of the system at that point. Forcing

the potential away from the open circuit can prevent one of two or more reactions from occurring, thus, for example, all oxidation may be due to a single reaction rather than two reactions that may occur at the OCP. Importantly, using the potentiostat to hold the potential at a potential other than OCP can induce reactions to occur that would otherwise not, complicating the analysis. However, just as importantly, forcing a reaction to occur can indicate the presence of a chemical species that might otherwise go undetected.

For example, Figure 4.7 displays what is termed an Evans diagram comparing potential versus the log of the current (or current density) for two oxidation-reduction reactions, one for hydrogen/hydrogen ion and one for a generic metal/metal ion. If only hydrogen and hydrogen ions or metal and metal ions were in the system, each pair would represent the sole oxidation reaction and sole reduction reaction. Above the potential at E_{H^+/H_2}, the oxidation of hydrogen will occur (the anodic reaction); below that potential, the reduction of H^+ will occur (the cathodic reaction). Likewise, the metal will oxidize at potentials above $E_{M^+/M}$ and metal ions will be reduced below that potential [9]. When acid and solid metal are combined in the same system, the acid will oxidize the metal through the reaction:

$$2H^+ + 2M \rightarrow H_2 + 2M^+ \tag{4.3}$$

The potential this reaction occurs at is the OCP (E_{corr} in the figure) and is the mixed potential; the current generated by the reaction is termed the corrosion current (i_{corr} in the figure). If the potential is held below $E_{M^+/M}$ (at the red line for example), the metal oxidation reaction will not occur. (This is the basic principle behind cathodic protection of metals, where the potential is held below $E_{M^+/M}$, thus preventing the anodic dissolution (oxidation) of the metal; the reaction $2H^+ + 2e \rightarrow H_2$ would still occur but the electrons needed would be supplied by the potentiostat.) At the potential marked by the red line, if any M^+ ions are present, the ions will get reduced to

solid metal. Conversely, if the potential is held above E_{H^+/H_2} (at the blue line for example), if any hydrogen were in the system, it would get oxidized, adding to the total current generated by the metal already being oxidized. In the situation where the potential is held between E_{H^+/H_2} and $E_{M^+/M}$ but away from E_{corr} (at the green line for example), the reactions occurring remain the same but the rates change. The reaction rate for $M \rightarrow M^+ + e$ will be retarded and the current for i_{corr} will decrease.

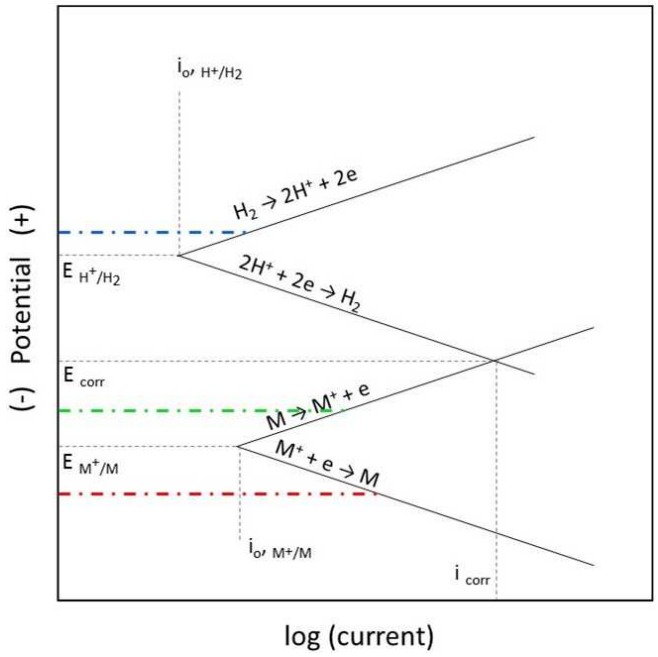

Figure 4.7. Evans diagram displaying a simple oxidation-reduction system, a metal in an acid solution. One reduction reaction ($2H^+ + 2e \rightarrow H_2$) and one oxidation reaction ($M \rightarrow M^+ + e$) will occur (e represents an electron) at a potential equal to E_{corr}. Diagram drawn based on information in references [5, 9].

Figure 4.8 presents a more complicated diagram but is more applicable to the current work. In this diagram, an extra oxidizing agent is added to the system, M_2^+, for this example a metal ion capable of oxidizing the original metal (now labeled M_1) but, importantly, could represent <u>any</u> ion capable of oxidizing M_1. The other lines are as in Figure 4.7. In this situation, both M_2^+ and H^+ are oxidizing M_1; thus, the total current flowing for reduction is increased (green line) as well as the total current for oxidation (blue line). The mixed potential for M_2^+

reacting to M_1 has the effect of increasing E_{corr} to a more positive potential, E_{corr} (new). Demonstration of these effects is important in the current work because multiple oxidation and reduction reactions all occur in the system at the same time.

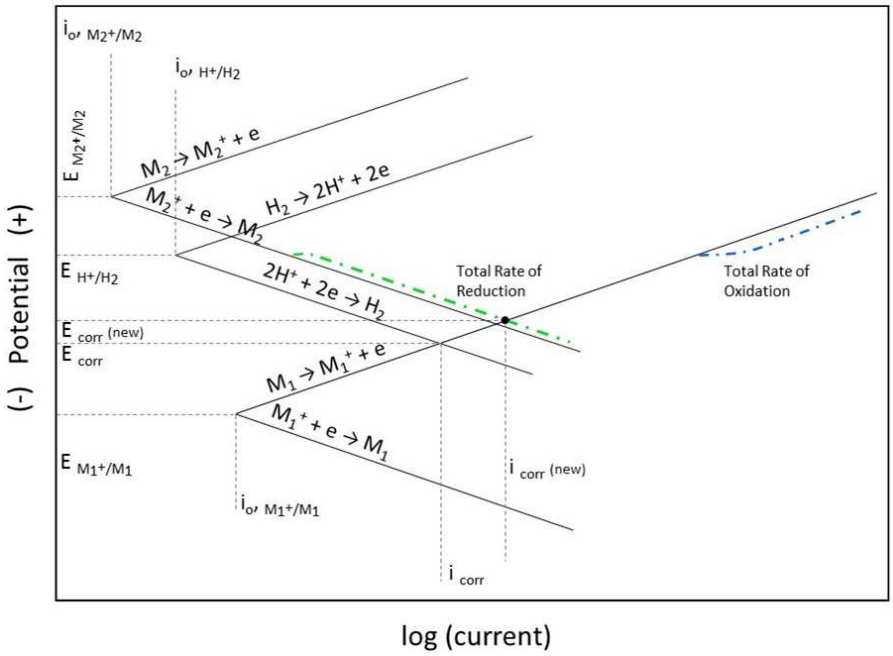

Figure 4.8. Evans diagram displaying the effects of adding an extra oxidizing agent to the system presented in Figure 4.7. Diagram drawn based on information in references [5, 9].

The data from the potentiodynamic polarization technique is graphed such that the current (or current density) observed is charted against the electrochemical potential of the cell at each point; Figure 4.9 presents a simple example of what may happen to an active metal in an electrolyte solution. Often, most activity is observed on the anodic branch of the plot, that portion at potential higher than the OCP. Oxidation reactions occur in this region; for corroding metals, this reaction will be oxidation of the metal, but other species being oxidized might also display activity in this region. Occasionally, activity is also observed on the cathodic branch, that portion of the graph at potential lower than the OCP. Activity in this region is associated with reduction reactions; in an aqueous solution, these might include oxygen reduction at neutral and acidic pH, water reduction if other reactions are not occurring, and, importantly for this

thesis, metal reduction [5]. The potential is typically applied from negative of the OCP (cathodic arm) to positive of the OCP but can be moved either direction. The rate the potential is moved (in millivolts per second, mV/s) and the length of time the current is measured at each potential step (sample period in seconds) are chosen by the operator as deemed fit.

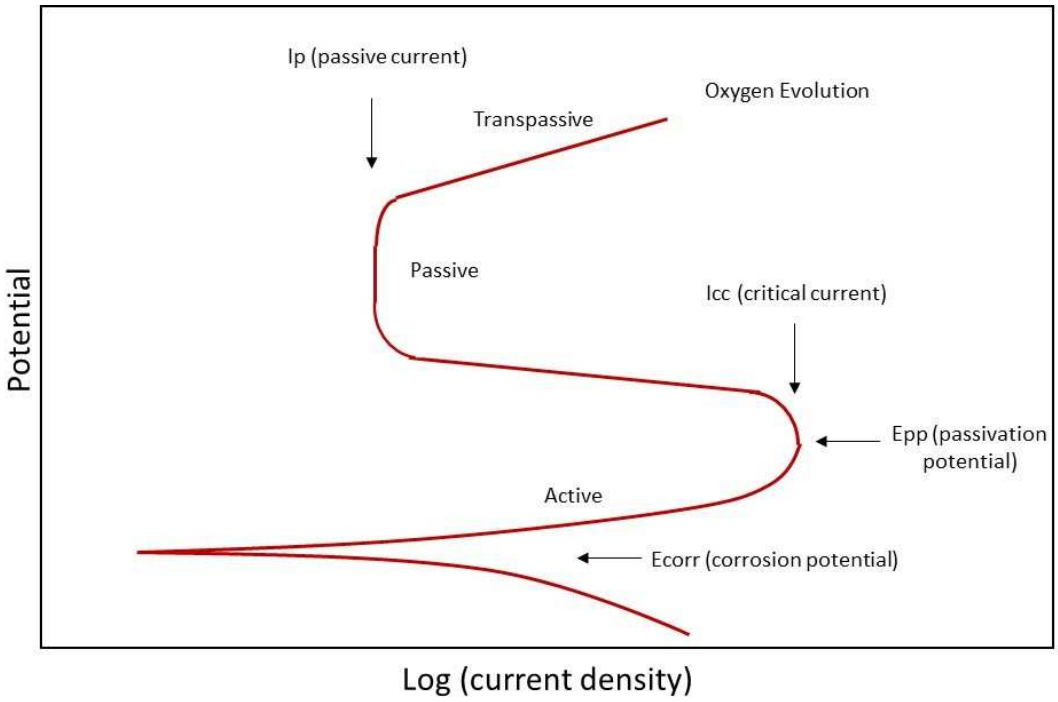

Figure 4.9. A simple, generic polarization graph presenting the most common activities observed for a metal/electrolyte system. Note there are no actual values on the axes. Diagram is redrawn from Reference 10.

In Figure 4.9, the OCP is delineated as "Ecorr;" the cathodic branch is below that point, and the anodic branch is above that point. Note the two branches immediately above and below Ecorr correspond to the two reactions on either side of $E_{M+/M}$ from Figure 4.7. The current observed on the cathodic branch at the very bottom is likely caused by oxygen or water reduction, as noted earlier, but this branch is also the branch at which metal ion reduction reactions may be observed. The "active" portion is where the oxidation of the metal occurs. At "Epp," a critical point may (or may not) be reached where the potential is at such favorable conditions as to so rapidly oxidize the metal that mass transport of metal ions away from the

surface begin to impede the transport of oxidizing agents to the surface and the current is decreased. Eventually a point is reached where the formation of metal oxides is rapid enough to precipitate on the surface and begin to impede the flow of current so the current density declines to the "passive" region. At the point "ip" the potential is pushed to such a high level as to begin to break down the oxide layer and corrosion processes rapidly increase in the "transpassive" region, as indicated by the rapid increase in current density; it may also be so high as to oxidize the water and generate gaseous oxygen.

4.3. Pourbaix diagrams

For this thesis, Pourbaix diagrams were used in conjunction with polarization measurements as a means to help predict the existence of possible ionic species present in a system. Pourbaix diagrams predict the stability of various solid and ionic species of metals in various aqueous conditions based on thermodynamics [5]. Pourbaix diagrams are also termed "potential-pH diagrams" because those are conditions that can be altered in the aqueous environment. Most importantly, these diagrams are mathematical constructs; just because a species may be stable based on these calculations of thermodynamics does not mean a system has the kinetics necessary to see a species form. A line in the diagram represents a reaction between two species at a particular potential or pH. The equation used to generate these lines is the Nernst equation:

$$E = E^o - \frac{RT}{nF} \ln \frac{[C]^c [D]^d}{[A]^a [B]^b} \tag{4.4}$$

The potential, E, for a reaction is calculated from the standard potential, E^o, which is the reaction of interest at standard conditions of 25°C and 1M (1 mole/liter) concentrations versus the Standard Hydrogen Electrode (SHE). R is the universal gas constant, F is the Faraday constant, n is the number of moles of electrons transferred in the reaction, and T is the absolute

temperature. The terms A-D are, properly, the chemical activities of the species involved, which are based on their concentrations, but at low concentrations the activities tend to be 1 so these are often just replaced by the concentration values. The pH values factor into the equation in the concentration terms because the pH value is simply a concentration of hydroxide or hydronium ions involved in the reactions.

Sample Pourbaix diagrams for iron-water systems are displayed in Figure 4.10. Note the difference in appearance between Figure 4.10a and 4.10b, notably the regions representing $Fe(OH)_2$ and Fe_3O_4, respectively. These differences arise because different species are considered in each diagram. It is not observed in Figure 4.10 but later examples will also consider changes due to temperature, important for the work in this thesis; the diagrams in the figure consider 25ºC for the temperature. Changes in the temperature will obviously affect the T term in equation (1.4) above but can also affect the solubility of the various species under consideration, thus, affecting the A-D terms of the equation as well.

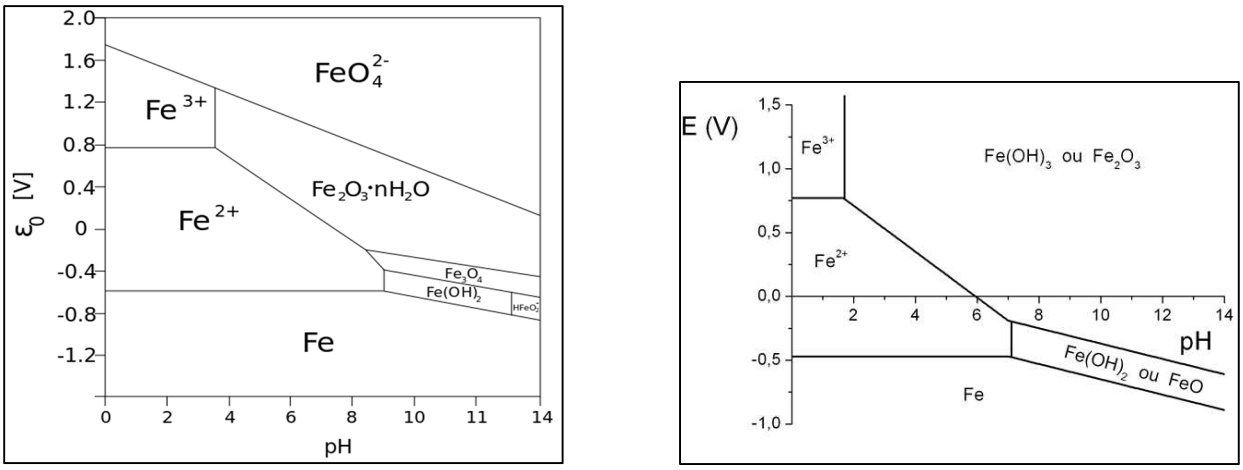

a) b)

Figure 4.10. Pourbaix diagrams for the Iron-Water system considering different species. Figures reprinted from reference [11], with permission from Creative Commons.

4.4. References

[1] D. Loveday, P. Peterson, B. Rodgers, JCT Coatings Tech, 1 (2004) 46-52.

[2] D. Loveday, P. Peterson, B. Rodgers, JCT Coatings Tech, 1 (2004) 88-93.

[3] D. Loveday, P. Peterson, B. Rodgers, JCT Coatings Tech, 2 (2005) 22-27.

[4] M.E. Orazem, B. Tribollet, Electrochemical Impedance Spectroscopy, John Wiley & Sons, 2008.

[5] D.A. Jones, Principles and Prevention of Corrosion, Prentice-Hall, Inc. 2005.

[6] S. Krause, "Impedance Methods," in Encyclopedia of Electrochemistry, Chapter 2.6, Vol. 3, A.J. Bard and M. Stratmann, eds., Wiley-VCH GmbH & Co. KGaA, 2003.

[7] F.J.J. Kellner, K. Schütze, C. Kreutz, S. Virtanen, Surface and Interface Analysis, 41 (2009) 911-917.

[8] C. Wagner, W. Traud, Corrosion, 62 (2006) 843-855.

[9] G.S. Frankel, D. Landolt, "Kinetics of Electrolytic Corrosion Reactions," in Encyclopedia of Electrochemistry, Chapter 1.3, Vol. 4, A.J. Bard and M. Stratmann, eds., Wiley-VCH GmbH & Co. KGaA, 2003.

[10] National Association of Corrosion Engineers, NACE International, http://events.nace.org/library/corrosion/AnodProtect/passivecurve.asp., accessed 2014.

[11] Figures 1.10a and 1.10b reprinted from http://commons.wikimedia.org/wiki/File:Pourbaix_Diagram_of_Iron.svg, with permission from Creative Commons, accessed 2014.

CHAPTER 5. ELECTROCHEMICAL IMPEDANCE SPECTROSCOPY STUDY OF THE INCORPORATION OF PHENYLENEDIAMINE OLIGOMERS IN EPOXY-AMINE COATINGS

5.1. Introduction

This chapter presents the results of EIS studies performed on epoxy-amine coatings on aluminum substrates in which phenylenediamine oligomers were incorporated. As discussed previously, this study was undertaken to further examine the unusual EIS behavior observed for organic-inorganic sol-gel coatings in which epoxy functionalized silanes were cross-linked with various amine compounds. The study attempted to determine whether the behavior is related to the aluminum oxide layer on the substrate, the sol-gel structure, or to the phenylenediamine in the coatings by removing the sol-gel structure from the coating.

5.2. Experimental methods

5.2.1. Materials and reagents

Aluminum alloy AA6061 substrates, 3" x 6", were obtained from Q-Lab. 0.2 μm PTFE filter disks were from VWR and 0.47 μm Supor-800 filter membranes from Pall-Gellman. Bisphenol A-based Epon 830 epoxy resin was kindly supplied by Momentive. Tris(4-hydroxyphenyl)methane triglycidyl ether (THMTE), tris(2-aminoethyl)amine (TAEA), m-xylylenediamine (XD), and ferrous sulfate were from Sigma-Aldrich. Sodium hydroxide, o-phenylenediamine, m-phenylenediamine, p-phenylenediamine, copper (II) acetate, cerium (III) nitrate, chromium (III) nitrate, and molybdenum (III) chloride were from Alfa Aesar. Cobalt (II) chloride was from Mallinckrodt, manganese (II) sulfate was from MP Biomedicals, hydrogen peroxide was from JT Baker, and acetone was from BDH. All chemicals were used as received. The structures of the monomers are displayed in Figure 5.1.

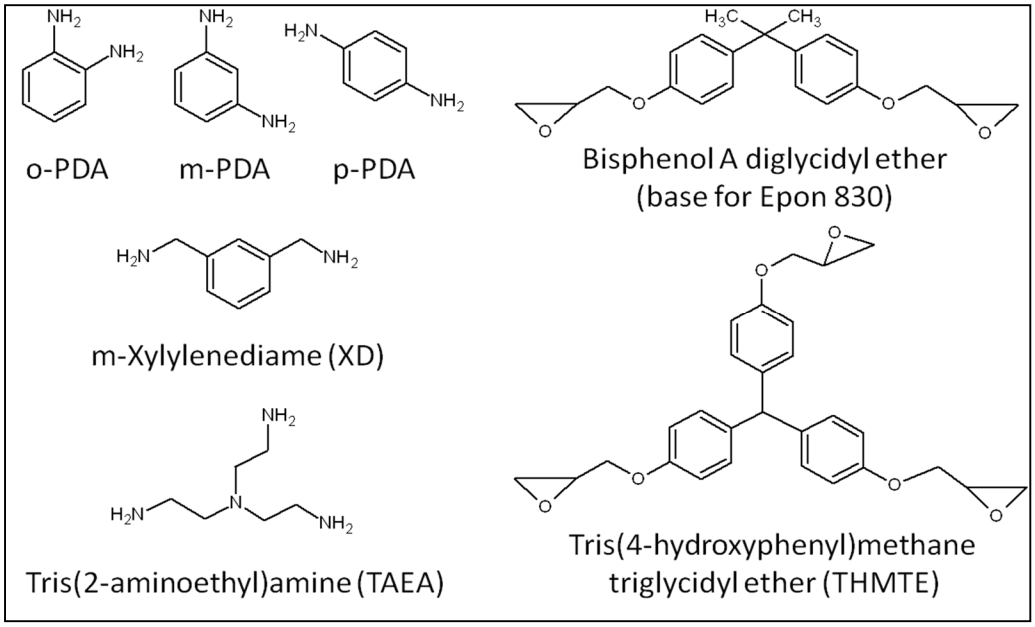

Figure 5.1. Structures of monomers used in the study.

5.2.2. Sample preparation

5.2.2.1. Substrate preparation

AA6061 substrates were cut to 2" x 3" in size. The panels were degreased in methanol for 2 minutes under sonication and rinsed with distilled water, then treated in a solution of ferric sulfate, nitric acid, and sodium bifluoride under nitrogen saturation for 10 minutes, rinsed with 18 MΩ Millipore water, and dried in a stream of air.

5.2.2.2. Oligomer synthesis

10 grams of PDA monomer in ca. 150 mL 18 MΩ water (Millipore) was heated to 50°C to dissolve the monomer and maintained at that temperature. Catalytic amounts of various metal salts (10mg) were dissolved in 3-4 mL of water and added to the PDA solution. 3 mL of 30% hydrogen peroxide (H_2O_2) was diluted to ca. 50 mL in Millipore water. H_2O_2 solution was added to the PDA solution using two methods: 1) in approximately 2mL increments over several hours to attempt to reduce the amount of over-oxidized, insoluble product; or 2) all immediately added to the PDA solution which was then stirred only one-half hour. The solution was cooled to room

temperature, approximately 1.0 mL of 1.0M NaOH solution was added to slightly alkalize the solution to reduce the solubility of the oligomers and increase yield, and then cooled to approximately 2°C in a NaCl/ice bath to crystallize the oligomers. The slurry was suction filtered through 0.47 μm filter membranes, rinsed with ice water, and the crystals air dried. Table 5.1 displays the metal salts used, whether H_2O_2 was added quickly or slowly, and the percentages of the formed oligomer sizes, as determined by ESI-TOF mass spectrometry. No monomer size molecules were detected indicating unreacted monomer rinsed away during filtration.

Table 5.1.
Percent of oligomers of various sizes generated by each metal catalyst. Q = H_2O_2 added all at once; S = H_2O_2 added in increments over several hours.

	CrQ	MoS	CoQ	FeQ	FeS	CeQ	MnQ	CuQ	CuS
Dimer	19.17	19.07	15.44	42.98	27.98	14.74	18.64	12.03	10.05
Trimer	16.25	62.81	15.90	26.46	12.18	22.24	24.89	20.49	49.16
Tetramer	44.36	16.74	58.47	13.01	34.03	48.61	56.47	47.89	35.10
Pentamer	20.23	1.38	10.18	17.55	25.80	14.40	0.00	19.59	5.70

5.2.2.3. Coating synthesis and application

MALDI-TOF mass spectrometry measurements of o-PDA oligomers by Sun et al. revealed structures consistent with oligomers containing 6 phenyl rings [1]. Their product was formed using $AgNO_3$ as the oxidant; the oxidant and solution conditions can alter the structure of the crystals obtained indicating the oligomer/polymer molecular weights may differ and affect the crystal structures obtained. However, their crystals easily dissolved in THF, indicative of oligomeric-sized molecules, which yielded a molecular ion peak at 638. In the current work, catalytic metal salts were the oxidant, in turn re-oxidized by the hydrogen peroxide. The crystals formed for the current work also easily dissolved in THF (and acetone), thus initially were assumed to be of approximately the same molecular weight. This value was then used for

formulating, along with assuming 3 reactive amines per oligomer, such that the levels of additional amine cross-linking agents could be adjusted accordingly. However, later work with ESI-TOF mass spectrometry revealed different masses for the current oligomers (see Table 5.1).

For preliminary samples, the oligomers used were from iron catalyst with slow addition of H_2O_2. Either 0.25g or 0.50g of oligomer was dissolved in 10 mL of acetone with sonication; this mixture was filtered through 0.2 μm filter disks to remove insoluble polymer, which comprised approximately 2-3% of the total mass. When PDA monomers were used, either 0.125g or 0.25g quantities were used due to the greater amount of available amine per mass versus the oligomers; the amounts of additional amine cross-linking agents were also adjusted when monomeric PDA was used to attempt to maintain constant amine content. The monomers were also dissolved in acetone and filtered to remove any air oxidized polymer. For comparison, coatings with neither PDA monomer nor oligomer were also synthesized, with commensurate increase in the second amine cross-linker. Table 5.2 displays the various coating components utilized; in the text, coatings synthesized with oligomer are designated with "o," those with monomer, "m." The additional amine was added to the PDA/acetone mixture and well agitated, then the epoxy was added and mixed with sonication. The coatings were allowed to sweat-in for 10-15 minutes and applied to the prepared aluminum substrates by spin-coating yielding cured coating thickness ca. 4-6μm with most of the variation due to substrate roughness (measured by SEM imaging). Coatings were cured at 25°C over saturated potassium acetate solution (relative humidity 23%) for 24 hours followed by saturated sodium chloride (relative humidity 75%) for another 24 hours.

For later samples, ESI-TOF mass spectrometry had revealed a range of molecular sizes depending on the metal catalyst used and whether H_2O_2 was added quickly or slowly (see Table

5.1). The sizes of the oligomers were determined to be lower than the hexamer size initially assumed, ranging from dimer to pentamer; the initial use of the hexamer size as the molecular weight of the oligomers led to underestimation of the available reactive amine content from the oligomers and an approximate epoxy:amine ratio of 1:1.35, a somewhat high ratio. This underestimation led to re-calculation of the formulas for later coatings to bring the epoxy-amine ratio down slightly, to approximately 1:1.25.

Table 5.2.
Amounts of monomers used for each preliminary coating.

COATING	0.50g Oligomer	0.25g Oligomer	0.25g Monomer	0.125g Monomer	No PDA
TX = THMTE + XD	0.74g XD	0.83g XD	0.48g XD	0.62g XD	0.87g XD
EX = Epon 830 + XD	0.74g XD	0.83g XD	0.48g XD	0.62g XD	0.87g XD
ET = Epon 830 + TAEA	0.53g TAEA	0.60g TAEA	0.35g TAEA	0.45g TAEA	0.63g TAEA
3.60g Epon 830 or 2.84g THMTE used in each sample					

5.2.3. Characterization

5.2.3.1. Oligomer characterization

PDA oligomer molecular weights were determined with a Bruker Daltronics BioTOF HRMS system with electrospray ionization (ESI-TOF-MS). Methanol with sodium trifluoroacetate was the solvent with positive ion source, although most often hydrogen ion from methanol appeared to provide the positive charge to the oligomer molecules for detection.

5.2.3.2. Infrared spectroscopy

Oligomers, monomers, and cured coatings were characterized by infrared spectroscopy utilizing a Nicolet 8700 FT-IR (Thermo Scientific). Coatings were cast on release film, cured, and ground in a cryo-mill to obtain a powder.

5.2.3.3. Scanning electron microscopy (SEM)

To determine coating thickness and examine for the presence of any microstructure, cross-sections of cured samples were studied with a JEOL JSM6490LV (JEOL USA Inc.) scanning electron microscope in secondary electron imaging mode operated at 15kV. No microstructure could be observed. Coating thicknesses were ca. 5μm.

5.2.4. Coating performance - electrochemical impedance spectroscopy (EIS)

Triplicate samples of each coating were immersed under dilute Harrison's solution (DHS) (0.35% ammonium sulfate and 0.05% sodium chloride in water). Further samples were later immersed under concentrations of ammonium sulfate-only (0.35% and 0.60%) and sodium chloride-only (0.10% and 0.265%). The choice of 0.265% NaCl was to keep the total ion concentration consistent with that of 0.35% ammonium sulfate for this latter study. For electrochemical cells, one-inch diameter PVC pipes (5.0 cm^2 area) were adhered to the samples using Marine Goop® adhesive. EIS was measured with Reference 600 potentiostats (Gamry Instruments) with platinum mesh counter electrodes and saturated calomel reference electrodes. A perturbating voltage of 5mV (rms) was applied to the samples over a frequency range of 100,000 Hz to 0.01 Hz. EIS data were circuit modeled using ZView modeling software from Scribner Associates, Inc.

5.3. Results and discussion

5.3.1. Oligomer synthesis

The synthesis and characterization of PDA oligomers was not the focus of this research. However, the author is unaware of any reports recording attempts to synthesize the oligomers in the manner described and several differences were observed while working with the resulting oligomers. Thus, some notes and discussion are included so other researchers might investigate

whether the method is useful for their needs. Other researchers have determined the o-PDA oligomers crystallize at reduced temperature under slightly basic conditions through pi-pi interactions, stacking into wire and rod shapes which are under study as conductive one-dimensional microstructures similar to carbon nanotubes with potential applications such as sensors and catalysts [1-6]. The structures obtained could be altered depending on oxidant and solution conditions. Metal salts have been used as oxidants such as silver [1], iron [2-3], and copper [4] but not in catalytic amounts with re-oxidation to continue the reaction as used in the present work. Hydrogen peroxide has been used in combination with horseradish peroxidase to oxidize PDA [7] but did not appear to oxidize PDA by itself in this study. Persulfate salts are also commonly used [6, 8-9]. Oligomers of o-PDA were easily synthesized and recovered from solution with all the metals listed in Table 5.1, some of which were chosen for further use in this study. Oligomers were synthesized from p-PDA using iron as the catalyst, although iron did not work well with m-PDA; none of the other metals were studied with the latter two PDA isomers so it is not known if the other metals might also polymerize those two isomers. It will be noted the oligomers of p-PDA synthesized with iron catalyst were examined in coatings and displayed the same EIS behavior, to be discussed, as those from o-PDA.

For the present purposes, the method of using catalytic amounts of metal salts with re-oxidation by hydrogen peroxide was chosen so, ideally, little or no residual oxidizing ions such as Fe^{3+} would become incorporated into the coatings which might interact with the aluminum substrate. Also, more expensive metal salts, or more hazardous metals, could be used in catalytic quantities rather than in the large quantities which would be required to synthesize sufficient quantities of material to incorporate into coatings. The range of oligomer size obtained by the various metals as determined by ESI-TOF-MS is displayed in Table 5.1. The values in

Table 5.1 were generated by the raw counts of molecular weights as a percentage of the total; peaks smaller than approximately 5% of the largest peak were not included, only the more significant peaks were counted to obtain a reasonable ratio of oligomer sizes. Notably, very little or no oligomer of hexamer size or larger was detected. A range of peaks about each expected molecular weight was detected, suggesting a range of PDA oxidation equal to minimally oxidized oligomers (single bonds between nitrogen atoms and rings, "PANI-ES" type segments) to more completely oxidized oligomers (double bonds between nitrogen atoms and rings, "phenazine" type segments) [8-9]. For example, a minimally oxidized trimer would give approximate M.W. 320 while a fully oxidized trimer would give approximate M.W. 312; the two structures are presented in Figure 5.2. Additionally, large peaks of lower molecular weights than would be expected were detected which suggest the loss of $-NH_2$ groups and HCN groups during the ionization step as observed by Losito, et al. [10]. Contributions from these peaks are included in the totals and fractions for each molecular weight for each sample, for this range of molecular weights is simply a phenomenon of the ESI-TOF-MS method. Samples of the EIS-TOF-MS graphs obtained are displayed in Figure 5.3 for comparison.

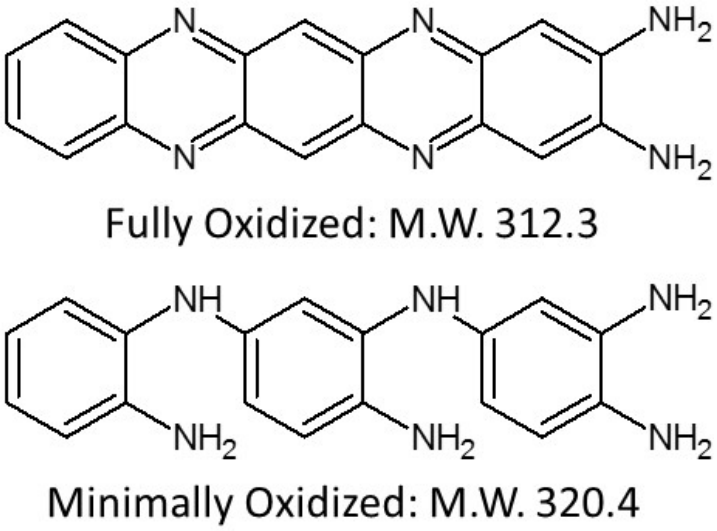

Figure 5.2. Comparison of fully oxidized versus minimally oxidized o-PDA trimer.

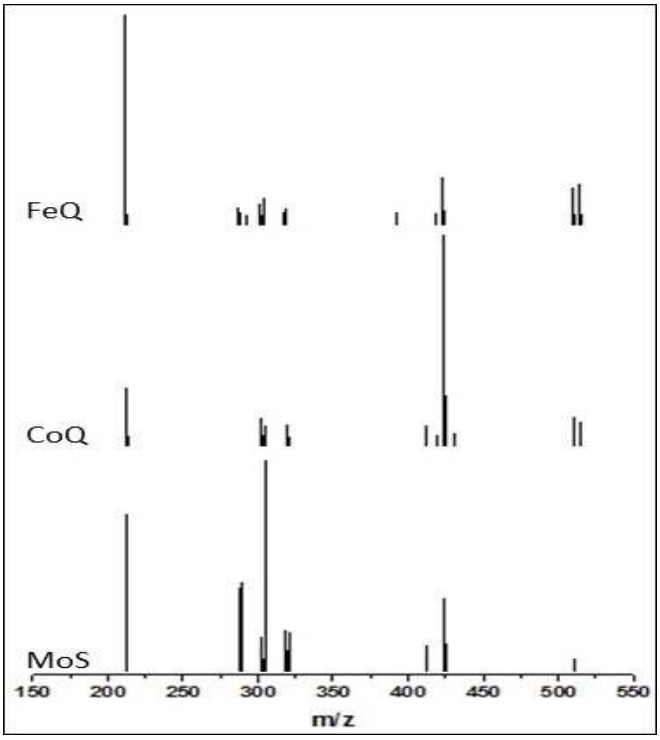

Figure 5.3. Selected spectra of ESI-TOF-MS results. Results indicate higher dimer production with Fe, higher tetramer production with Co, and higher trimer production with Mo.

5.3.2. Preliminary coatings

Several studies have incorporated various amine cross-linking agents synthesized from PDA and aniline precursors [11-13]. And Fu, et al. studied thermal properties and kinetics of epoxy resins cured with p-PDA in THF demonstrating the feasibility of using PDA as sole cross-linking agent [14]. In the present case, initial attempts were made to synthesize epoxy coatings with EPON 830 in various solvents with only PDA monomers and oligomers as the amine cross-linking agents, however, the coatings did not form well. Coatings made with monomer phase separated at room temperature; upon heating (~50^{o}C) coatings formed but were quite brittle. Coatings made with oligomers-only fared worse; large amounts of oligomers were needed to provide sufficient amine reactivity, these coatings also phase separated at room temperature, and upon heating resulted in soft, insufficiently cross-linked coatings. Therefore, other amine cross-linking agents were chosen as the primary cross-linking agent with lower amounts of PDA

monomers and oligomers added, approximately 20% of amine content. The second epoxy, THMTE, was chosen for comparison because 1) it added additional phenyl rings to impart additional aromatic character to the overall coating structure, thus enhancing the possibility for inter-chain electron hopping between conductive fragments of PDA and 2) the tri-functionality would serve to increase cross-link density. The tertiary structured TAEA was also chosen to increase cross-link density but the aliphatic nature of the molecule would reduce the overall aromatic character of the coating. Xylylenediamine provides lower cross-link density but also increases overall aromatic character of the coating.

Representative infrared spectra of monomers and cured coating oEX are displayed in Figure 5.4. Due to air oxidation of the monomer, the spectra of o-PDA monomer and oligomer were very similar except the small aromatic secondary amine N-H bend at 1338cm^{-1} was somewhat stronger for the oligomer sample. The epoxide stretch at approximately 912cm^{-1} of the epoxy monomers disappeared in the cured coatings with the concomitant appearance of the broad OH stretch centered at approximately 3384cm^{-1} (in both ET and TX coatings also). The sharp double peak primary amine stretch visible at approximately 3387cm^{-1} and 3364cm^{-1} in the oligomeric and monomeric PDA was absent in the cured coating, for XD and TAEA it appears obscured by water but should be present. However, the broad N-H stretching of XD and TAEA from approximately 800 to 1000cm^{-1} was absent in the cured coating suggesting much of the primary amine of those two monomers reacted. A strong peak at 1272cm^{-1} indicative of primary aromatic amine C-N stretch from o-PDA monomer and oligomer was also absent in the cured coating. The strong N-H bend of primary amine was visible at 1609cm^{-1} (XD) and 1595cm^{-1} (TAEA). For ET coatings the peak was absent also indicating much of the primary amine

reacted; for EX and TX coatings, a peak present at 1609cm^{-1} in the epoxy and cured coatings obscured whether it was absent in the coating.

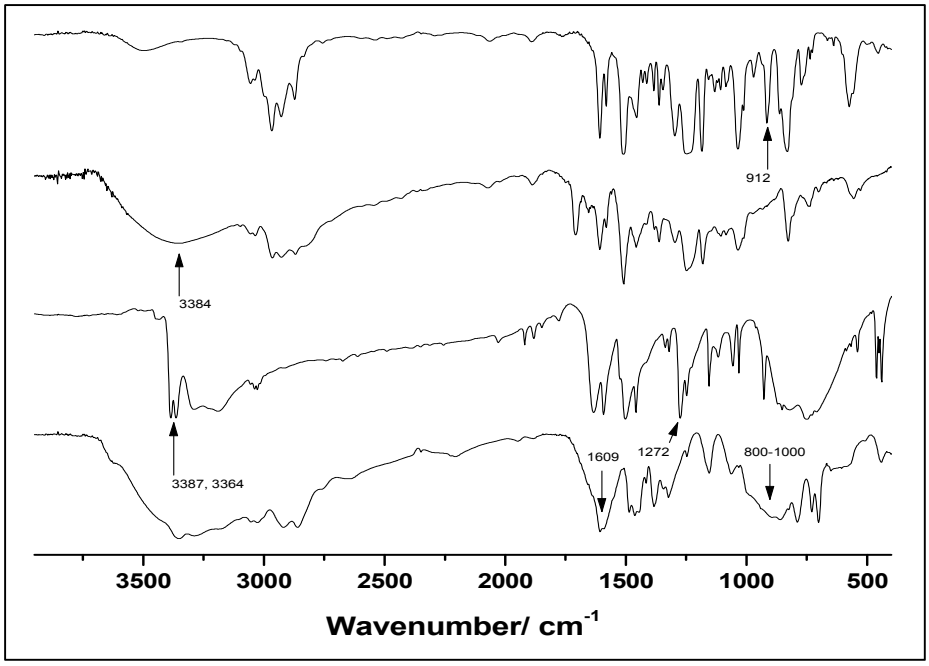

Figure 5.4. Select FTIR results, transmittance (a.u.). From top: Epon 830; cured coating EX; o-PDA oligomers; and xylylenediamine. A peak visible at 1706cm^{-1} in the cured coating was likely the carboxyl peak from residual acetone solvent; the strong double peak at approximately 3387/3364cm^{-1} was obscured by, most likely, water in the xylylenediamine. The arrows denote peaks mentioned in the text.

In the sol-gel coatings studied earlier, the PDA monomer could be expected to be concentrated in the interstitial space between the colloidal particles; this concentrating effect would enable the PDA to remain in sufficiently close proximity so as to be able to polymerize in oxidizing conditions. The PDA monomers in the present coatings, however, would be expected to be dispersed sufficiently such that it would be more difficult to polymerize any unreacted monomer as might be possible in the sol-gel coatings. Indeed, coatings cross-linked with PDA monomers displayed Randle's cell behavior, indicative of a lower porosity coating and quite different than the sol-gel coatings. Figure 5.5 presents the result for sample mTX (0.25g monomer) as an example; samples mEX and mET displayed similar results. When coatings

incorporating oligomeric PDA isomers were measured, however, the behavior changed dramatically. Initially, the coating displayed Randle's cell behavior as expected for an epoxy coating, very capacitive at high frequencies and turning resistive at low frequency and becoming more resistive with time. It is interesting to note the coating became quite resistive at low frequencies, with a phase angle near -10°. However, after several days/weeks of constant immersion, the impedance declined sufficiently to reveal the resistive response initially observed at low frequencies changing to capacitive response. The results for coatings oTX and oET (0.50g PDA oligomers) are displayed in Figures 5.6 and 5.7. Coating TX, with higher total aromatic character, revealed the change by 17 days in both the Bode and phase angle graphs. Coating ET required 8-9 weeks to reveal the behavior but the latter coating should be more hydrophobic owing to the greater aliphatic character of the coating so this result is not unreasonable.

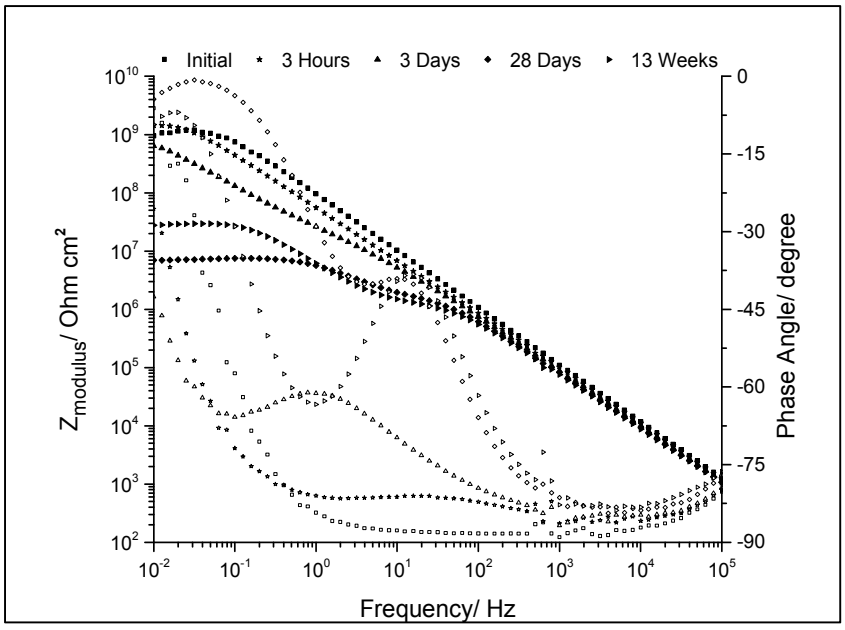

Figure 5.5. EIS results for sample TX made with monomeric o-PDA incorporated into the coating. A second time constant can be observed to form at approximate 10Hz after 28 days of exposure and the coating is very resistive at low frequency. Hollow symbols are phase points that match impedance symbol shapes.

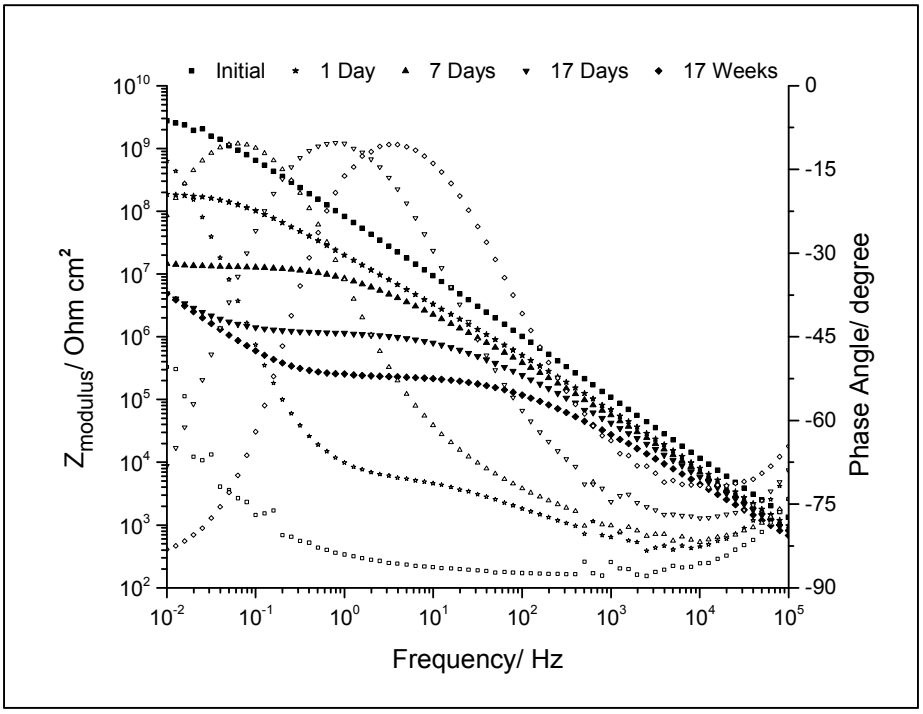

Figure 5.6. EIS results for sample TX made with oligomeric o-PDA incorporated into the coating. Even after 22 weeks of immersion (not displayed), the low frequency impedance was little changed from 17 days of immersion.

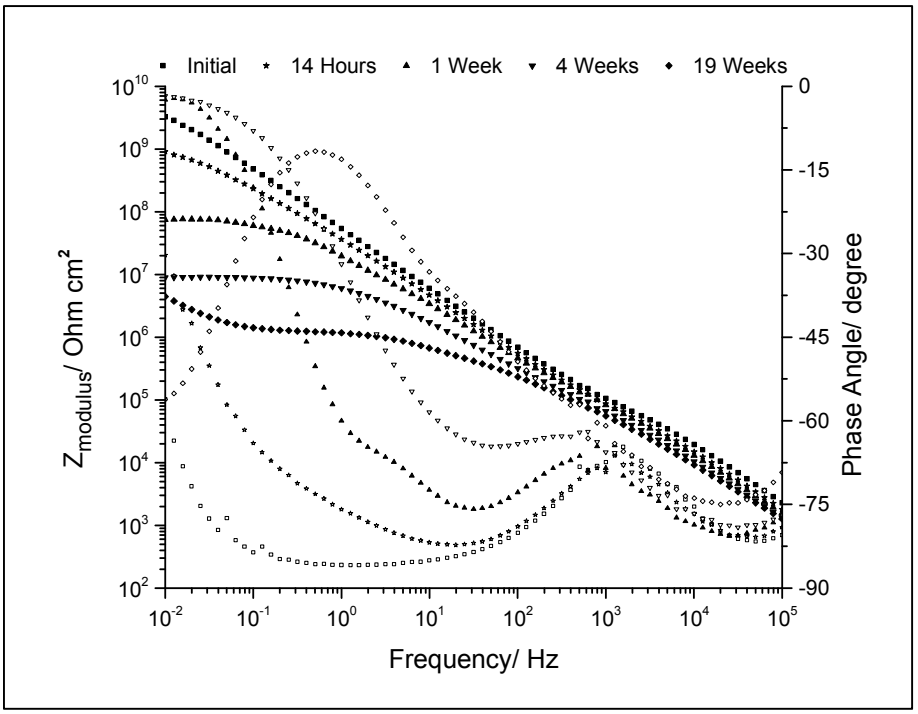

Figure 5.7. EIS results for sample ET made with oligomeric o-PDA incorporated into the coating.

Interestingly, the coating synthesized with XD and Epon 830 (EX) did not reveal the same behavior during EIS measurements, even though the coatings contained the same amount of o-PDA oligomers (0.50g); an example is displayed in Figure 5.8. In fact, the first few high frequency data points reveal resistive response, indicative of a thin coating with less than ideal barrier properties, as well as unstable measurements at low frequencies indicative of rapid electrolyte penetration. This response was likely related to the much lower cross-link density expected with these two monomers yielding a more linear structure. In a study by other authors, EIS measurements were performed on bisphenol A-based epoxy coatings cross-linked by poly (Ani-*co*-p-PDA) end-capped by amino groups on steel and compared to those cross-linked with triethylenetetramine [11]. Those results also revealed the typical Randle's cell-type behavior of a barrier coating, even with conductive polymeric sequences incorporated in the structure. Both THMTE epoxy and TAEA amine are branched monomers which would increase the cross-link density of the coatings formulated with those monomers in the current study. With three functional epoxides versus 6 functional amine groups per molecule, coating TX formulated with THMTE would require incorporating even more branched monomer than coating ET formulated with TAEA, to maintain the same epoxide:amine ratio. Additionally, the phase separation observed between EPON 830 and PDA monomer or PDA oligomers when only PDA or oligomers were examined as cross-linking agents may be occurring at a micro-scale that would leave unreacted functional groups, thus, localized porous regions.

The circuit models used to fit the data are displayed in Figure 5.9, the latter model the same as the model used to fit the data in the sol-gel study [15]. The Randle's cell contains the solution resistance, Rsoln, the coating capacitance, Ccoat, and the pore resistance, Rpore; it fits the data quite well during the early measurements. There was a transition region from 1 to 2 or 3

days exposure where a second time constant began to reveal itself in the Nyquist and phase angle graphs. The software could not fit the low frequency data without large errors with the Randles cell model but also could not yet incorporate the low frequency capacitance/constant phase element, Cunk; this term was chosen because several concepts will be presented which might explain the source of this capacitance. By 4 or 5 days usually, however, the model in Figure 5.9b which incorporates the second CPE became viable as the impedance fell low enough to reveal the presence of the low frequency capacitance. It should be noted Cunk could be placed in series to the pore resistance, thus in parallel to coating capacitance, and the modeling software would return nearly identical values for the circuit elements. As noted in the earlier sol-gel study, this behavior is indicative of a transmission line model [15-16].

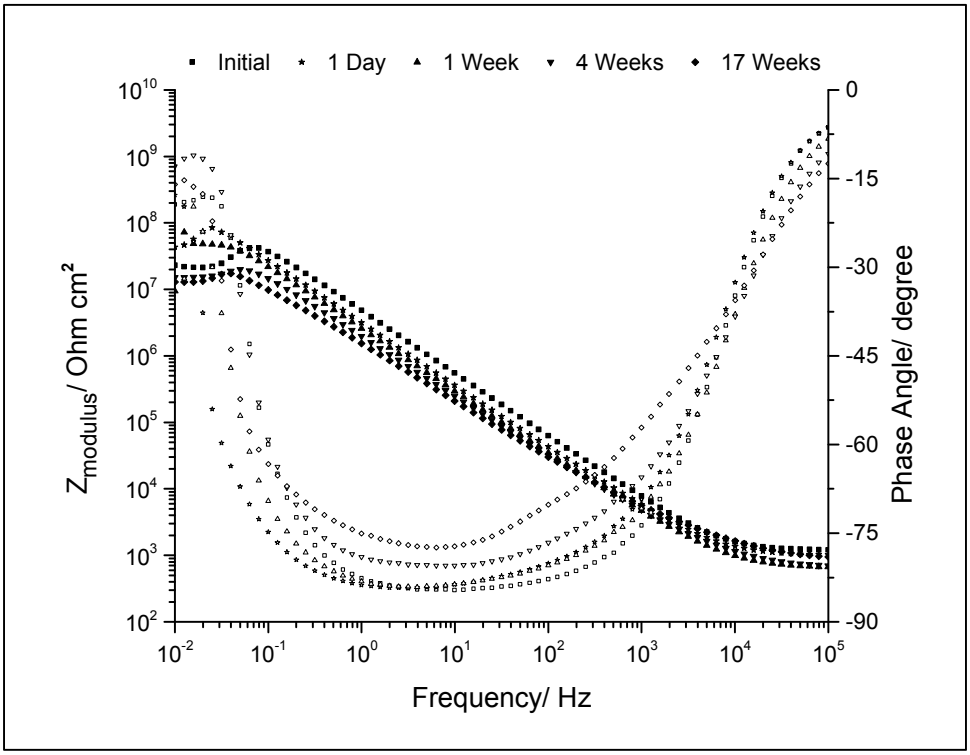

Figure 5.8. EIS results for sample EX made with oligomeric o-PDA incorporated into the coating.

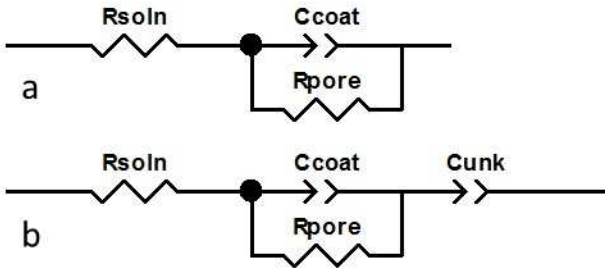

Figure 5.9. Circuit models used to fit the data. Cunk represents the low frequency capacitance.

The EIS results can now be compared to those of the sol-gel coatings discussed previously in Chapter 3. In the sol-gel coatings the electrolyte easily penetrates the porous layer to contact the thin, dense layer; both layers are thus immediately revealed in the data. For the present coatings, only the nature of the barrier properties of the epoxy-amine coating was initially revealed but as the electrolyte penetrated deeply enough with concurrent decrease of impedance, the low frequency capacitance was observed in the coatings containing PDA oligomers (TX and ET). As with the PDA cross-linked sol-gel, the resistance in the middle frequencies continued to decline as the electrolyte penetrated still further, while the low frequency impedance remained relatively unchanged; for coating TX for example, the low frequency impedance was still approximately $5x10^6$ ohm·cm^2 after 4 months of immersion, nearly the same as it was after 17 days. Whereas *in-situ* polymerization of the PDA cross-linking agents in the sol-gel study explained the decline of the resistive plateau, with the coating becoming more conductive over time, the polymerization of PDA was completed before addition to the present epoxy coating. Therefore, further polymerization in situ would not be expected and would not account for the reduction in resistance at the middle frequencies; the decline of the resistive plateau is explained simply by deeper penetration of the electrolyte over time resulting in decline of the coating pore resistance. As noted, the EIS behavior was not observed when monomeric PDA was included in the coatings; this result indicates the oxide layer is either not

responsible for the low frequency capacitance observed, or coatings containing monomeric PDA do not stabilize the oxide layer while coatings containing oligomeric PDA will somehow stabilize the layer. Thus, it appears the coating itself is somehow responsible for the observed behavior.

In addition to in-situ oligomerization of PDA in the sol-gel coatings yielding a less resistive coating over time, a further explanation was presented for these results in which the electrolyte was penetrating the coating to a particular depth, but not completely, and the low frequency capacitance was due to as-yet unpenetrated, pristine coating; once the electrolyte penetrated to sufficient depth, the capacitance of the pristine layer was revealed [15]. A model of this scenario is presented in Figure 5.10. Amand, et al. [17] presented a somewhat different model for some non-sol-gel coatings in which, rather than proceeding along an even front and leaving a layer of pristine coating, the electrolyte penetrated some pores to greater depths and others to lesser depths; the low frequency capacitance was attributed to the aluminum oxide layer contacted by electrolyte in the first few pores to reach the substrate, with continuing decline of the pore resistance as electrolyte reached the substrate through an ever greater number of pores. Applied to the current coatings, however, that model would require the coating to stabilize the aluminum oxide layer over several weeks/months of immersion, as observed for oTX and oET. Even with an oxide layer present, the alloying elements render the aluminum alloy susceptible to pitting corrosion in the presence of electrolyte [18]. It would seem as more electrolyte contacts the oxide layer through more pores, some amount of pitting would occur and yield change in the signal (double-layer capacitance/charge transfer resistance) but that was not observed. Additionally, those authors noted their model did not fit the data observed in sol-gel coatings using less aggressive electrolyte than 0.5% NaCl [17].

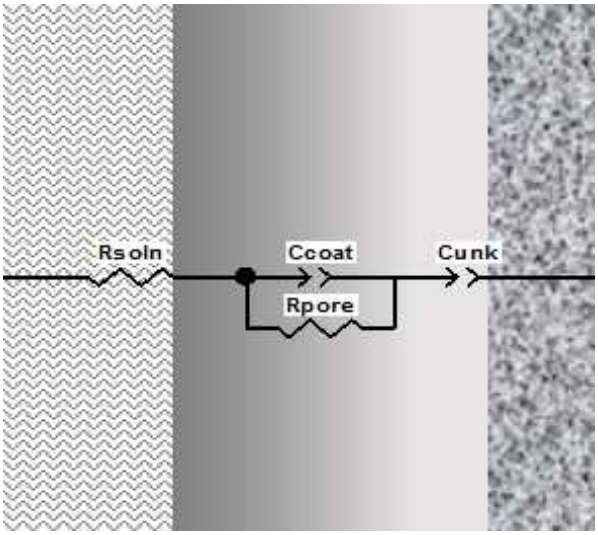

Figure 5.10. Circuit model from Figure 5.9b, where Cunk represents a layer of pristine coating.

5.3.3. Coatings with different concentrations of o-PDA oligomers

Neither of the preceding models adequately explains the behavior observed when PDA is included in the present coatings. Coating mTX formulated with PDA monomer (Figure 5.5) revealed the electrolyte contacted the aluminum oxide layer so there would not appear to be an evenly distributed solvent front leaving a pristine layer for that coating, as suggested in [15]. Neither does it appear the solvent penetrated just a few pores to make contact with the aluminum oxide layer while the PDA monomer in the coating stabilized the layer, as suggested by [17]; had the coating stabilized the oxide layer, the low frequency capacitance should have been observed for at least a few of the measurements. This result suggests the aluminum oxide layer alone was not responsible for the observed behavior.

The only difference, then, is the presence of the PDA oligomers. It should be noted that the PDA monomer does not have high solubility in water; one reason for maintaining the oligomer reaction temperature at 50^{o}C was to completely dissolve the 10g of PDA monomer. If the temperature fell below that level, the monomer would rapidly begin to precipitate. The oligomers were even less soluble; during other unpublished experiments, the oligomers would

not re-dissolve in water alone. They could be dissolved in a few mL of solvent such as ethanol and added to water but upon standing would generally agglomerate with only a small fraction remaining dissolved as attested to by the color of the solution. Therefore, the addition of the oligomers to the coatings may simply have the effect of making the coatings more hygroscopic, although this still does not explain the different results obtained for coating EX.

An additional explanation would be if the coatings with oligomers is acting as osmotic membranes, removing the salts from the water as the electrolyte penetrates the coating; a thin layer of pure water at the interface could be expected to produce a capacitive response separate from the coating capacitance and resistance, as was observed. Indeed, sorbents based on copolymers of PDA and its sulfonate were found to adsorb heavy metal ions [19] while nanoparticles of polymerized m-PDA were found to adsorb silver ions [20]. Therefore, these coatings may be capable of adsorbing, especially, the ammonium and sulfate ions which are the main constituents of the dilute Harrison's solution used as the electrolyte for the current and previous studies [15, 21].

Closer examination of coating oTX formulated with two levels of oligomers may bolster these explanations. An example of oTX formulated with 0.50g oligomers was presented in Figure 5.6; an example of oTX formulated with 0.25g oligomers is presented in Figure 5.11; the same time points were included in the graphs for comparison. The low frequency capacitance was well defined by 7 days for the coating with 0.25g oligomers in Figure 5.11 (and actually was observed by 3 days immersion) whereas it was just beginning to present itself at 7 days when the higher level of oligomers was incorporated and required several more days to become well defined. For the higher level of oligomers, the impedance at the point where the phase angle was most resistive, i.e. nearest 0, in the resistive region at 17 days was 1.15×10^6 ohm·cm^2; for the

lower level of oligomers, the impedance was 1.21×10^5 ohm·cm^2, a nearly full order of magnitude difference for the same amount of immersion time. With lower oligomer content to remove the salt, the salt front would advance closer to the water front which would leave the coating saturated with salt to a greater depth, thus the coating would be less resistive than the coating with higher oligomer content. The additional oligomers in the higher oligomer coating may also simply render that coating more hydrophobic, impeding the penetration of the solution.

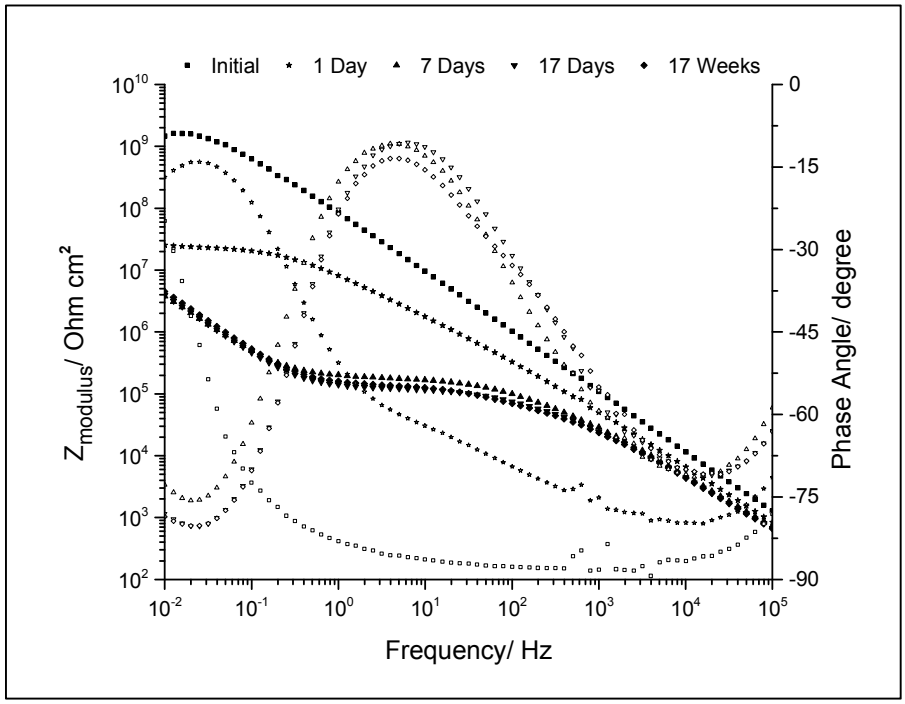

Figure 5.11. EIS results for sample TX made with oligomeric o-PDA incorporated into the coating.

The diffusion of water/water uptake of the coating can be determined by analysis of the coating capacitance at higher frequency [22-24]. It is observed in Figures 5.6, 5.7, and 5.11 the impedance at high frequencies declined over time. This behavior was not observed in the earlier study with sol-gel coatings (refer to Figure 3.6); the high frequency capacitance generally remained stable from the first measurement to the last for those coatings. The following

expression has been derived to calculate the diffusion coefficient of water from capacitance measurements [24]:

$$\frac{\ln(C_t/C_o)}{\ln(C_s/C_o)} = \sqrt{\frac{4Dt}{L^2\pi}} \quad (5.1)$$

where Ct is the coating capacitance at time t, Cs is the coating capacitance at saturation, Co is the initial coating capacitance, D is the diffusion coefficient, and L is the coating thickness (assumed to be 5μm for this study from SEM results). The capacitance at each time, t, was of greater value for the coatings with lower oligomer content, with very similar C_o and C_s values, yielding a larger diffusion coefficient, thus, the water uptake appeared to be faster in the coating with lower oligomer content.

5.3.4. Significance of salt species and concentration

DHS is comprised of two salts, NaCl and $(NH_4)_2SO_4$, which could penetrate the coating at different rates, especially if the coating is acting as an osmotic membrane. To this end, a set of samples was produced from one formulation of TX, with samples immersed in two concentrations of NaCl and two concentrations of $(NH_4)_2SO_4$. As noted earlier, one concentration of NaCl (0.265%) was chosen so the number of ions was the same as for the level of $(NH_4)_2SO_4$ found in DHS (0.35%). When immersed in 0.265% NaCl, the samples rapidly failed and never achieved steady state even during the initial measurement. A second set of samples was then immersed in 0.1% NaCl. This lower concentration was chosen to determine if the coating could act as an osmotic membrane for a reduced level of NaCl nearer to that found in DHS but without the presence of $(NH_4)_2SO_4$. These samples also rapidly failed with no detectable differences from those of the higher concentration. For the samples immersed in $(NH_4)_2SO_4$-only, the response was less capacitive at higher frequencies than previous samples (as attested by the phase angle); also, the water uptake was detected in the EIS results with this

salt, with noticeable change in the first 24 hours. This suggests the TX coating was somehow different than earlier coatings, perhaps due to aging of the xylylenediamine cross-linker, such that the curing characteristics had changed. The coatings appeared to fail before the EIS behavior was observed; points of corrosion were detected within the cells.

While these results unsuccessfully displayed the EIS behavior of interest, they do suggest $(NH_4)_2SO_4$ may have a pore-blocking effect in coating TX (and ET) such that water uptake is retarded (and measureable) whereas NaCl is able to rapidly penetrate the pores. The measured radii of the various ions in aqueous solution are displayed in Table 5.3 [25]. In DHS solution, once adsorbed, the large ammonium and sulfate ions may be sufficiently large to block pores, disallowing sodium and chloride ions to pass, and the samples did not simply fail as they did when sodium chloride-only was the electrolyte. Thus, in the samples utilizing DHS, the water molecules might pass, albeit more slowly, similar to a clogged screen, but eventually a layer of pure water develops a front ahead of the salt ions. This model may explain why coating oEX, with an expected lower cross-link density, did not display the same EIS results even though the level of oligomers was the same as oTX and oET; the larger pores were sufficiently large such that the sodium and chloride ions could still pass around adsorbed ammonium and sulfate ions.

Table 5.3.
Ionic radii in aqueous solution for the salt ions used in this study.

Ion	Na^+	Cl^-	NH_4^+	SO_4^-
Radius (aqueous, in nm)	0.097	0.180	0.260	0.242

5.3.5. Coatings with oligomers of different length

The oligomers synthesized by the metals presented in Figure 5.3 were utilized to make comparable coatings to examine the effect of different lengths of the oligomers. While not monodisperse, the oligomers synthesized with iron and H_2O_2 added quickly were predominantly dimers; those from molybdenum and H_2O_2 added slowly were predominantly trimers; and those

from cobalt and H_2O_2 added quickly were predominantly tetramers. Interestingly, the coating mixture using predominantly trimers was noticeably more viscous after the sweat-in period; the mixture did not form usable coatings, which were full of large fish-eye structures and, thus, could not be measured with EIS. Examination of the ESI-TOF-MS results in Figure 5.3 may provide an explanation: it can be observed a sizable portion of the trimers were detected at m/z 287 and 288 for those synthesized with molybdenum and H_2O_2 added slowly. These values would suggest a much larger number of unreacted primary amine groups remained in these oligomers indicating lower oxidation is obtained with molybdenum (as discussed in Section 5.2.1.). These extra primary amine groups then reacted at a sufficiently faster pace so as to increase the viscosity of the coatings, even though the sweat-in time was the same as the other two coatings. This increased viscosity would also suggest the PDA oligomers may react to the epoxide groups at a faster pace than the other amine cross-linking agents depending on the level of primary and secondary amine available in each oligomeric unit.

Figure 5.12 compares the triplicate samples of predominantly dimer and predominantly tetramer after 10 days of immersion. It is observed the coating resistance was lower for tetramer than for dimer for all samples, even though the mass of PDA oligomer was the same for each. This difference was observed from when the graphs first displayed the low frequency capacitance. While fewer in number, longer fragments of conductive polymer in the coatings would have a better chance of interacting with each other for electron movement, thus yielding an overall less resistive coating. The longer fragments might also disrupt the cross-link density to a larger extent, depending on the amount of reaction between the PDA amine groups and epoxides, as just noted, thus yielding a somewhat more porous coating. Conversely, for the dimer, a larger number of oligomer units, from the same mass used, would be dispersed

throughout the coating and may simply serve to increase the hydrophobicity of the coating and slow water ingress. The larger capacitance values for the coating with tetramer yielded a larger water diffusion coefficient, similar to the result obtained when two different amounts of identical oligomers were used. Because the PDA oligomers are only about 20% of the total amine content, it is not clear whether this result indicates lower pore resistance with tetramers was due to different rates of water uptake or the longer conductive fragments rendered the coating less resistive.

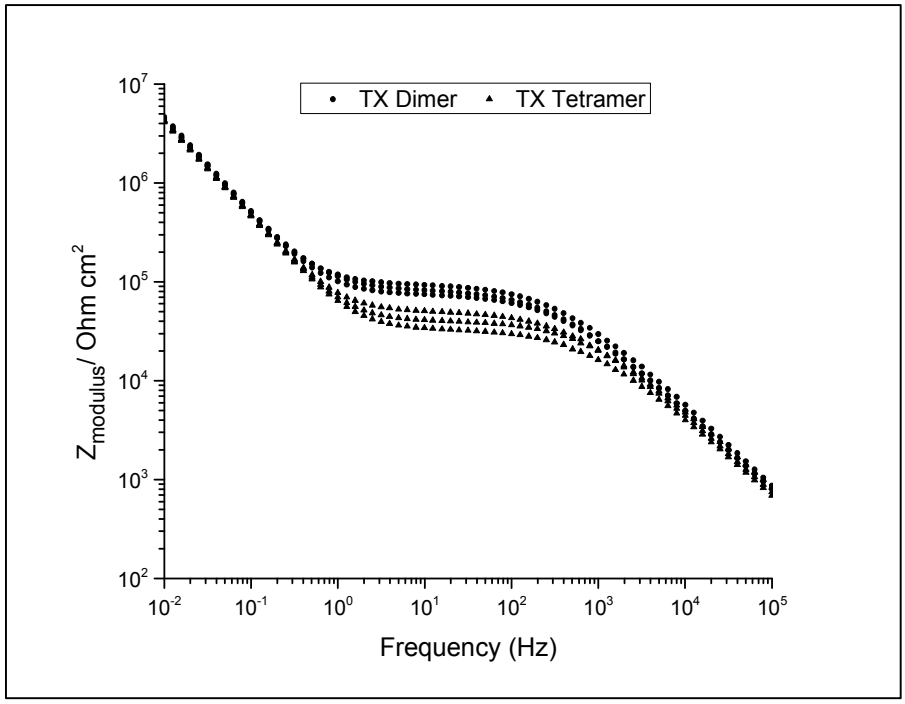

Figure 5.12. Comparison of coating TX made with PDA dimers versus tetramers after 10 days of immersion.

5.4. Conclusions

Monomers and oligomers of o-phenylenediamine were incorporated into epoxy-amine coatings to study their effects on EIS measurements and compare them to the results obtained with hybrid organic-inorganic sol-gel coatings also cross-linked with phenylenediamine. Coatings incorporating PDA monomers did not display the same results as the sol-gel coatings.

However, coatings which incorporated PDA oligomers at first displayed Randle's cell behavior for the first days/weeks of constant immersion but eventually displayed similar EIS behavior to the sol-gel coatings as the overall impedance declined to sufficiently low values. This finding suggests the EIS behavior was not due to the different structure of the epoxy-amine coating nor the aluminum oxide layer, unless for some reason oligomeric PDA is capable of stabilizing the oxide layer while PDA monomer is not. This finding also suggests the EIS behavior was not simply due to the sol-gel structure of the earlier studies because that structure was not present in the current coatings.

Different metal catalysts with hydrogen peroxide were used to synthesize the PDA oligomers; different length oligomers oxidized to various degrees were formed depending on the method of synthesis. These differences altered the EIS response of the coatings into which they were incorporated, likely due to structural differences incurred in the coatings, such as larger gaps around the larger oligomer fragments, or to differences in the coating resistances imparted by the different oligomer lengths.

The cross-link density of the coatings appeared to have a measureable effect on the EIS results. The lower cross-link density expected from coating EX yielded different EIS response from the expected higher cross-link density expected of coatings TX and ET with coatings TX and ET displaying similar results to the sol-gel coatings while coating EX did not. The unusable coating made using PDA oligomers synthesized by molybdenum catalyst indicated the oligomer structures might also have an effect on the final coating structures, either by reacting to the epoxide groups at a more rapid pace or somehow catalyzing the curing reaction between the epoxide and other amine cross-linking agents present.

Rather than the EIS response being caused by any conductivity due to the incorporated PDA oligomers, the results suggest the presence of the PDA oligomers may cause the coatings to act as osmotic membranes, specifically adsorbing ammonium and sulfate ions, which may in turn block pores for sodium and chloride to pass. A layer of pure water would be expected to yield a capacitive response, and when combined with the coating capacitance and coating resistance responses, might be expected to present the observed behavior. When an electrolyte of sodium chloride-only was used, the solution appeared to easily penetrate the coatings and the EIS results revealed rapid failure without displaying the unusual behavior.

5.5. References

[1] X. Sun, S. Dong, E. Wang, Macromolecular Rapid Communications, 26 (2005) 1504-1508.

[2] X. Sun, M. Hagner, Langmuir, 23 (2007) 10441-10444.

[3] Q. Hao, B. Sun, X. Yang, L. Lu, X. Wang, Materials Letters, 63 (2009) 33*4*-336.

[4] L. Wang, S. Guo, S. Dong, Materials Letters, 62 (2008) 3240-3242.

[5] Y. Li, R. Lenigk, X. Wu, B. Gruendig, S. Dong, R. Renneberg, Electroanalysis, 10 (1998) 671-676.

[6] Y. Zhang, H. Li, Y. Luo, X. Shi, J. Tian, X. Sun, PLoS ONE, 6 (2011) 1-11.

[7] D. Ichinohe, T. Muranaka, T. Sasaki, M. Kobayashi, H. Kise, Journal of Polymer Science Part A: Polymer Chemistry, 36 (1998) 2593-2600.

[8] R.H. Sestrem, D.C. Ferreira, R. Landers, M.L.A. Temperini, G.M. do Nascimento, European Polymer Journal, 46 (2010) 484-493.

[9] R. H. Sestrem, D.C. Ferreira, R. Landers, M.L.A. Temperini, G.M. do Nascimento, Polymer, 50 (2009) 6043-6048.

[10] I. Losito, F. Palmisano, P.G. Zambonin, Analytical Chemistry, 75 (2003) 4988-4995.

[11] B. Yao, G. Wang, X. Li, Z. Zhang, Journal of Applied Polymer Science, 112 (2009) 1988-1993.

[12] K-Y. Huang, C-L. Shiu, P-S. Wu, Y. Wei, J-M. Yeh, W-T. Li, Electrochimica Acta, 54 (2009) 5400-5407.

[13] T. Viswanathan, Q. Feng, A. Toland, Journal of Elastomers and Plastics, 30 (1998) 197-206.

[14] T. Fu, G. Zhang, S. Zhong, C. Zhao, K. Shao, L. Wang, H. Na, Journal of Applied Polymer Science, 105 (2007) 2611-2620.

[15] K.J. Croes, A.J. Vreugdenhil, M. Yan, T.A. Singleton, S. Boraas, V.J. Gelling, Electrochimica Acta, 56 (2011) 7796-7804.

[16] J.F. Rubinson, Y.P. Kayinamura, Chemical Society Reviews 38 (2009) 3339-3347.

[17] S. Amand, M. Musiani, M.E. Orazem, N. Pébère, B. Tribollet, V. Vivier, Electrochimica Acta, 87 (2013) 693-700.

[18] D.A. Jones, Principles and Prevention of Corrosion, Prentice-Hall, Inc. 2005.

[19] M.-R. Huang, H.-J. Lu, X.-G. Li, Journal of Materials Chemistry, 22 (2012) 17685-17699.

[20] W. Yu, L. Zhang, Y. Meng, S. Dai, Z. Su, L. Chai, H. Wang, Synthetic Metals, 176 (2013) 78-85.

[21] A.J. Vreugdenhil, V.J. Gelling, M.E. Woods, J.R. Schmelz, B.P. Endersen, Thin Solid Films, 517 (2008) 538-543.

[22] E.P.M. van Westing, G.M. Ferrari, J.H.W. de Wit, Corrosion Science, 36 (1994) 957-977.

[23] F. Bellucci, L. Nicodemo, Corrosion, 49 (1993) 235-247.

[24] K.N. Allahar, B.R. Hinderliter, D.E. Tallman, G.P. Bierwagen, Journal of the Electrochemical Society, 155 (2008) F201-F208.

[25] Y. Marcus, Chemistry Reviews, 88 (1988) 1475-1498.

CHAPTER 6. POLARIZATION STUDIES AND DEVELOPMENT OF A WORKING MODEL FOR THE DEPOSITION OF MAGNETITE ON STEEL FROM A CHEMICAL BATH

6.1. Introduction

This chapter presents the potentiodynamic polarization studies performed to attempt to determine a working model for the deposition of a magnetite coating on steel. As discussed in Chapter 3, an industrial client has sold for several years a complex, highly alkaline chemical bath that generates a layer of magnetite on steel as a coating. After determining the optimal concentrations of components through trial and error, they performed studies such as measuring the elemental content and component concentrations after different levels of use, which could not reveal the mechanisms for how the bath functioned and they could not resolve issues some of their customers encountered when using the bath. They approached NDSU to see if electrochemical methods could provide a better understanding of the bath mechanisms. Study of similar systems in the scholarly literature suggested potentiodynamic polarization might be a viable method to study the system [1].

6.2. Preliminary studies of the complete bath

Two major questions were approached first to obtain background information and also to determine if polarization measurements would be useful to study this coating system. These questions were to a) observe any changes in the measurements as the temperature of the bath was raised incrementally from 150ºF to 200ºF and b) follow the progress of the bath as it was used under its normal operating conditions, from new until completely consumed. As noted in Chapter 3, the correct bath temperature was necessary for proper function. Both experiments

revealed potentiodynamic polarization measurements may provide valuable insight into the mechanisms of the bath as the technique had demonstrated in the literature [1].

6.2.1. Methods

From preliminary experiments, it was determined the optimal conditions for the potentiodynamic polarization measurements would be to sweep the potential from -0.4V to +1.5V about the open circuit potential at 10mV/s with a sample period of 0.5s. The potentiostat collected an OCP measurement for 10 seconds prior to the start of the polarization measurement. For the temperature and bath consumption studies, a ½" x 3" "test" strip of cold rolled steel provided by the client was immersed into the bath (250mL) so that approximately 1 ½" of the strip was immersed and functioned as the working electrode; this immersion yields a surface area of exposure of approximately 4.7cm^2. A platinum mesh was used as the counter electrode and mercury/ mercury oxide (Hg/HgO) as the reference electrode. The Hg/HgO electrode had a plastic body that could withstand the high temperature and pH and is more accurate at high pH than the more commonly used silver/silver chloride electrode. The silver/silver chloride begins to lose accuracy at approximately pH 12 due to the alkaline error where, with low H^+ concentration, the electrode begins to respond to sodium ions in addition to H^+ ions [2]; another commonly used electrode, the saturated calomel electrode, cannot be used above 70ºC due to the change in concentrations caused by heating yielding an unsaturated condition.

For the consumption study, a measurement was made initially on a "test" strip, then two "consumption" strips of steel 1" x 3" were completely immersed in the bath consecutively for 5 minutes each. Then another "test" strip was measured followed by two more "consumption" strips; the process was repeated until the bath was completely consumed. It was observed, generally, the first three sets of consumption strips were very black but thereafter the coating,

while still very dark, began to have a more brownish coloring. It took 6 or 7 sets of "consumption" strips plus test strips to completely consume the bath. At the end point when the bath no longer functioned, very little product of any kind formed on the surface of the steel, as determined by just a slight discoloration of the steel occurring as viewed by eye.

6.2.2. Bath temperature study

For the temperature study, a sample of the bath was heated to 150^{o}F and one test strip measured by potentiodynamic polarization at that temperature. The bath temperature was increased in 10^{o}F increments and the measurements were repeated until 200^{o}F was reached. The small total volume of steel immersed in the solution ensured the bath was still in nearly new condition by the end of the experiment so concentrations of byproducts had not yet built to a significant level. The experiment was repeated several times with excellent reproducibility.

The behavior of the bath at increasing incremental temperatures revealed several changes due solely to temperature; each data set for each temperature from 150^{o}F to 200^{o}F is provided in Figure 6.1. Arrows delineate the most relevant changes. At point A, a small peak appears at 200^{o}F that was not as large or absent at lower temperatures; the appearance and behavior of this peak was somewhat sporadic making it difficult to decipher but was identified and is discussed later in the chapter. The peak at point B weakens with increasing temperature, possibly indicating the slowing of a reaction. The peak at point C becomes much stronger at temperatures from 170^{o}F and higher, indicating a reaction is likely strengthening at higher temperature. A "curl" develops on the cathodic arm that is essentially undetectable at 150^{o}F but becomes stronger with each increase in temperature, point D. The open circuit potential, OCP, value also increases toward more positive values with temperature and continually displays higher current

with each temperature increase, point E; this behavior may relate to the increased activity observed at peaks A, C, and D at the same time peak B decreased.

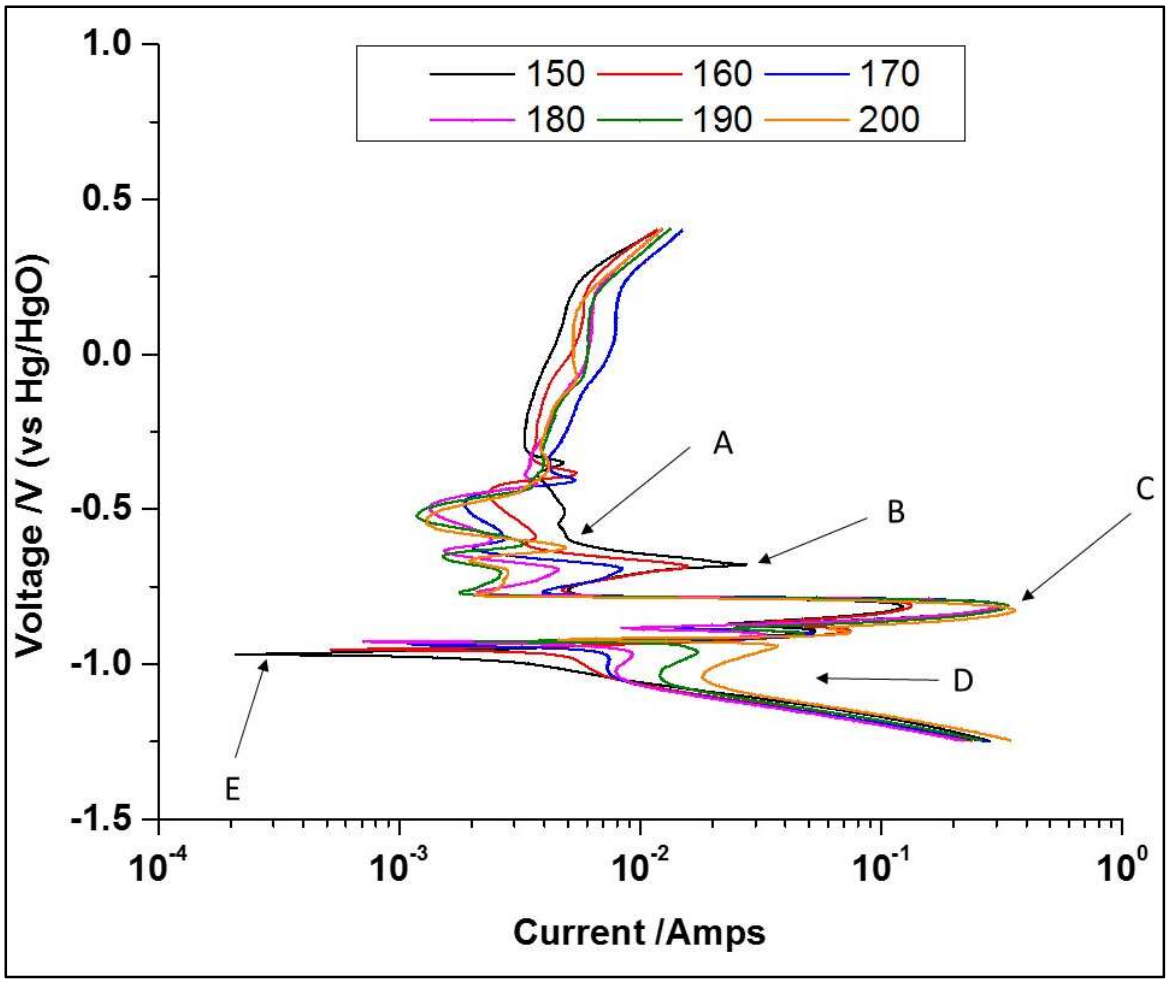

Figure 6.1. Polarization results of the bath temperature study. Values in the legend are in degrees Fahrenheit.

6.2.3. Bath consumption study

The results of several test strip potentiodynamic scans are overlaid for comparison in the graph in Figure 6.2; the inclusion of all measurements made as the bath was consumed renders the graph indecipherable. Much activity was detected with each measurement and these activities changed as the bath was consumed. The most notable changes are in the areas denoted by arrows. At point A, the passive region, the current density continually shifted to lower values

as the bath was consumed. The behavior indicates that although this region is generally stable through this range of potentials, indicating the formation of an oxide layer; something in the bath is actively affecting the rate of the oxide layer formation and greater current flow is observed initially but the activity becomes decreased as the chemicals are consumed. At point B, equivalent to point B in Figure 6.1, the peak appeared for Test 4 and Test 6 also but it is absent in Tests 1-3 and 7. At point C, a peak is visible which gradually disappears as the bath is consumed; the peak was visible but relatively unchanging in Figure 6.1. It can be observed the peak is not present in Test 7; it is very difficult to discern in Test 5 in Figure 6.2 but the peak is still just visible, again indicating the consumption of a chemical. Point E is the point at which the potentiostat measured the OCP (before each measurement) for all measurements except Tests 6 & 7; it can be observed the potential value became slightly more positive with each measurement. Point D depicts the cathodic branch of the measurement; it is observed the peak that forms at the top of the "curl" increases in intensity as the bath was consumed but is essentially absent at the end point. Finally, a strong, low current peak at point F is detected for Tests 5-7, with the potentiostat measuring approximately this value as the OCP prior to the polarization measurements for Tests 6 and 7. The potentiostat did not measure this value as the OCP prior to the polarization measurement for Test 5, even though it is quite strong; this indicates there was still sufficient activity of the bath components that the more negative value (~-0.85V) was detected as OCP prior to the polarization measurement; the presence of the peak for Test 5, therefore, may be due to some phenomenon induced by the potentiostat.

6.2.4. Summary

The aforementioned measurements confirmed polarization measurements may indeed provide useful information in the analysis of this coating system. It was not determinable from

these measurements, however, what bath components were responsible for the various behaviors indicated by the changes in current densities as the temperature changed or the bath was consumed. Therefore, further studies were needed to determine which activity was related to which bath component and to look for synergism/antagonism between bath components present in this complex formulation that could help explain the observed behaviors.

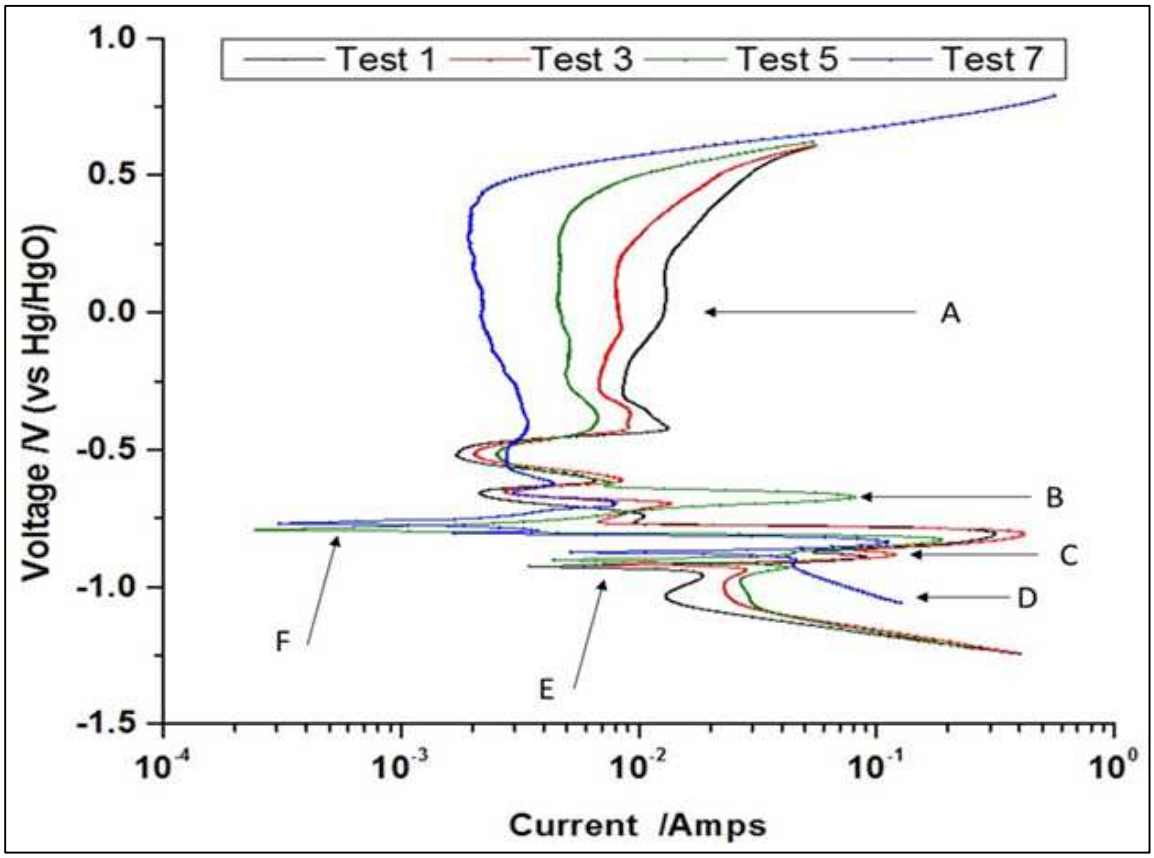

Figure 6.2. Polarization results of the bath consumption study.

6.3. Studies of the bath components

To determine the source of the observed peaks in the full bath, samples of steel were immersed in various combinations of the bath components at increasing temperatures. The potentiostat settings were the same as those described in section 6.1. The chemical concentrations were at the same concentrations found in a new bath. With the number of possible of combinations, however, 10°F increments were deemed excessive and too time

consuming so measurements were made at 150°F, 175°F, and 200°F. The components were not measured individually in water. Due to the high pH of the complete bath, the reactions would likely be different than at neutral pH because, as will be revealed shortly, the iron species generated in the bath would not be the same. Therefore, all were measured individually at the normal hydroxide concentration of the bath. These measurements were followed by all possible pairs at the normal hydroxide concentration with other combinations measured as necessary. As a baseline, the steel was measured in hydroxide solution alone to determine what activities might be due solely to the steel at the high pH and temperature of the bath.

6.3.1. Hydroxide-only at normal bath pH

Figure 6.3 displays the results of steel in hydroxide-only solution at the three temperatures. Four notable peaks are observed. At point A, ~ -0.67V, the current density is similar for 150°F and 175°F but declines at 200°F; there is also a slight negative shift in the potential at the tip of the peak. At point B, ~ -0.82V, the strongest peak is observed, with possibly more current density at 200°F and also a slight negative shift at the tip. At point C, ~ -0.89V, the peak is much stronger at 200°F than lower temperatures. At point D, the OCP is found at ~ -0.96V; notably, it does not change with temperature as observed in Figure 6.1, indicating the positive shift in potential observed in Figure 6.1 is due to the other chemicals present in the bath. Additionally, at point E, a "valley" of reduced activity is observed between Peaks A and B which will display differences in the presence of some of the other chemicals. Comparing to Figure 6.1, it is observed several of the peaks, thus activities, are present simply due to the steel and hydroxide alone, with slight shifts in the potential from when the complete bath was used. Notably different is the passive region which has lower current density than the complete bath (point F) and the "curl" is absent from the cathodic arm of the graph (point G).

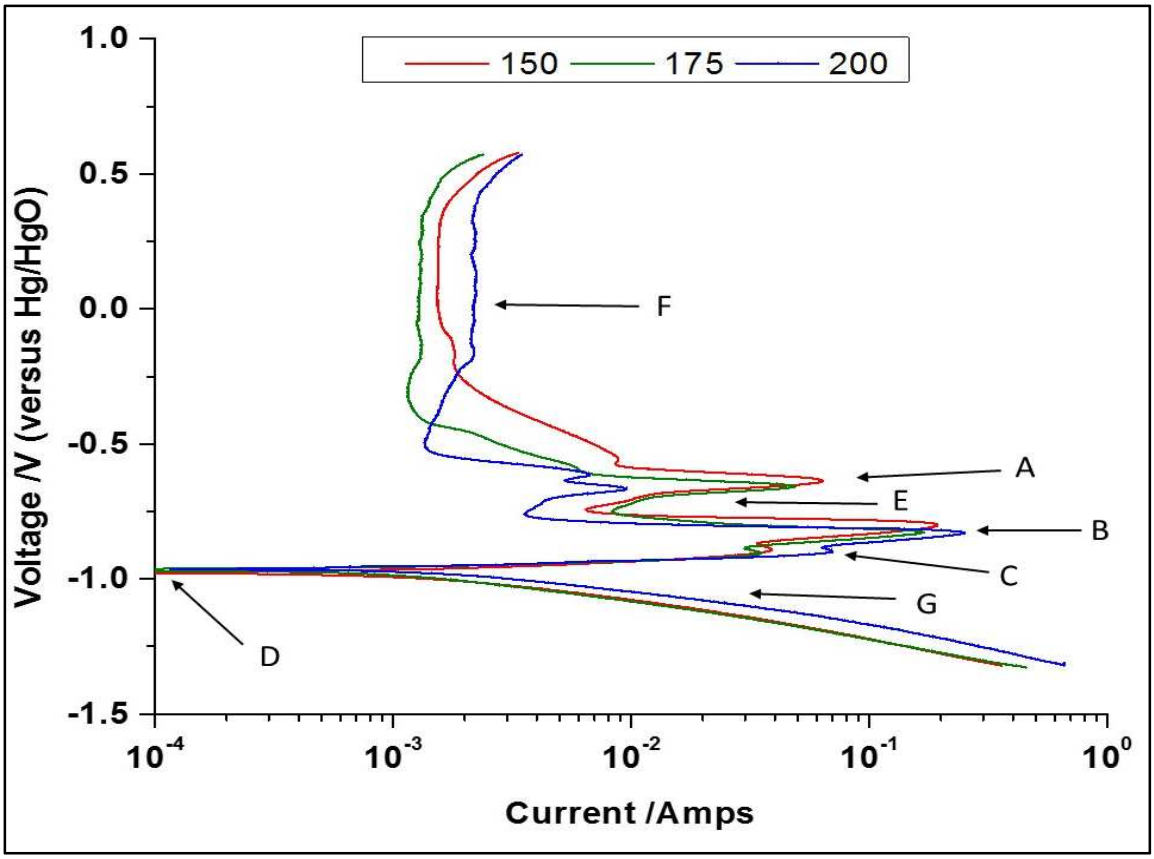

Figure 6.3. Polarization results for water/hydroxide/steel only.

The three peaks, A-C, observed in hydroxide-only solution, Figure 6.3, are identified first. Study of a Pourbaix diagram of the iron-water system at 100°C helps identify the peaks at -0.82V and -0.89V (points B and C); the diagram is displayed in Figure 6.4 [3]. A horizontal red line is overlaid on the figure equal to the OCP observed in Figure 6.3 (adjusted to reflect the difference between the Hg/HgO reference electrode and Standard Hydrogen Electrode used in the diagram). A blue line is overlaid at the point of lowest activity, a slight valley, between peaks B and C. A vertical red line indicates the approximate pH of the bath. It is observed the OCP intersects the pH line solidly in the region of stability for $HFeO_2^-$ species, indicating that species is very likely present in the system; thermodynamically, it should be stable, as noted in Chapter 4. At this pH, the blue line intersects the line which separates $HFeO_2^-$ from that of Fe_2O_3 (or, more likely, $Fe(OH)_3$ which is not considered in this particular diagram, but was, for

example, in Figure 4.10b); the separation of the two peaks most likely indicates a transition between two competing reactions. While it is possible some of the activity observed at Peak B is due to oxidation of $HFeO_2^-$ caused by the potentiostat, some of the activity is also likely due to the direct formation of an Fe^{3+} species; the reaction is likely occurring at the open circuit potential, but a condition is reached where the reaction can occur at a more rapid pace, the Fe^{3+} species becomes more stable, thus, higher current density is observed at this potential. It is important to note that in the full bath during deposition, the solution obtains a dark red color which is most likely the complexing agent reacting with Fe^{3+} present in the bath.

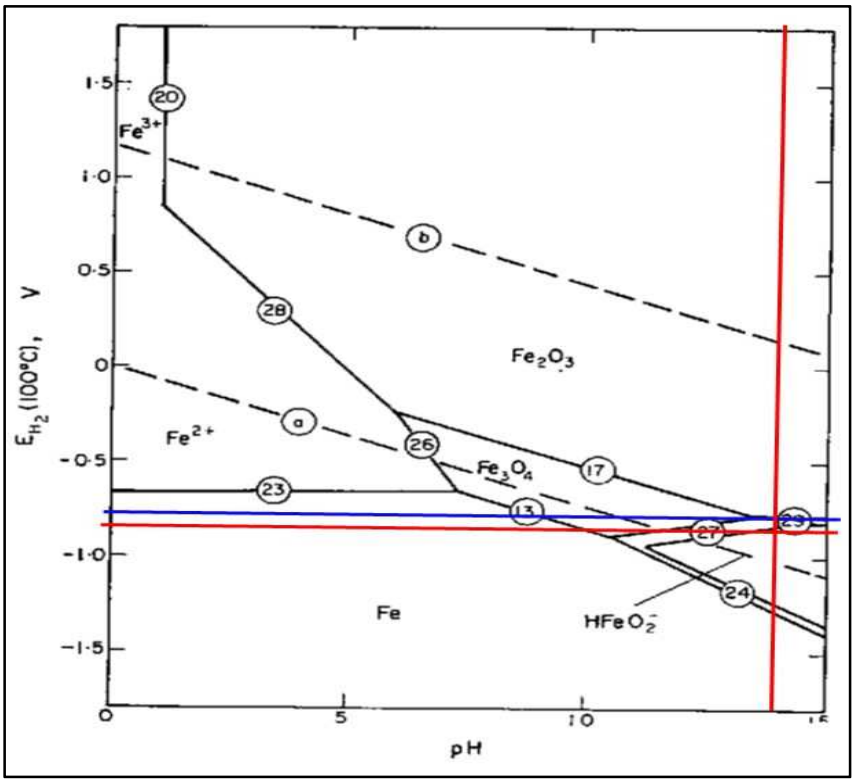

Figure 6.4. Pourbaix diagram for the water-iron system at 100°C. Red vertical line is approximate pH of the bath; red horizontal line is at the OCP measured in Figure 6.3; and the blue horizontal line at the "saddle" between the peaks B and C in Figure 6.3. The circled numbers on the various lines refer to reactions between the species on either side each line which were considered in the original reference. Colored lines are added. Reprinted and adapted from reference [3], with permission from Elsevier.

Another Pourbaix diagram is displayed in Figure 6.5, one of the iron-water system calculated at 25°C [3]. In this case, the red OCP line and vertical pH line are again overlaid at the same positions but with a green line indicating the potential of the sharpest peak at -0.82V. It is observed both lines intersect with the pH line in the Fe_3O_4 region of stability. It is also observed the region of stability for $HFeO_2^-$ encompasses a much smaller area than at 100°C. Even though thermodynamically magnetite is stable in hydroxide-only at these conditions, the figure would indicate, kinetically, magnetite and $HFeO_2^-$ may not be obtainable. Comparison of these two diagrams suggests the ability to form $HFeO_2^-$ at higher temperatures is at least partially responsible for the bath to function correctly. Thus, the hypothesis is that two soluble iron species are formed at this temperature and pH due solely to the hydroxide and water: Fe^{3+} (of some form) and $HFeO_2^-$.

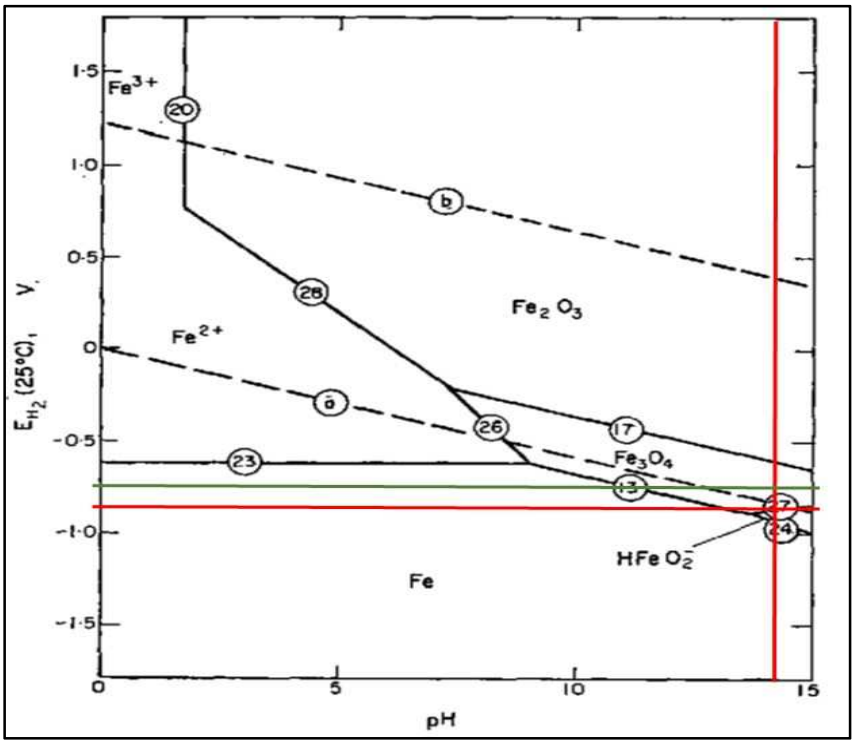

Figure 6.5. Pourbaix diagram for the water-iron system at 25°C. Red vertical line is approximately the pH of the bath; red horizontal line is at the OCP measured in Figure 6.3; and the green horizontal line at the potential of peak C from Figure 6.3. Colored lines are added. Reprinted and adapted from reference [3], with permission from Elsevier.

Neither Pourbaix diagram reveals any other iron species at more positive potentials along the vertical pH line, indicating something else in the steel-hydroxide-water system is responsible for the peak observed at -0.67V (Peak A in Figure 6.3). In cold rolled steel, the alloying elements are sulfur, phosphorus, and carbon in very small quantities (each 0.2-0.4%) and manganese [4]; in the alloy studied, manganese is present at 0.6-0.9%. A Pourbaix diagram for the manganese-water system at 95°C is displayed in Figure 6.6 [5]. As before, the blue line is inserted at the bottom of the peak at -0.67V with a red vertical line at the approximate pH of the system; it is observed the gap between the peaks at -0.67V and -0.82V approximately coincides with the transition between $Mn(OH)_2$ and Mn_3O_4. Not pictured in the figure is the transition from Mn metal to $Mn(OH)_2$ which occurs at very negative potentials below which the measurements of this study were made. Thus, the peak at -0.67V likely represents the transition between $Mn(OH)_2$ and Mn_3O_4 and is quite possibly induced by the potentiostat. The fact that current is much lower at 200°F than lower temperatures suggests the formation of $Mn(OH)_2$ may be sufficiently high at higher temperature so as to essentially passivate the manganese and the peak is suppressed. Importantly, some of the bath components will be shown to create increased activity in that peak at 200°F when present suggesting they interfere in the formation of $Mn(OH)_2$ and are more active in the vicinity of the manganese inclusions in the steel.

To further demonstrate the peak at -0.67V is related to manganese, a sample of pure iron was measured in the full bath at 200°F; the result is displayed in Figure 6.7. Due to cost, only a small amount of pure iron was available so only samples in the full bath were measured; additionally, the sample size was smaller than that of the steel pieces, with approximately 1.5 cm^2 immersed into the bath, thus accounting for some of the decrease in currents observed. Discussion of portions of Figure 6.7 is premature and will be considered in detail later but

several features are notable. For the present discussion, the peak at -0.67V is completely absent; in fact, this region is very passive and the transpassive region appears to begin at approximately -0.5V, whereas for steel the transpassive region started well above 0V. Concurrently, the peak associated with $HFeO_2^-$ at -0.89V is greatly decreased, in fact, nearly nonexistent; this behavior indicates the production of $HFeO_2^-$ is intimately tied to the presence of manganese. Two other peaks are also important: first, the "curl" on the cathodic arm is present and active, although somewhat lessened (probably due to lower surface area); second, the peak representing Fe^{3+} at -0.82V is also lessened but very active. The behavior indicates the activity observed on the cathodic arm is related to reduction of Fe^{3+}; under corrosion conditions, activity observed on the cathodic arm indicates reduction of some species in the system, usually hydrogen (in acidic conditions), oxygen (in acidic or neutral conditions), or water, but also occasionally, metal [6].

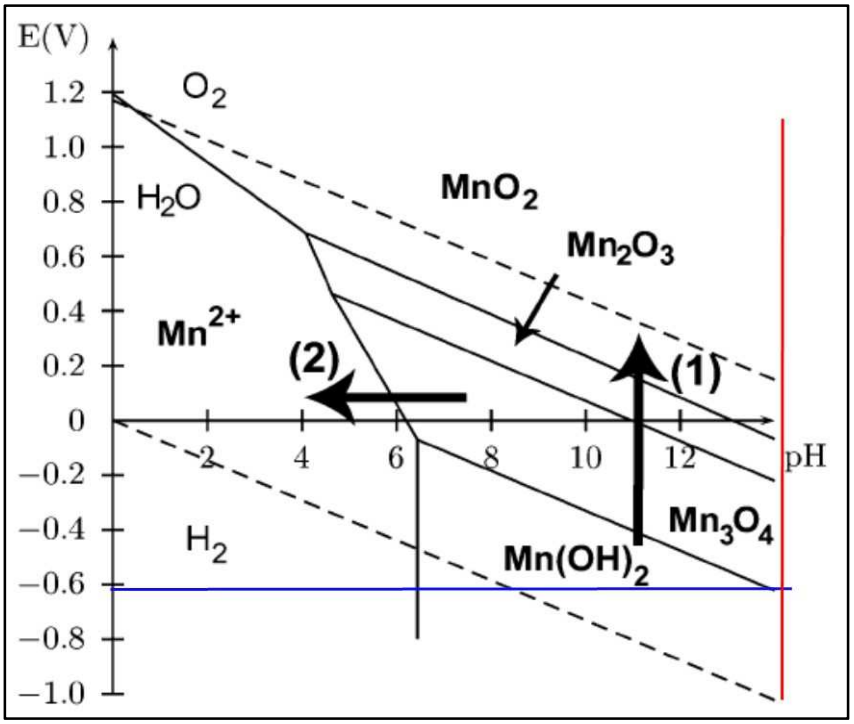

Figure 6.6. Pourbaix diagram for the water-manganese system at 95°C. Red vertical line is at approximately the pH of the bath; blue horizontal line is at the gap between Peaks A and B measured in Figure 6.3. Colored lines are added. Reproduced and adapted from reference [5], with permission of The Royal Society of Chemistry.

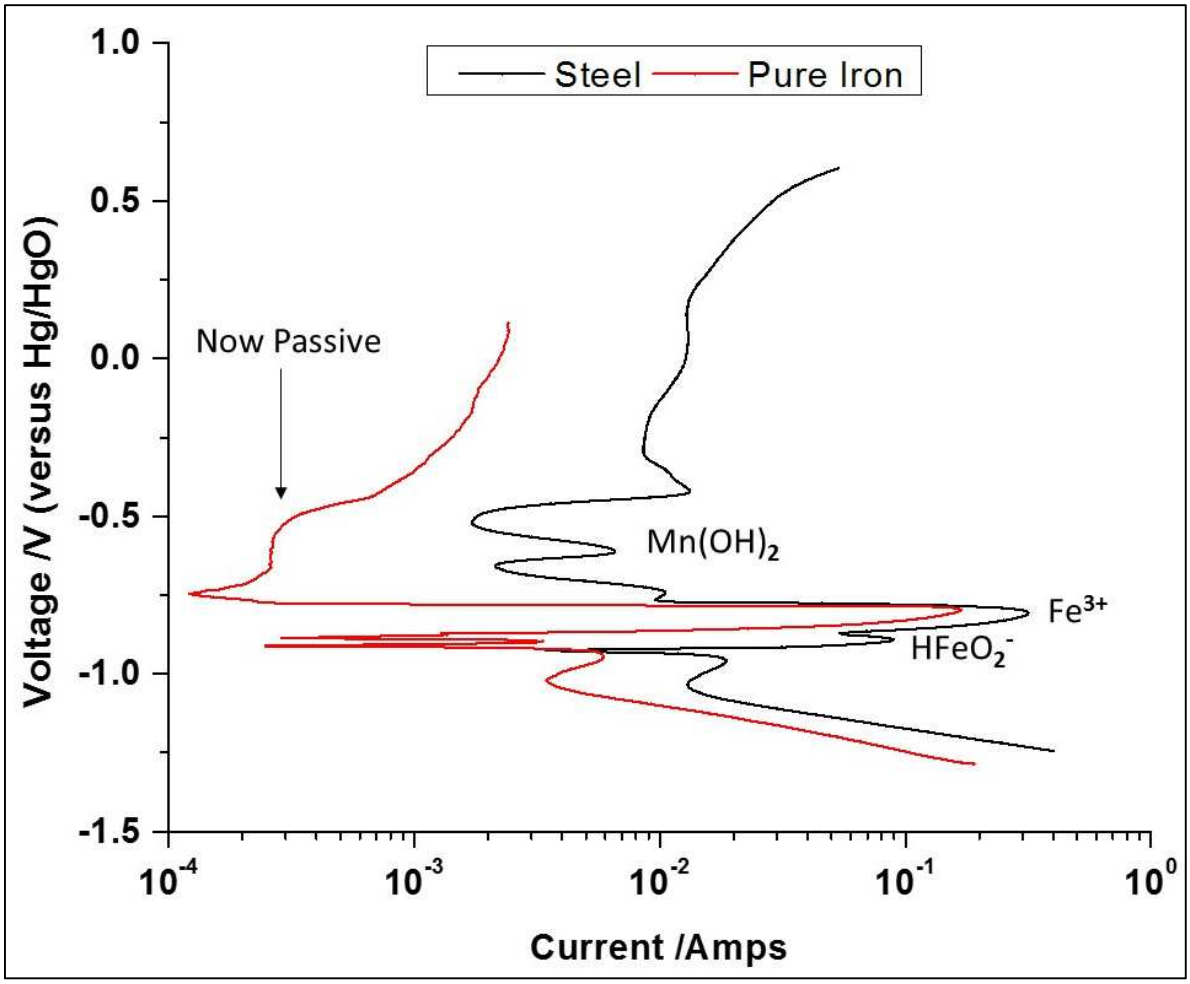

Figure 6.7. Polarization results comparing steel to pure iron in the complete bath at 200°F. The peak that likely represents the transition from $Mn(OH)_2$ to Mn_3O_4 is absent from the graph of pure iron. That region, indicated by the arrow, now appears to be the passive region, transitioning to the transpassive region. It must be noted the peak labeled as $Mn(OH)_2$ (steel) is not the actual manganese peak but another peak near it; this is discussed later in the text.

In summary, these results suggest two soluble iron species are formed by hydroxide and water alone, Fe^{3+} of some form and $HFeO_2^-$; this understanding was important because initially it was believed nitrate was necessary to oxidize iron from the surface. A reaction involving manganese is either present or can be induced by the potentiostat. The peak likely represents the transition from $Mn(OH)_2$ to Mn_3O_4. The OCP does not shift more positive as the temperature increases indicating one of the other components in the full bath is responsible for that behavior. The cathodic "curl" is not present, neither is the shift of the passive region to higher currents

observed, again both indicating other components in the bath are responsible for those phenomena.

6.3.2. Individual components at normal bath pH

Figures 6.8 - 6.13 display the results for each of the other components at the normal bath pH. The results for each component are summarized in the figure caption and each figure has the graph of hydroxide-only at 200°F included for comparison; the numbers at the top are temperature in °F. The most important observations are: the "curl" observed in the cathodic arm is determined to be related to nitrite and it becomes more active as the temperature increases; peak C from Figure 6.3, representing $HFeO_2^-$, is not observed in the presence of nitrite or nitrate; peak A from Figure 6.3, representing activity around the manganese, is not decreased at 200°F and the other peaks are relatively unaffected by thiosulfate; peak A is strong and consistent at all temperatures (not decreased at 200°F) and the other peaks are relatively unaffected by the charge transfer agent; and peak C is less defined in the presence of the complexing agent at 200°F.

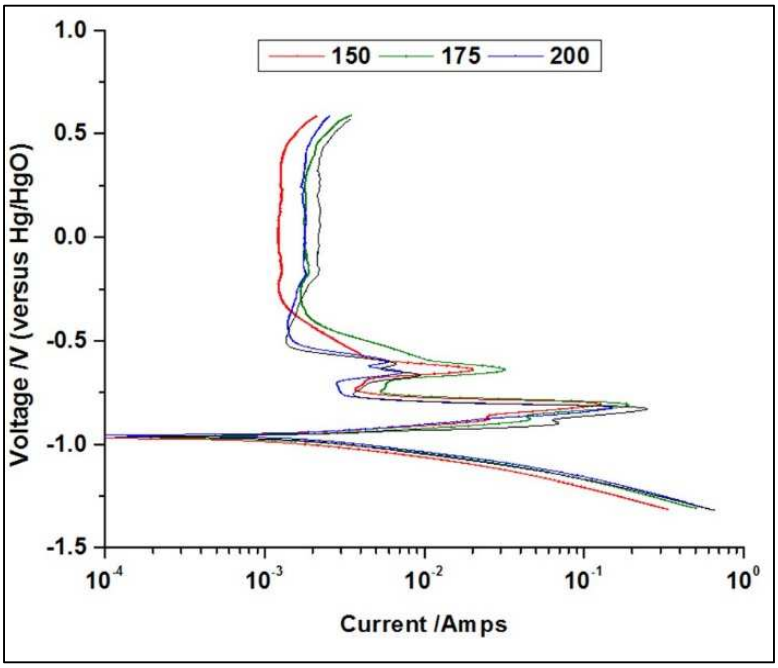

Figure 6.8. Results for complexing agent in hydroxide. Very similar to hydroxide-only results. $HFeO_2^-$ peak absent at 200°F; Fe^{3+} peak broader at lower temperatures.

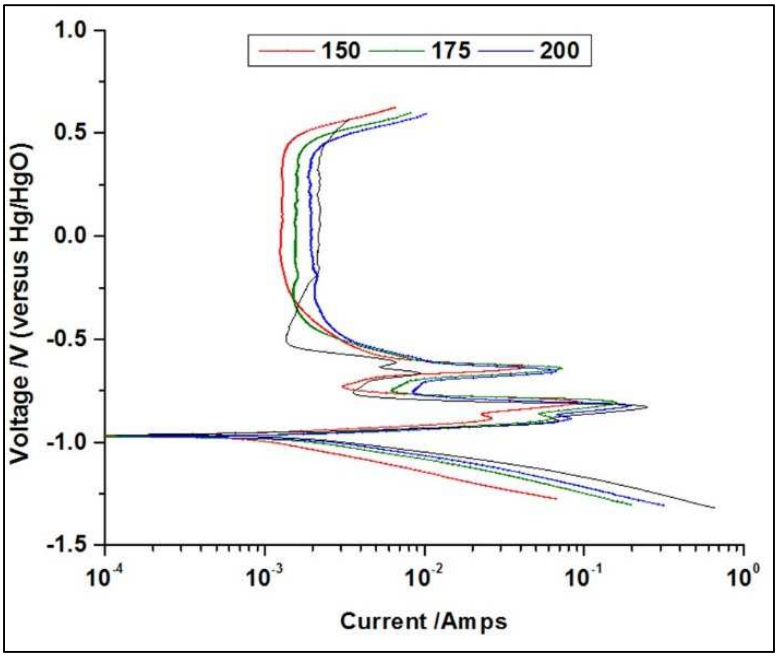

Figure 6.9. Results for charge transfer agent in hydroxide. The only significant difference is that there is high current in the region around the manganese.

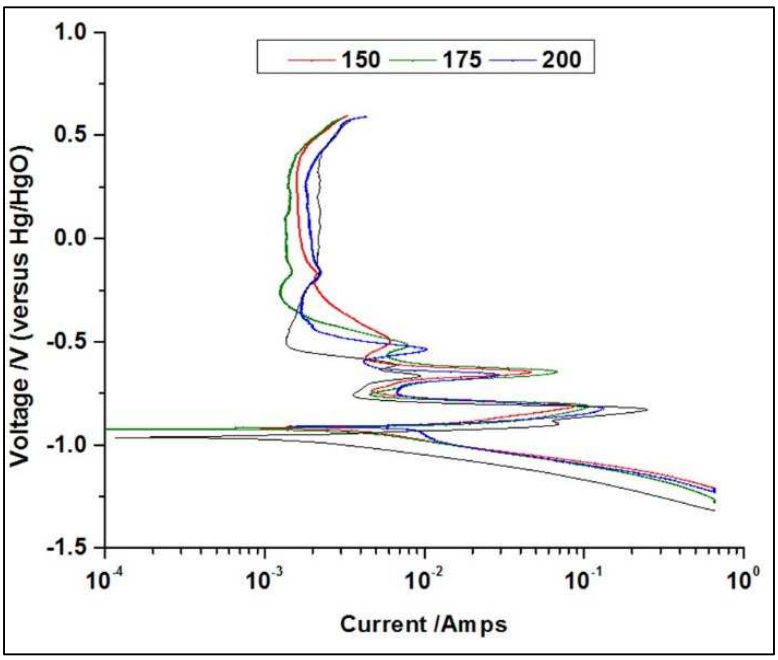

Figure 6.10. Results for sodium nitrate in hydroxide. OCP is ~40mV more positive but, importantly, changes only approximately 10mV with increasing temperature; $HFeO_2^-$ peak is absent; slightly less current around Fe^{3+} peak; slightly more current at Mn peak at 200°F. Appearance of a peak at ~-0.54V at 200°F.

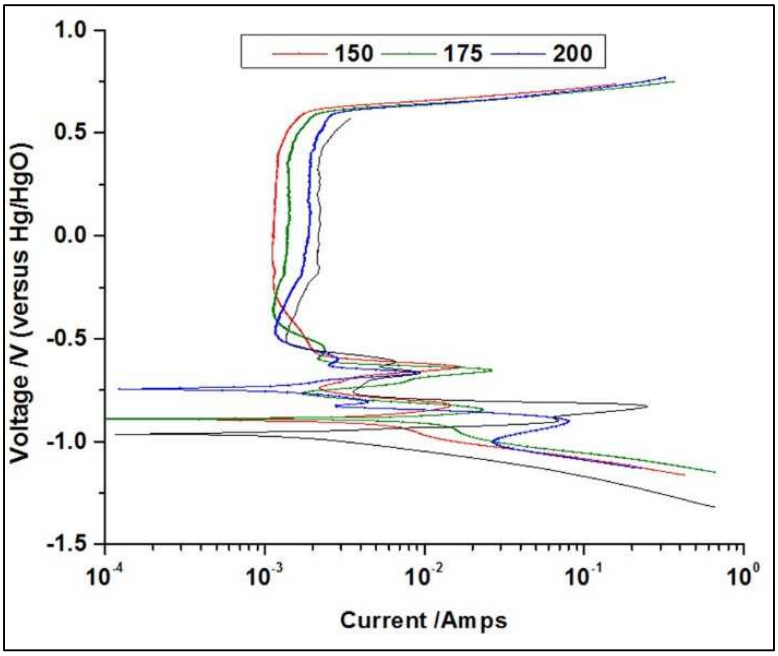

Figure 6.11. Results for sodium nitrite in hydroxide. OCP is approximately 90mV more positive at lower temperatures; at 200°F, it is at approximately -0.74V, nearly 200mV higher. The "curl" in the cathodic arm is present; the peak for $HFeO_2^-$ is absent; Fe^{3+} is subdued at lower temperatures and nearly nonexistent at 200°F.

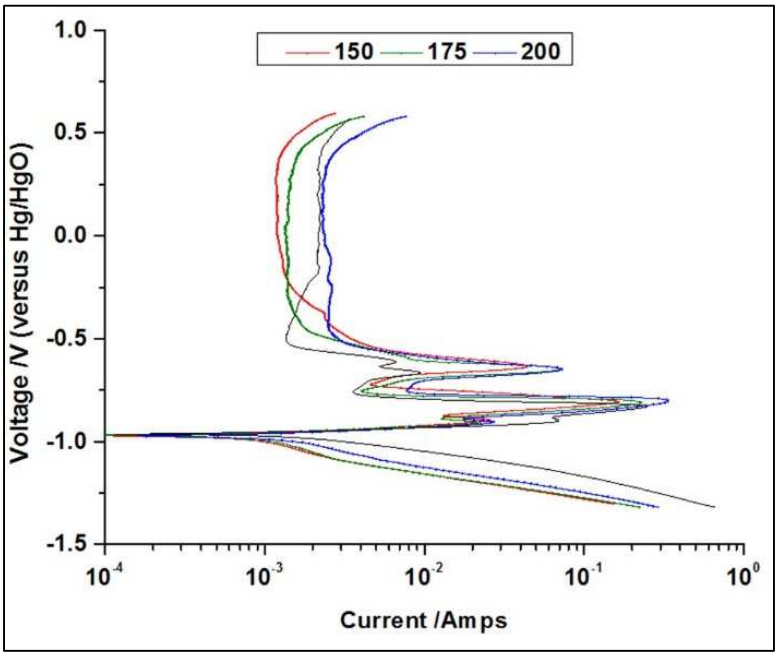

Figure 6.12. Results for sodium thiosulfate in hydroxide. OCP is unaffected by presence of thiosulfate; $HFeO_2^-$ peak is subdued by its presence at all temperatures; top edge of Fe^{3+} peak is at slightly more positive potentials in the presence of thiosulfate; very active at all temperatures around the manganese.

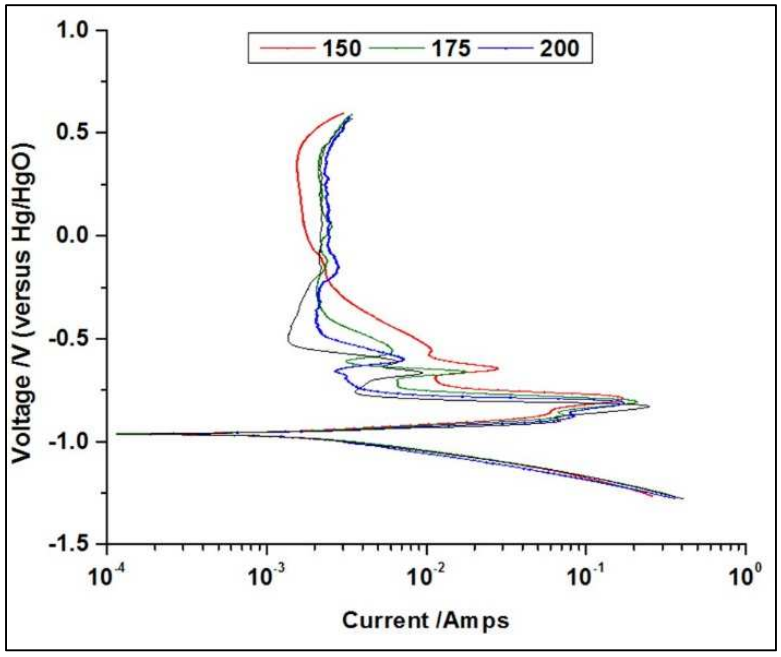

Figure 6.13. Results for tin compound in hydroxide. OCP is unaffected; $HFeO_2^-$ peak is stronger at lower temperatures, about the same as hydroxide-only at 200°F; appears to be no activity around the manganese at 200°F. A new weak peak appears at approximately -0.60V.

These results begin to reveal which bath components may be associated with each iron species generated by the high hydroxide content in the bath. Most notably, the cathodic curl is observed to relate to the presence of the nitrite in the bath. As observed in the results presented in Figure 6.7, when pure iron was measured in the full bath, an Fe^{3+} species was likely the iron species being generated and the curl was observed on the cathodic arm, which would indicate nitrite is reacting with Fe^{3+}. Indeed, metal reduction is observed on the cathodic branch of the polarization graph [6]; since the activity is observed on the cathodic branch, this behavior would indicate nitrite is acting as a *reducing* agent in this system, rather than as an oxidizing agent as it would normally react and as was initially believed. Note that the "curl" is not observed until the temperature has reach about 180°F, perhaps more easily observed in Figure 6.1, where at 170°F it does not quite form the sharp peak just below the OCP but by 180°F it is quite distinct.

Importantly, at 200°F, the Fe^{3+} peak is nearly nonexistent with only nitrite in the bath. Nitrite has been investigated as a corrosion inhibiting agent for steel at low temperatures by oxidizing the steel and forming a passivating layer [7-11]. By itself in this bath, nitrite is perhaps playing the role of inhibitor but through a different mechanism at increased temperature. It may be reducing the Fe^{3+} at such a pace as to greatly decrease the level of Fe^{3+} detected. Also, the peak associated with $HFeO_2^-$ is absent altogether. One explanation is, simply by Le Chatlier's Principle, if both iron species are getting generated but one is being consumed (by nitrite in this case) while the other is not, more activity should be observed by generation of additional molecules of the species being consumed, thereby favoring that reaction [12]. Conversely, little Fe^{3+} appeared to be generated either, so the nitrite may simply be preventing the formation of $HFeO_2^-$ as well through whatever mechanism it is working.

The OCP value is observed to increase when nitrite and nitrate were introduced; the OCP is unchanged from hydroxide-only in the presence of any of the other individual components. The hypothesis for the change in OCP caused by nitrite will be discussed at a later time. For the moment, however, note the peak representing $HFeO_2^-$ is also absent when nitrate is added to the system; the hypothesis is nitrate oxidizes $HFeO_2^-$ to another species, thus, the peak is not observed in this combination. The oxidation of more iron to a second species with temperature increase (as greater Fe^{3+} was observed at 200°F in the hydroxide-only study, Figure 6.3) plus this extra oxidation of $HFeO_2^-$ would cause the total level of iron oxidation to increase above that of hydroxide-only. It would occur through a more circuitous route forming $HFeO_2^-$ first, then to a different species; again by Le Chatlier's Principle, consumption of a reaction product would draw a reaction toward the product side of the chemical reaction. This extra oxidizer would be equivalent to the extra M+ species discussed in the Evans diagrams in Chapter 4; as noted there,

the M+ species could be something other than another metal ion. This would shift the OCP to more positive potentials.

6.3.3. Pairs of components at normal bath pH

The sources for most of the peaks observed in Figure 6.1 have now been determined; however, none of the previous results identified the cause of the shift of the passive region to higher current densities. There are fifteen possible pair combinations of the 6 bath components in hydroxide. The results are displayed in Figures 6.14 - 6.28. They are compared to Figure 6.3 and again include the graph of hydroxide-only at 200ºF for comparison and again the numbers at the top are degrees Fahrenheit. A summary is again included in each figure caption. In some instances the behavior is very erratic but erratic behavior suggests certain antagonistic properties between the two components; at other times, certain peaks are either enhanced or absent, again suggesting certain synergistic/ antagonistic behavior.

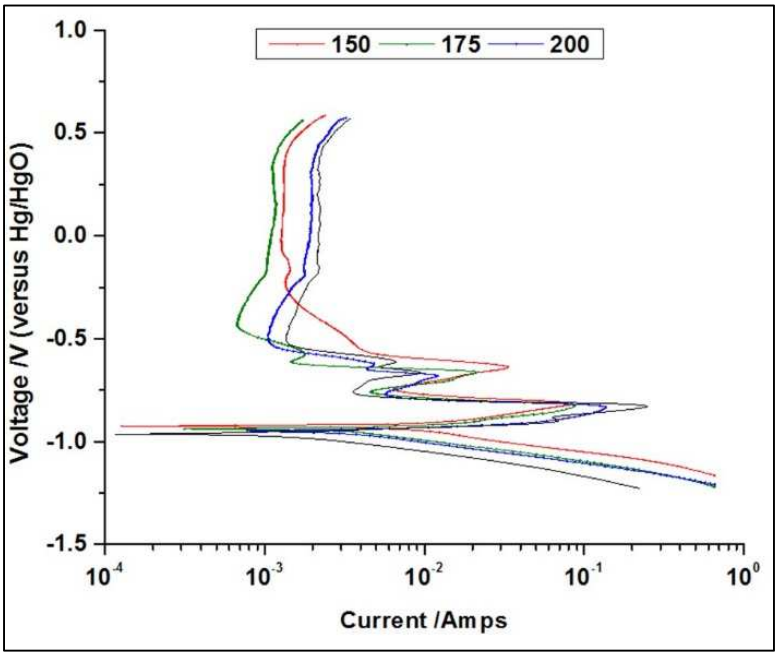

Figure 6.14. Results for nitrate and nitrite. No curl in cathodic arm; no peak representing $HFeO_2^-$, which perhaps has become part of Fe^{3+} peak at 200ºF; Fe^{3+} peak somewhat subdued at lower temperatures than hydroxide-only; less activity around manganese at lower temperatures.

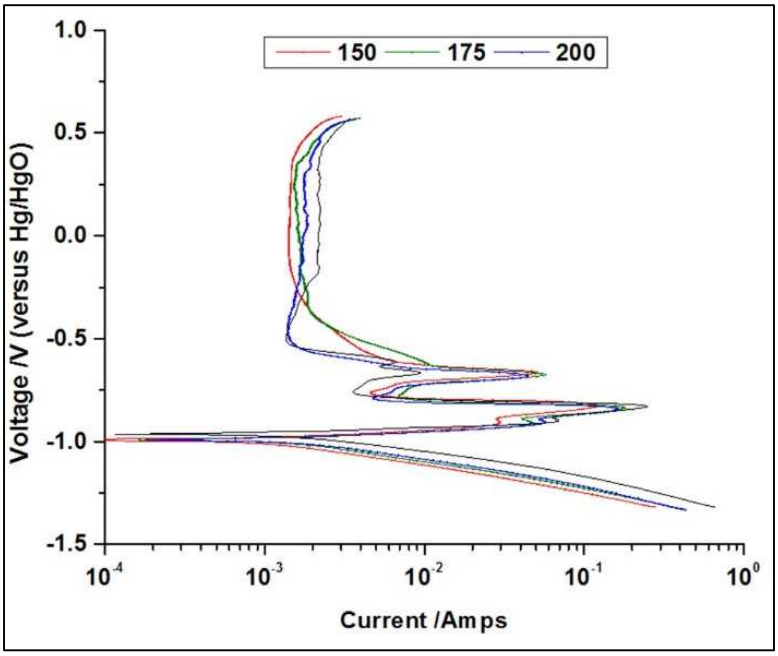

Figure 6.15. Results for nitrate and complexing agent. Active around manganese at all temperatures; OCP peak is slightly lower, phenomenon not observed in nitrate nor complexing agent alone; slightly decreased activity at Fe^{3+} peak.

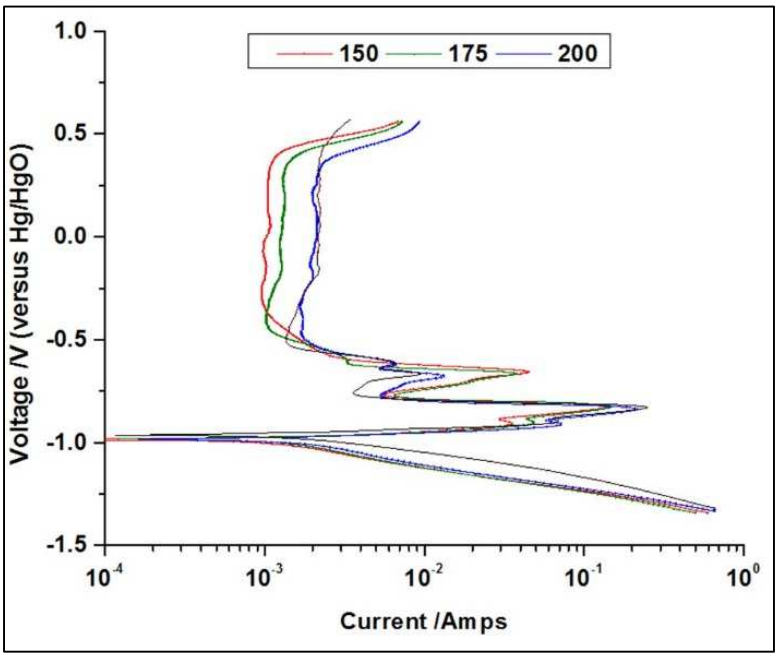

Figure 6.16. Results for nitrate and charge transfer agent. Very similar to hydroxide-only; slight decrease of OCP.

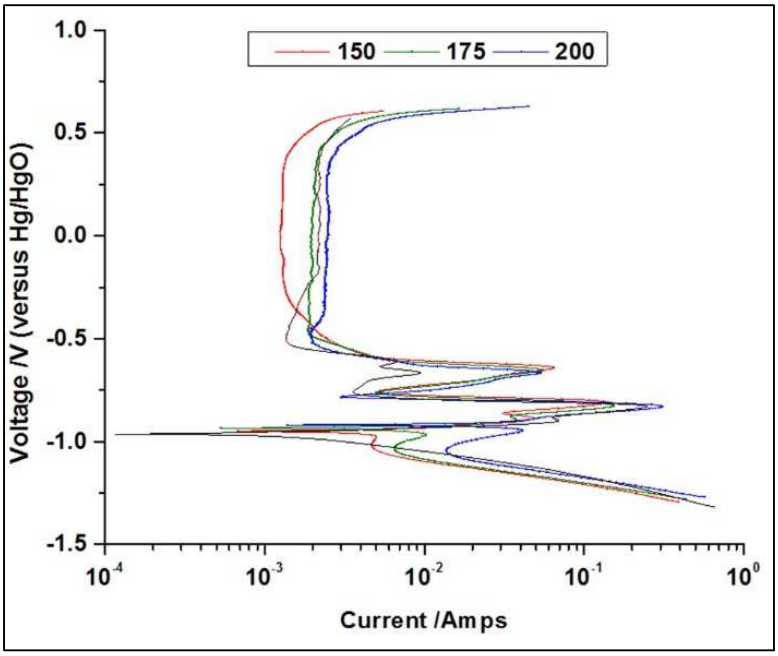

Figure 6.17. Results for nitrite and thiosulfate. Cathodic curl is present; peak representing $HFeO_2^-$ (faint at 200°F) present; active around manganese; increasing OCP with temperature.

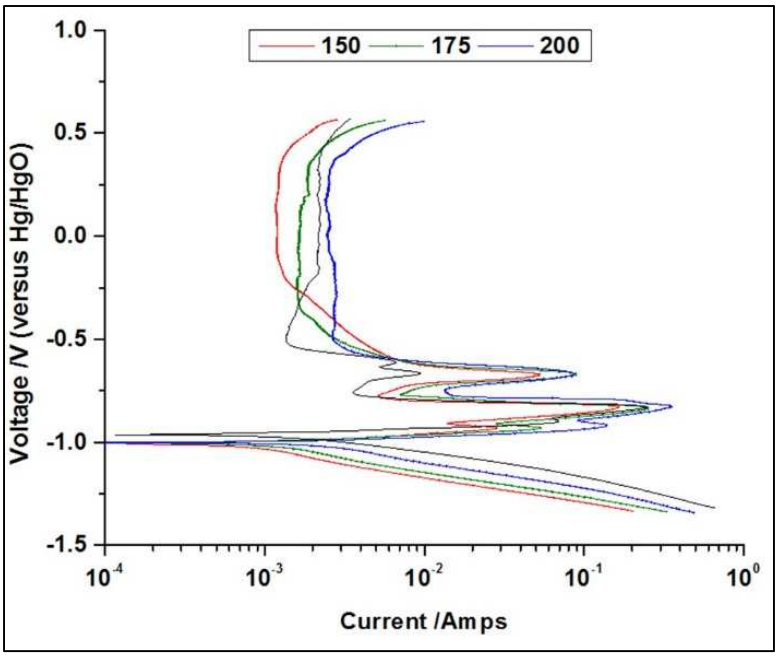

Figure 6.18. Results for nitrate and thiosulfate in hydroxide. OCP is somewhat lower than hydroxide-only, and nitrate or thiosulfate alone; $HFeO_2^-$ peak also at slightly lower potentials than hydroxide or thiosulfate alone; active around manganese at all temperatures; Fe^{3+} peak similar to thiosulfate alone. While OCP and $HFeO_2^-$ peaks have shifted more negative, manganese and Fe^{3+} unchanged.

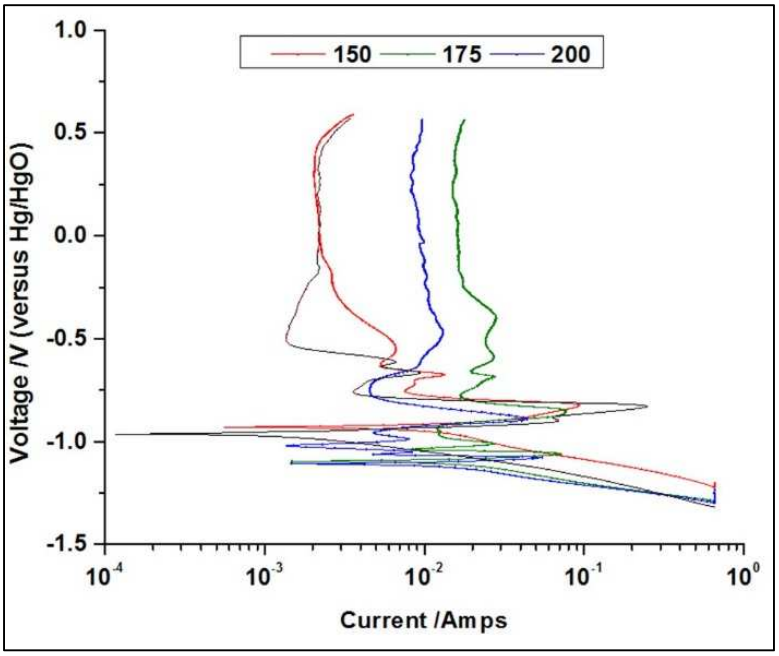

Figure 6.19. Results for nitrate and tin compound. Behavior is very erratic; but, tin can be observed to not be very active at 150ºF as behavior is similar to nitrate alone with decreased activity of Fe^{3+} peak and increase of OCP; then erratic behavior begins at 175ºF with OCP at much lower potential, approximately 140mV lower than hydroxide-only and tin alone; shift of passive region to higher currents. At 200ºF, the shoulder of $HFeO_2^-$ appears to be a separate peak with no Fe^{3+} formation.

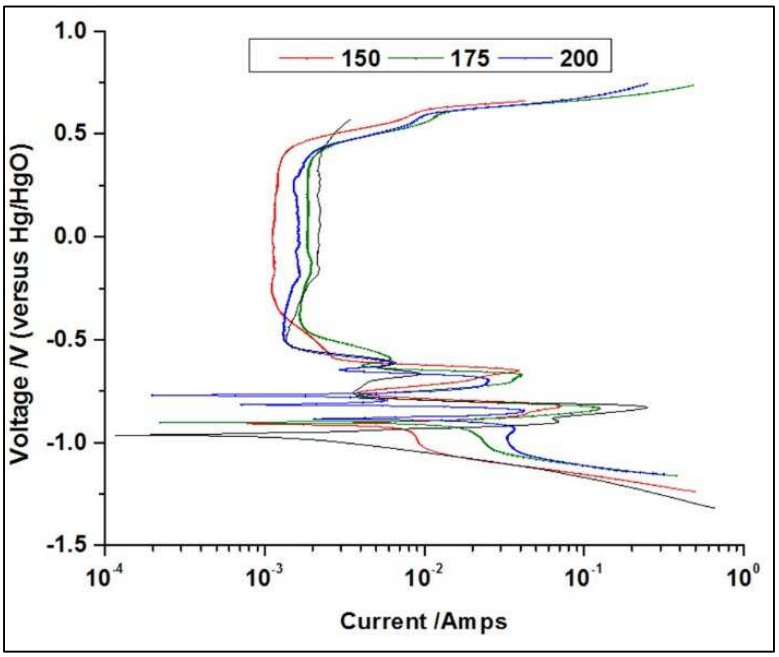

Figure 6.20. Results for nitrite and charge transfer agent. Increase in OCP with temperature; nitrite curl present but suppressed, almost more like a passive area; no $HFeO_2^-$ peak; Fe^{3+} suppressed but not as much as in nitrite alone; activity around manganese altered, broad peak.

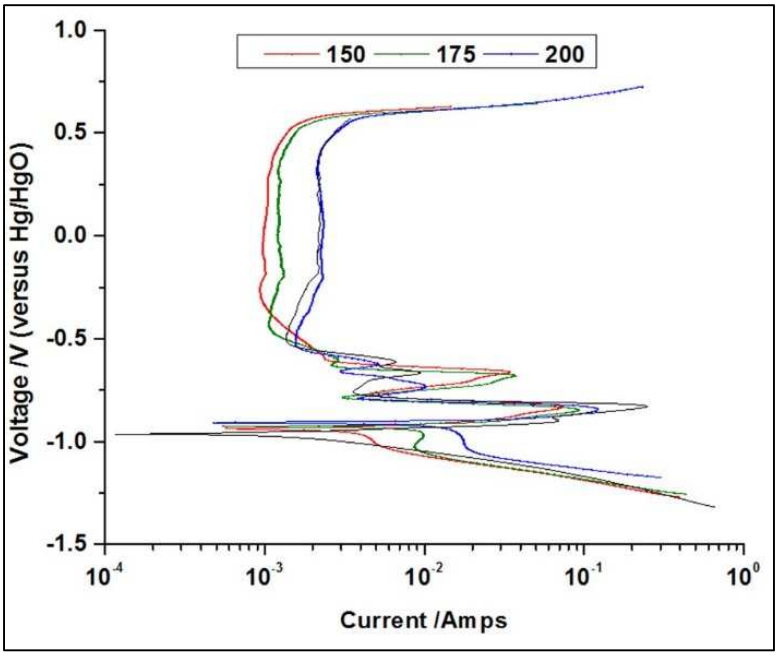

Figure 6.21. Results for nitrite and complexing agent in hydroxide. OCP again increased versus hydroxide-only; curl on cathodic arm is not as strong as in nitrite alone; current for Fe^{3+} not decreased as with nitrite only; peak appears at -0.74V which has not been observed before; manganese peak approximately the same current at lower temperatures but broader than hydroxide-only results.

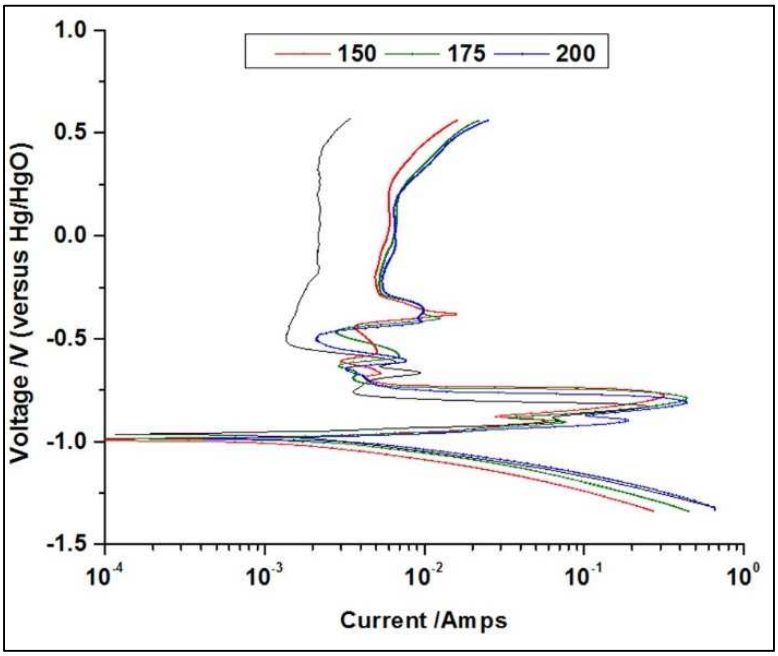

Figure 6.22. Results for thiosulfate and tin compound. OCP is slightly lower; passive region is shifted to higher current; Fe^{3+} peak is very broad, the top edge and peak itself at much higher potential which may represent a different species, as discussed in the section 6.4.4.

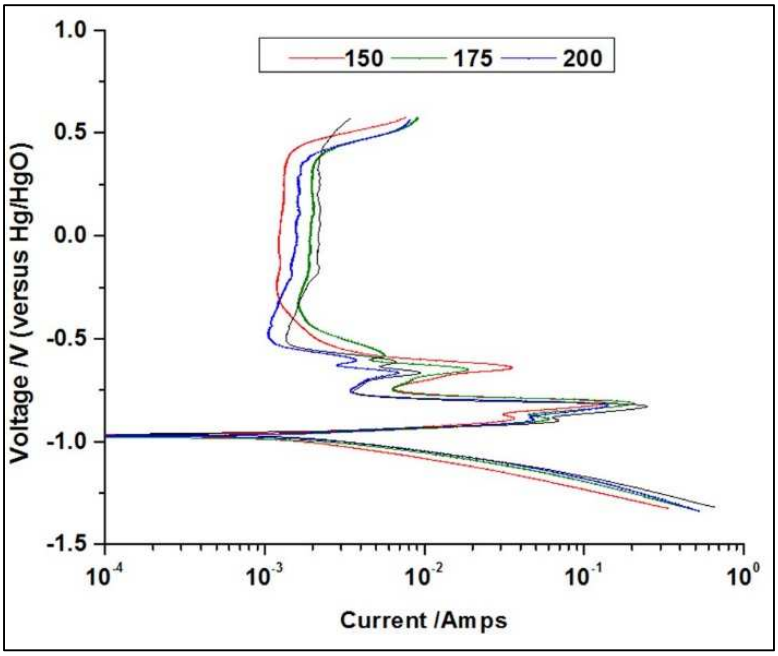

Figure 6.23. Results for complexing agent and charge transfer agent. Very little change from hydroxide-only results. Note the manganese peak at -0.67V is subdued whereas it was quite strong when only charge transfer agent was present (Figure 6.9).

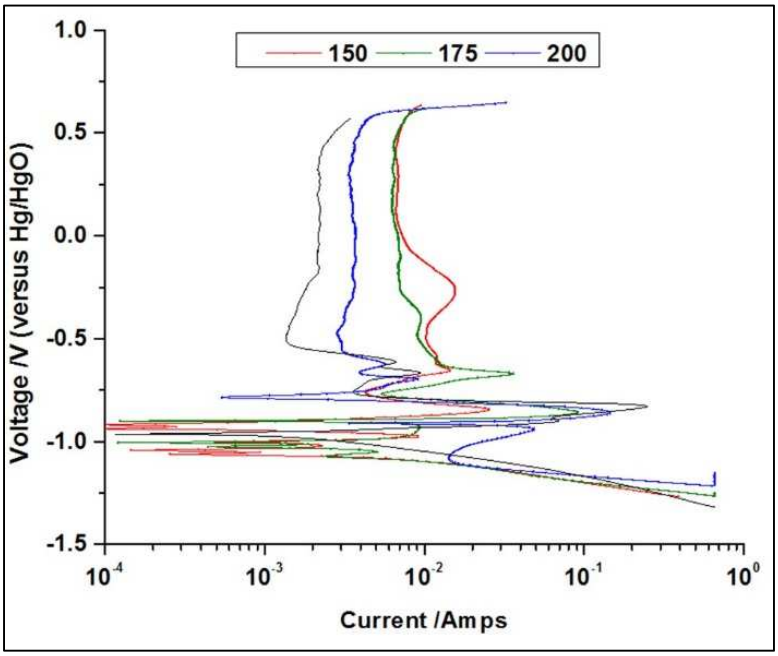

Figure 6.24. Results for nitrite and tin compound. Behavior is very erratic at lower temperatures, difficult to discern what may be happening. Cathodic curl is resolved at 200°F; $HFeO_2^-$ peak does not seem present at 200°F; passive region is shifted to higher current at lower temperatures, less at 200°F but still higher current than hydroxide-only.

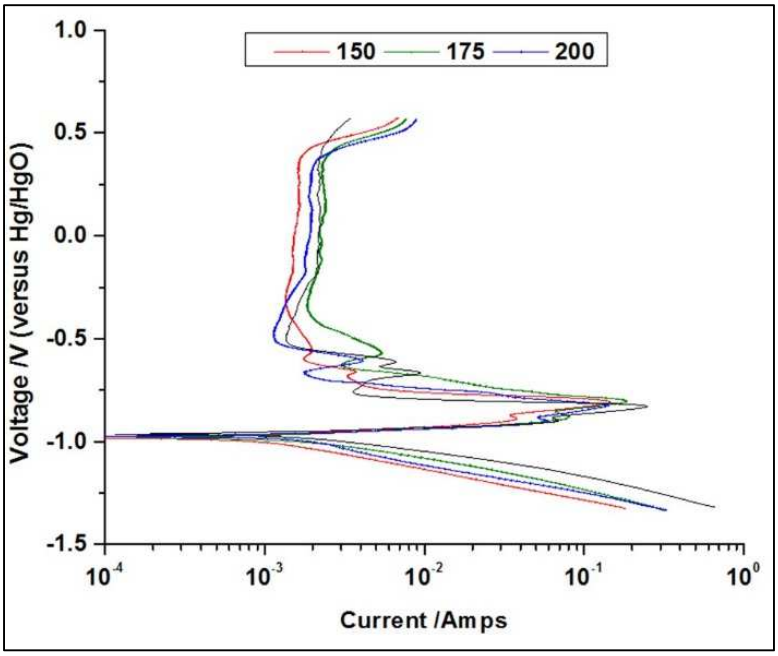

Figure 6.25. Results for tin compound and charge transfer agent. OCP same as hydroxide-only; Fe^{3+} peak very broad at "base" of it; activity around manganese is suppressed at 150°F, nonexistent at 200°F and appears to part of Fe^{3+} peak at 175°F. Appearance of peak at -0.60V at 200°F and another at -0.56V at 175°F.

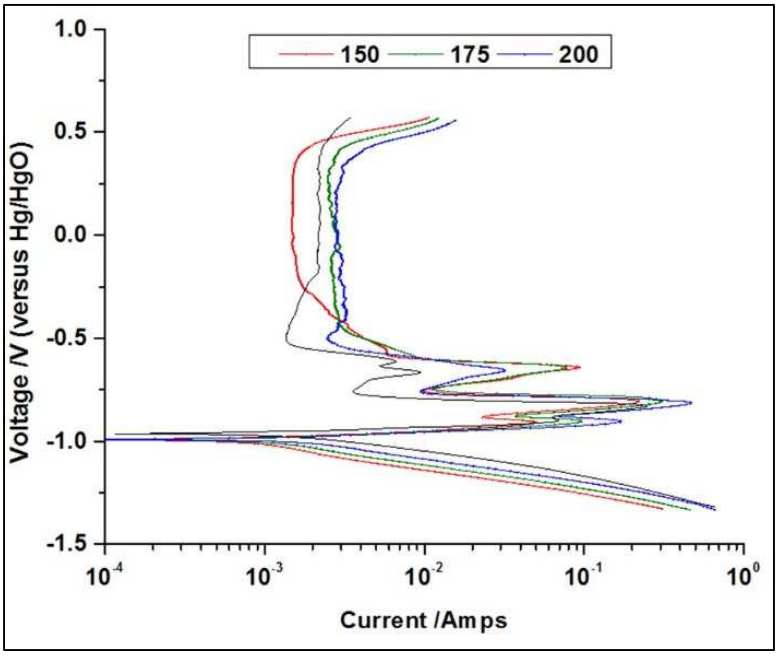

Figure 6.26. Results for thiosulfate and charge transfer agent. OCP is slightly lower; Fe^{3+} peak is quite broad; manganese peak is very broad.

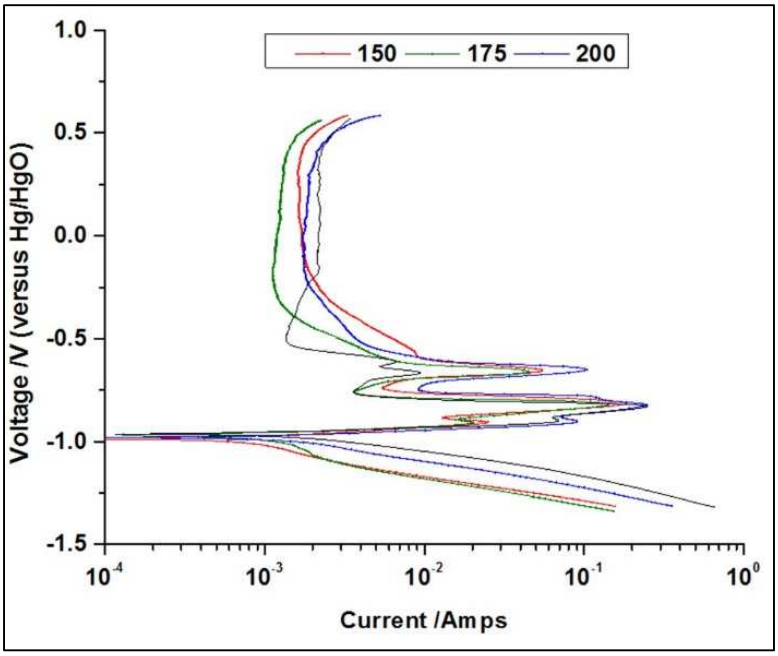

Figure 6.27. Results for thiosulfate and complexing agent. Very similar to thiosulfate alone; $HFeO_2^-$ peak present (current level is not very consistent at each temperature, though); higher activity around manganese at 200°F.

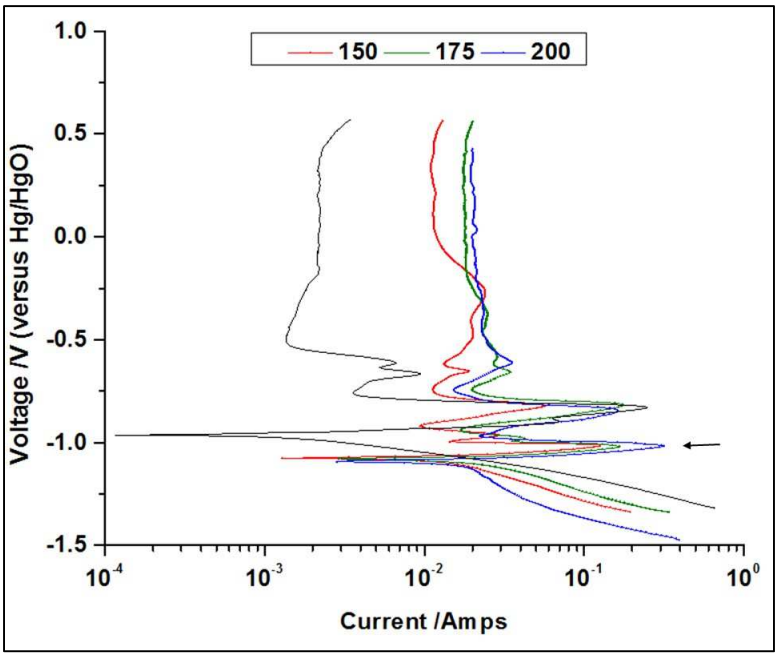

Figure 6.28. Results for tin compound and complexing agent. Passive region shifted to very high current; OCP shifted to very low potential; cannot determine if $HFeO_2^-$ peak is present because Fe^{3+} peak appears very broad; manganese peak essentially hidden due to shift of passive region. An additional peak appears at the arrow which may be due to oxidation of tin; because the entire scan is shifted very low due to the low OCP, it is very possible some tin was reduced and deposited on the surface which was later re-oxidized at that potential.

The peak representing $HFeO_2^-$ is not present in the nitrate/nitrite pairing (Figure 6.14), as observed when one or the other component was present alone. It appears to be absent altogether at the lower temperatures but at 200°F, the peak representing Fe^{3+} is very broad, and encompasses the shoulder peak from hydroxide-only solution; it may indicate, rather than absence of $HFeO_2^-$, the formation of that species is increased to the extent it does not form the separate, distinct shoulder peak. It will also be noted the OCP actually decreases (~20mV) as the temperature increases with concurrent slight increase in current as well.

When every other component was combined with nitrite, the Fe^{3+} peak is not suppressed; this behavior occurs to different degrees depending on the component. Only when nitrite was by itself did it appear to be passivating the steel. The current associated with the peak forming the top of the cathodic curl is suppressed in the presence of charge transfer agent or complexing agent when combined with nitrite; but that peak is strong when thiosulfate or tin compound is present, and, as noted, nonexistent when nitrate is present. These behaviors indicate each component, in some manner, affects the reduction of Fe^{3+} by nitrite and/or the mechanism by which it may passivate the steel. It is also interesting to note when the complexing agent is combined with charge transfer agent, only minor changes were detected versus hydroxide-only solution, whereas there was increased activity around the manganese when charge transfer agent was alone with the hydroxide; this suggests an antagonistic relationship between those components. However, no other changes were observed, suggesting those two components are only responsible for catalyzing the reactions involving nitrite, nitrate, and thiosulfate, the components which, along with hydroxide, are needed for magnetite formation.

Perhaps the most useful information from these results is the variety of activities observed in the results involving the tin component. In several combinations, the tin compound

is observed to shift the passive region to higher current densities, indicating the shift of the passive region to lower current densities in Figure 6.2, during the bath consumption study, was due, at least in part, to the depletion of the tin component with use. In combination with nitrate (Figure 6.19), it is also observed the passive region is shifted to higher current density at 175°F and 200°F, indicating the temperature must be 175°F before the tin compound is fully activated. Importantly, that combination appears to completely stop production of Fe^{3+} species; a peak can be observed in the vicinity of the Fe^{3+}/$HFeO_2^-$peaks but that peak appears to be solely from $HFeO_2^-$(~ -0.89V) and it is not a shoulder on the Fe^{3+} peak as usual because the strong peak typically associated with Fe^{3+} is absent. Additionally, the OCP shifted dramatically lower with increased temperature with nitrate and tin (also indicating increased activity for tin at increased temperature) and with tin in combination with complexing agent at all temperatures (Figure 6.28). The lowered OCP (at ~ -1.08V) appears to reveal an additional peak at ~ -1.02V that may have been hidden under the cathodic branch of the graph in other solutions but is most likely the result of tin deposited on the surface getting re-oxidized; the deposition would be the result of the very low starting potential applied because of the very low OCP value. Conversely, for tin in combination with nitrite, the passive region shifts to lower current density as the temperature increases, indicating an antagonistic relationship between these two components with reactions with nitrite perhaps somewhat favored in this combination. These observations are discussed in greater detail throughout Section 6.4 when the working model is presented.

6.3.4. Additional combinations

From the study of the previous results, it was determined that the next stage of the research should be to analyze a few baths comprised of altered compositions. One bath contained all components at normal concentrations except for nitrite and thiosulfate. These two

components appeared to create rather unusual behavior when combined with the tin compound so they were left out to observe how the rest of the bath functioned without them. The behavior had been very erratic when just nitrite and tin were combined; the Fe^{3+} peak was very broad with the top edge of the peak at much higher potentials than in hydroxide-only solution. Measurements were also made with the concentration of tin (Sn) compound altered to 0, 1/3, and 2/3 of normal. Figure 6.29 displays the combined results. The OCP is at approximately the normal position without tin present; the behavior becomes somewhat erratic in the OCP region when only 1/3 the tin is present; and it is shifted very negative when 2/3 or all of the tin is present. As with just tin and nitrate, with 2/3 or all tin present, an additional peak is observed at approximately -1.1V, the deposition and re-oxidation of the tin compound observed because of the lower potential at the start of the measurement. Finally, the passive region is shifted to higher current density at 1/3 tin and more so at 2/3 and all tin.

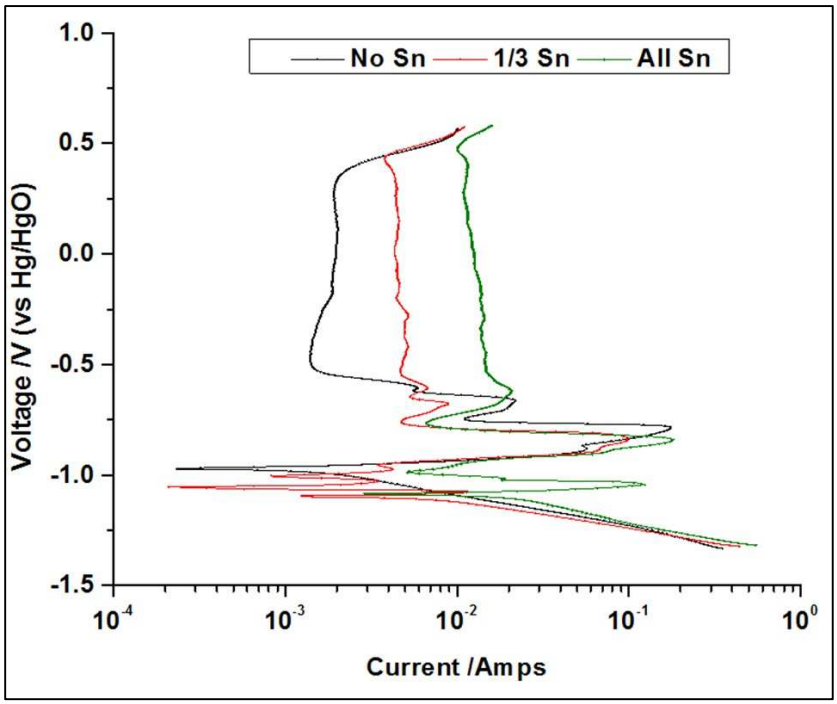

Figure 6.29. Results for nitrate, complexing agent, charge transfer agent, and hydroxide at normal concentrations with various concentrations of tin compound, at 200°F. Result for 2/3 tin was very similar to all tin result, thus, that graph is not displayed for clarity.

Another study was undertaken to observe the results when the concentration of hydroxide was adjusted; one question posed to NDSU by our client was whether the amount of hydroxide required could be lowered, for cost savings. To these ends, a bath was created in which all compounds were at normal concentrations except hydroxide, which was at 10% of normal. 100mL aliquots were used to measure the polarization at 200ºF. To each successive aliquot was added enough hydroxide to yield concentrations of 20% to 100%, in 10% increments. The results are displayed in Figure 6.30. At 10% of normal hydroxide levels, several phenomena are observed. The current level of the passive region is approximately the level observed in consumed bath or whenever tin compound is not present, even though tin was present at the normal concentration. The $HFeO_2^-$ peak appears to be either weak or nonexistent and the Fe^{3+} peak is decreased substantially. The curl on the cathodic arm is absent and the OCP is more positive than normal. In fact, the OCP measurement made prior to the polarization was much more positive than at normal hydroxide levels, approximately -0.68V versus -0.96V; it can be observed in the Pourbaix diagram (Figure 6.4) that this line (adjusted to -0.58V, to account for the reference electrode) would intersect the pH line in the Fe_2O_3 region of the graph. Little difference could be observed between 10 and 20% so that graph is not included. By 30% hydroxide, the cathodic curl is visible although it does not form the sharp peak normally observed just below the OCP. The $HFeO_2^-$ peak is now visible, although somewhat decreased from the complete bath. The Fe^{3+} peak is much stronger but not at normal levels and the passive region is now more active. Interestingly, at 40%, the curl on the cathodic arm decreases, as does the $HFeO_2^-$ peak, and the activity of the passive region is actually decreased from 30%. By 50%, the passive region is again more active, the cathodic curl is present, and the activity for Fe^{3+} is increased; however, activity for $HFeO_2^-$ is still subdued. By 70% hydroxide, $HFeO_2^-$, cathodic

curl, and Fe^{3+} peaks are all approximately at the levels observed in earlier work with the full bath. The OCP is observed to become more negative from 10 to 40%, then appears to stabilize at approximately -0.90V, where earlier it was usually approximately 0.93-0.95V. Oddly, $HFeO_2^-$ peak is decreased again by 90% hydroxide, with slightly higher activities for the passive region and Fe^{3+} peak. Further discussion of these observations is presented with the working model.

It must be noted the steel used for these measurements was from a different lot than the lot used for the earlier experiments. Some of the differences, most notably at 90% (and 100%) hydroxide, may be attributable to that. However, the chemicals were a couple years old by this point and may have decomposed or degraded. In work performed several months later still, a new bath did not generate the same thickness of magnetite as when the chemicals were first purchased. It was not clear whether the differences were caused by the steel, aged chemicals, or a combination thereof.

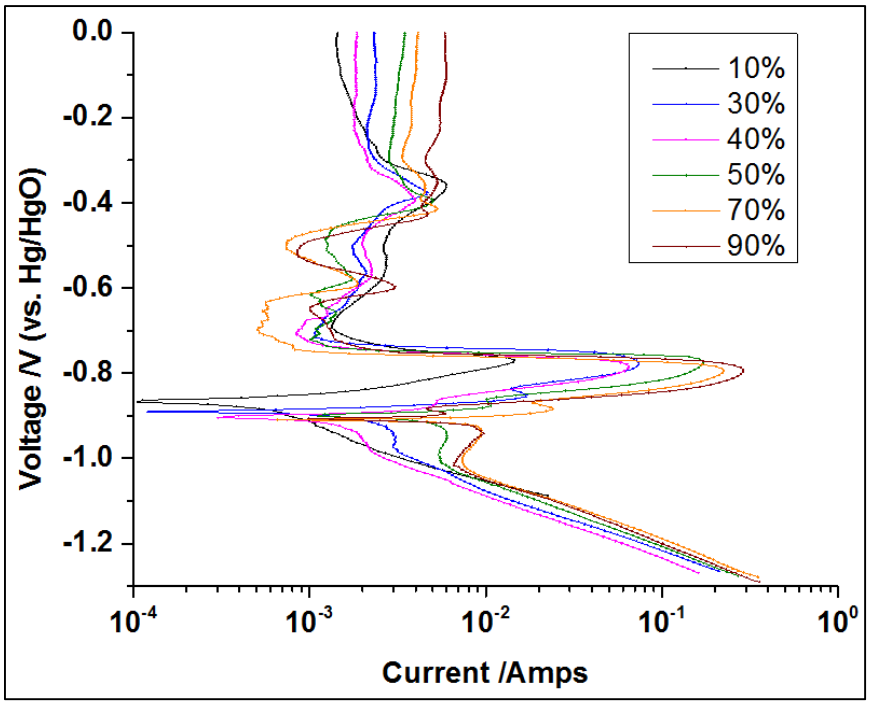

Figure 6.30. Results for adjustments of hydroxide concentration. Hydroxide was adjusted by 10% increments from normal concentrations; all other chemicals at normal bath concentrations, temperature at 200°F. For clarity, samples at 20%, 60%, 80%, and 100% are not included.

6.3.5. Summary

The study of the individual components and various combinations at their normal concentration and bath pH resulted in a large volume of useful data. Much of the activity observed in the bath can be attributed to the steel introduced to this level of pH and temperature, most notably, the apparent generation of soluble iron species, Fe^{3+} and $HFeO_2^-$. The results demonstrated the hydroxide level needs to be at or near the current level to generate these two species and not an iron (II) species such as $Fe(OH)_2$. Indeed, the solutions with reduced hydroxide levels of 10 and 20% were a green color immediately after the measurements, while those with 30, 40, and 50% of normal turned green upon standing overnight; those of higher concentration remained red. Simple experiments with Fe^{2+} and Fe^{3+} salts mixed with the complexing agent in water, then with NaOH added, revealed the Fe^{2+} solution turned green at alkaline pH and Fe^{3+} solution turned red at neutral and alkaline pH, yielding general agreement with the observations in Figure 6.30 with greater Fe^{3+} generated as the pH was increased. These observations are expanded on in Section 6.5.1.

Tin and nitrite added additional reactions and responses and were observed to become more active as the temperature increased, while the other components either enhanced or retarded the activities observed. The $HFeO_2^-$ peak detected in the hydroxide-only solution was not visible when nitrite, nitrate or a combination of both was introduced, indicating an altered balance in the reactions occurring. However, addition of thiosulfate appeared to restore some balance to the system when present and the peak was again observed. Tin both altered the current density of the passive region when present as well as lowered the OCP if certain other components were absent. Numerous synergistic and antagonistic relationships were revealed that yielded potential insights into the inner workings of the bath.

6.4. Studies of the open circuit potential

When steel is immersed in the bath and allowed to simply react at the open circuit potential, at some point during the deposition the OCP is observed to increase to more positive potential, quite rapidly, by approximately 200mV. During the course of the potentiodynamic polarization studies, occasional measurements were made where the open circuit measurement was allowed to make the rapid increase prior to beginning the polarization measurement; the results were significantly different than when the polarization measurement started after only 10 seconds of OCP measurement typically used. Additionally, during the consumption study, as previously noted, the OCP was much more positive for tests 6 and 7 than the first five measurements. Thus, a study was undertaken to attempt to determine the cause of the more positive OCP (as the bath was consumed) and the rapid increase during OCP measurement. Some inconsistencies were observed in some of the measurements that appeared could be related to de-oxidation of the steel so further measurements were performed to study whether de-oxidation was having any effect on the results.

6.4.1. De-oxidation of steel

When the study began, the client did not stress that the steel preparation steps were of major importance, just that they should be done; 1-2 minutes in hot alconox (soap) solution to degrease and 1-2 minutes in 5% sulfuric acid solution to de-oxidize the metal. Occasionally the steel piece remained in the alconox solution too long and the surface became noticeably different and was unusable; the phosphate in the soap appeared to passivate the steel. Also, the sulfuric acid was re-charged occasionally during use, meaning the concentration was declining, however slightly, from one piece of steel to the next, until it was recharged. The de-oxidation time was also not necessarily the same with each sample (but within a range of 10-20 seconds). With both

factors possibly changing for each sample, the total level of de-oxidation could conceivably be quite different. It was not known the change of acid concentration was having any effect until inconsistencies were observed obtaining the results presented in the section 6.4.2; because only 10 seconds were normally required to obtain a stable OCP, the varying behavior was not observed but neither should it have affected any results presented earlier. The difference in immersion time in acid was one possible explanation for the observations. Thus, a study was undertaken in which the acid was divided into portions with only one test strip immersed in each for different lengths of time such that the acid concentration was consistent from sample to sample. The time the steel was immersed in the soap solution was also identical. The results are displayed in Figure 6.31. It is observed the length of immersion time, from 60 to 90 to 120 seconds, greatly affects the length of time the sample is immersed in the bath before the rapid increase of OCP is observed, with shorter immersion time in the acid resulting in a longer period of time before increase of OCP in the bath. After 120 seconds of immersion, the effect is much decreased.

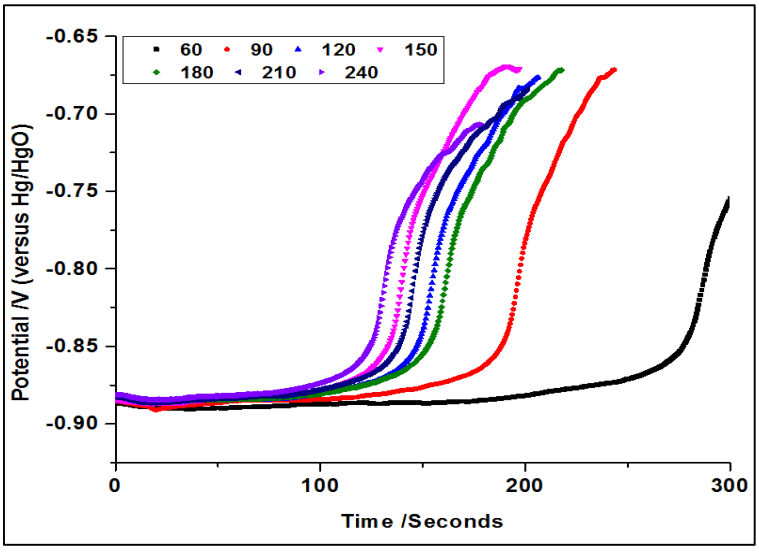

Figure 6.31. Open circuit potential measurements for steel samples immersed in full bath which were de-oxidized in acid solution for different lengths of time. Temperature at 200°F. Numbers in legend are the time each sample was de-oxidized, in seconds.

Two possible explanations may exist for this behavior. First, as the acid etches the steel, if iron is etched from the surface, there will simply be more iron underneath; however, if the manganese in the steel is etched away from an inclusion at the surface, there will likely be more iron underneath, thus reducing the surface area of manganese exposed to the bath. It was observed in the polarization results that different bath components appeared to influence the activity around the manganese peak; with less manganese present, the level of these activities may well be altered. A second possibility is that during immersion in the acid, iron sulfate will likely form, as well as the hydrogen gas which was observed bubbling off the surface. Even with rinsing after de-oxidation, iron sulfate may remain on the surface of the steel and somewhat passivate the surface when immersed in the bath [13]. However, iron sulfate is quite soluble in water and should rinse away, therefore the former explanation would seem more plausible.

6.4.2. Polarization measurements after OCP increase

Another study involved allowing the OCP to begin the rapid positive shift, then beginning the polarization measurement at various potentials during that shift. The results are displayed in Figures 6.32 and 6.33. In Figure 6.32, the OCP data for 5 measurements are graphed; the polarization measurement for each dataset is then graphed in Figure 6.33. The value listed in the legend of Figure 6.33 is the OCP at the moment each polarization measurement was started, thus, -0.859V just before the rapid increase, -0.758V just at the top of the rapid increase, and with a few more mV to the positive for each additional sample. Note the inconsistency (Figure 6.32) in how long it took to reach the point of the rapid increase, related to de-oxidation discussed in the previous section; however, that is not the focus for this portion of the study.

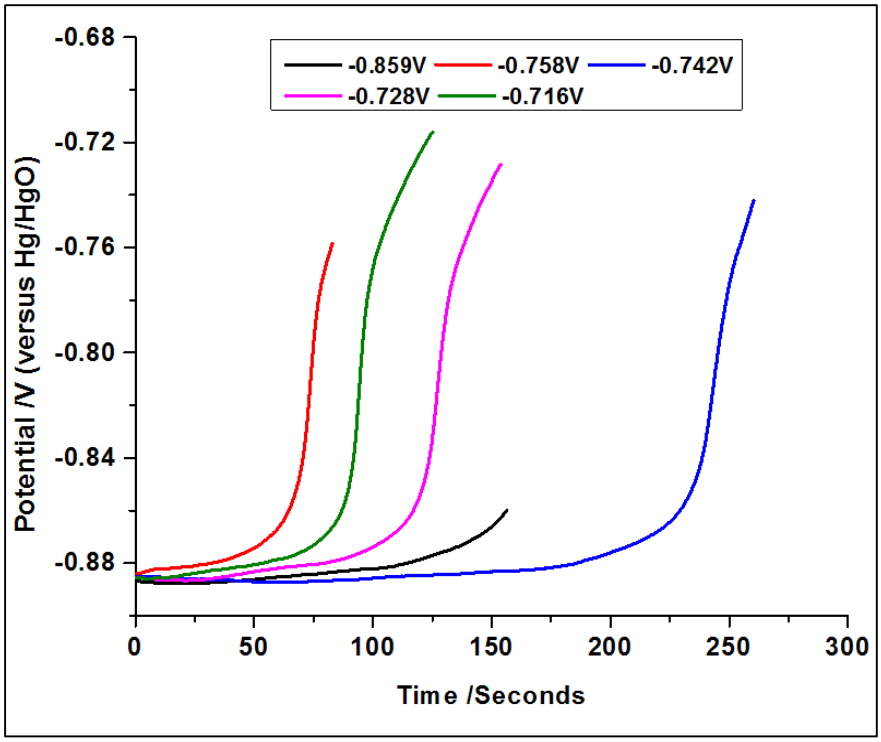

Figure 6.32. Open circuit potential results for steel samples in full bath at the time polarization measurements were begun. The values at the top are the final value for each plot.

More important are the effects on the polarization results displayed in Figure 6.33. Note the consistency from measurement to measurement, except for the sharp, low current peak that forms at approximately -0.78V to -0.80V. Also present is a distinct peak appearing at -0.61V that at first glance would appear to be the manganese peak. However, in several of the baths containing only some of the components, a small peak appeared on the periphery of the manganese peak at slightly more positive potentials; in the present case, the peak is clearly resolved and was also observed in Figure 6.1, peak A, especially at 200°F. During immersion in the bath, magnetite could be observed forming within tens of seconds, certainly less time than that needed to observe the rapid increase in the OCP. If the manganese is becoming covered by magnetite, no signal would be observed for manganese activity in that region at that potential. The peak is now identified: the peak is oxidation of magnetite to FeOOH. Several studies have identified activity at this potential as being related to oxidation of magnetite to goethite, FeOOH;

these observations were confirmed by Raman spectroscopy analysis of the corrosion products formed on the surface [14-17]. Oxidation of magnetite also explains why the peak did not appear in the pure iron samples even though the bath was complete and at normal temperature; $HFeO_2^-$ was not formed, thus, no magnetite was formed to become oxidized to FeOOH (Figure 6.7). Importantly, this is one instance in which the potentiostat is obviously forcing a reaction to occur, albeit, not necessarily an adverse occurrence for it aided in understanding the mechanisms of the bath.

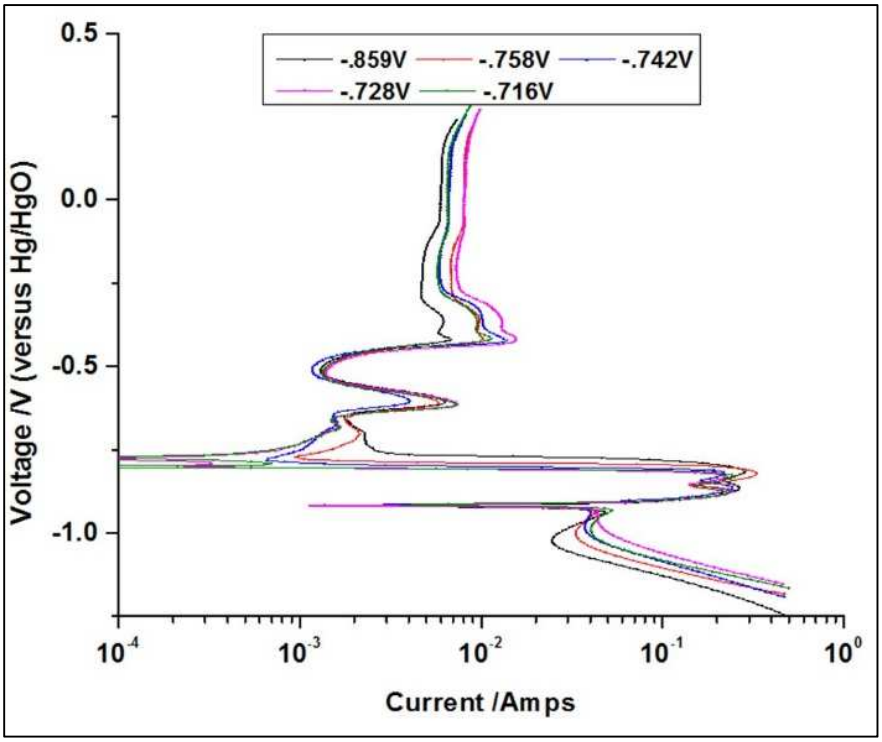

Figure 6.33. Polarization results for steel samples in full bath after OCP began rapid increase. Note the very low current peak that has gone off the scale at -0.8V when nitrite was present by itself (Figure 6.11) and when tin and nitrite were combined at 200°F.

The presence of the low current peak at -0.78V to -0.80V was observed in four situations: when nitrite was present by itself (Figure 6.11); when tin and nitrite were combined at 200°F (Figure 6.24); when the bath was near or at the point of consumption (Figure 6.2); and in the present situation after beginning the polarization measurement after the sharp increase of the

OCP (Figure 6.33). It appears to signal that the formation of a species normally in the bath is no longer occurring. A peak of low current at approximately -0.92V is still observed; this is approximately the potential where the OCP is normally measured by the potentiostat. However, the lower current of the peak at -0.78V is now approximately where the potentiostat measured the OCP after the rapid positive shift. Thus, the low current peak may represent: 1) a species which does not form in nitrite alone or nitrite/tin, noted by its absence; 2) a species which stops forming at some point during the deposition yielding the rapid increase of the apparent OCP; or 3) a species which does not form at all once the bath is at the point of complete consumption. All of these could describe magnetite. Combined with the preceding analysis in which magnetite is observed to be oxidized at approximately -0.61V, this region of the graph very likely represents magnetite formation. Magnetite must be formed somewhere more negative to -0.61V if it is detected by being oxidized to another species at that potential; whether it is caused by or accelerated by the potentiostat or occurs naturally is not clear. Under most circumstances, it is part of the Fe^{3+} peak and is not distinguishable from the Fe^{3+} peak. It is only under the above circumstances that the species makes its presence known – but actually by its *absence*.

However, magnetite is possibly observed forming in other combinations but does not distinguish itself as a peak separate from Fe^{3+}: in thiosulfate/tin compound (Figure 6.22); tin/CTA (Figure 6.25); thiosulfate/CTA (Figure 6.26); and thiosulfate/complexing agent (Figure 6.27). In each combination, the peak representing Fe^{3+} was somewhat broader due to the top edge occurring at slightly more positive potential; a gap can be observed between the top of the Fe^{3+} peak in hydroxide-only and the graphs for each combination in each of those figures, potentially indicating the formation of magnetite.

In only one instance, the magnetite might be clearly observed without the presence of the Fe^{3+} peak: that instance was in Figure 6.29 when nitrate/complexing agent/charge transfer agent/ hydroxide were combined without tin compound and compared to when tin compound was added. The tip of the peak is at much more positive potential (-0.78V) when the tin compound is absent than when the normal level of tin is present (-0.84V), which may be demonstrating the other Fe^{3+} species is not forming at all in that combination of four components. Thus, it appears the peak in each graph in that figure may well represent a different species. The purpose of this project was not to attempt to reformulate the bath, just determine how it functioned; at the time this data was collected, it was not understood. However, at a later time, this simpler combination of chemicals was briefly studied and a thinner layer of magnetite formed on steel, albeit at a slower pace, indicating that, indeed, the peak at -0.78V and the top edge of the peak determined to be Fe^{3+} species in other combinations is magnetite. By corollary, the sharp low current peak observed at -0.78V, such as in Figure 6.2 for the bath consumption study, would indicate the lack of magnetite formation.

A further observation in Figure 6.33 is the $HFeO_2^-$ peak appeared as strong as the Fe^{3+} peak, rather than appearing as a shoulder on the Fe^{3+} peak when the measurement was made after only 10 seconds of OCP measurement. Both tin and thiosulfate maintained the presence of $HFeO_2^-$ when combined with nitrate, and thiosulfate when combined with nitrite; it may be that once enough magnetite has formed and other competing reactions are subdued, forming or maintaining the presence of $HFeO_2^-$ becomes easier and its presence it more easily detected.

6.4.3. Summary

The results revealed several important points. First, the degreasing and de-oxidation steps are perhaps more important and may need to be performed more carefully than first thought. There are obvious differences. And these differences may explain differences observed

in the coatings when treating different types of steel that contain different quantities of manganese. Second, the results allowed for the positive identification of magnetite within the polarization results whereas previously the results suggested the presence of the magnetite but could not confirm it. Third, the peak detected at -0.61V, oxidation of magnetite to goethite suggests an upper limit at which the potentiostat begins to force reactions to occur that likely do not when the bath is operating at OCP. These observations are discussed further during the development of the working model.

6.5. Development of the working model

The formula for magnetite can be written in two ways: Fe_3O_4 or $FeO{\cdot}Fe_2O_3$. The latter formula is a more apt description of the molecule, because it is comprised of a combination of the two molecules, FeO and Fe_2O_3 and is often synthesized by co-precipitation of ferrous (Fe^{2+}) and ferric (Fe^{3+}) ions by a base [18]. For the present purposes, it is more important to use the latter formula for it helps understand how the bath forms the layer of magnetite. The working model developed from study of the polarization measurement results postulates two separate primary reactions are occurring in the bath simultaneously, one forming the FeO molecule and another forming the Fe_2O_3 molecule which combine to form Fe_3O_4.

6.5.1. The reaction forming FeO

From the polarization data presented earlier, it is quite obvious nitrite interacts with a component in the bath yielding the peak on the cathodic branch of the graphs. The most likely reaction would be the reduction of Fe^{3+}. As discussed, it is possible the activity that generated the peak ascribed to Fe^{3+} is due to the potentiostat driving a reaction which forces the formation of Fe^{3+}. However, at normal operating conditions, visually, a species is generated that can be observed forming a red color in the bath. None of the starting components imparts color to the

bath (it is a clear solution when new). Of the byproducts and species formed or potentially present in the bath which would yield a color upon steel immersion are then iron species; at neutral pH, Fe^{2+} species tend to turn solutions pale green if present and Fe^{3+} species tend to turn solutions yellow. As noted in Section 6.3.5, the complexing agent used in the bath is itself colorless but will complex with Fe^{3+} to form a red complex at neutral and alkaline pH. It may complex with Fe^{2+} at neutral pH but does not yield a color change; at alkaline pH, it complexes the Fe^{2+} to turn the solution green.

These color changes were observed during the study when the hydroxide concentration was altered (Section 6.2.4). At 10% (and 20%) normal hydroxide levels, the coating did not form, the cathodic "curl" was not observed, and the current associated with the Fe^{3+} peak was greatly decreased versus normal conditions (Figure 6.30). The level of current observed may, then, indicate the amount of iron metal oxidized to the Fe^{3+} state that the potentiostat can induce by holding the potential in the region of that peak. Importantly, both solutions had a green color after the measurements were completed, indicating the presence of iron in the 2+ oxidation state. When the hydroxide was increased to 30%, 40%, and 50% of normal concentration, the peak on the cathodic branch began to indicate higher currents and more activity was observed for the Fe^{3+} peak, especially at 50%. For these solutions, when allowed to cool and stand overnight, however, all turned green; when hot, the baths were the typical yellow color normally observed when the bath was fairly new and before the level of iron ions in the bath became significant. At 60% of normal hydroxide and higher, the polarization behavior was similar to that observed at normal concentration and the solution remained the normal color regardless of temperature. These observations thus indicate there is a transition of the iron species that is generated from Fe^{2+} to Fe^{3+} which occurs across the range of approximately 20% to 50% of the normal

hydroxide level; either some of both species are generated in that range or else Fe^{3+} is not stable at lower temperatures in that pH range and is converted to Fe^{2+}. The transition coincides with the increase in activity observed on the cathodic branch of the polarization graph when nitrite is present in the bath.

The shoulder peak representing $HFeO_2^-$ was also absent at 10% and 20% normal hydroxide levels and present at 30% and higher levels when the current of the cathodic peak was weakly present. This behavior could be construed that nitrite might be having an interaction with $HFeO_2^-$ since both phenomena appear at the same time. However, when pure iron was measured in the complete bath, the peak related to $HFeO_2^-$ was nearly nonexistent but the peak representing Fe^{3+} was quite strong (Figure 6.7). The current associated with nitrite on the cathodic branch was also present and strong. This is also strong evidence the nitrite is acting as a reducing agent and the species being reduced is Fe^{3+} of some form.

Based on the preceding observations, the reaction presented in Scheme 6.1 is postulated for the formation of FeO. At these high hydroxide levels, Fe^{3+} is possibly present in the form $Fe(OH)_3$, $Fe(OH)_4^-$, a hydrated version of the iron hydroxide ($Fe(OH)_x(H_2O)_y$), but most likely, FeOOH; several FeOOH species form at alkaline conditions but typically these will form precipitates [14-17, 19-21]. As noted in the background information, Chapter 3, our client informed NDSU that while the complexing agent (CA) is not necessary for the bath to function, the bath works "better" when the complexing agent is present as indicated by the quality of the magnetite forming on the substrate; the purple arrow denotes the reaction if complexing agent is not present. Therefore, the complexing agent is included in this reaction scheme.

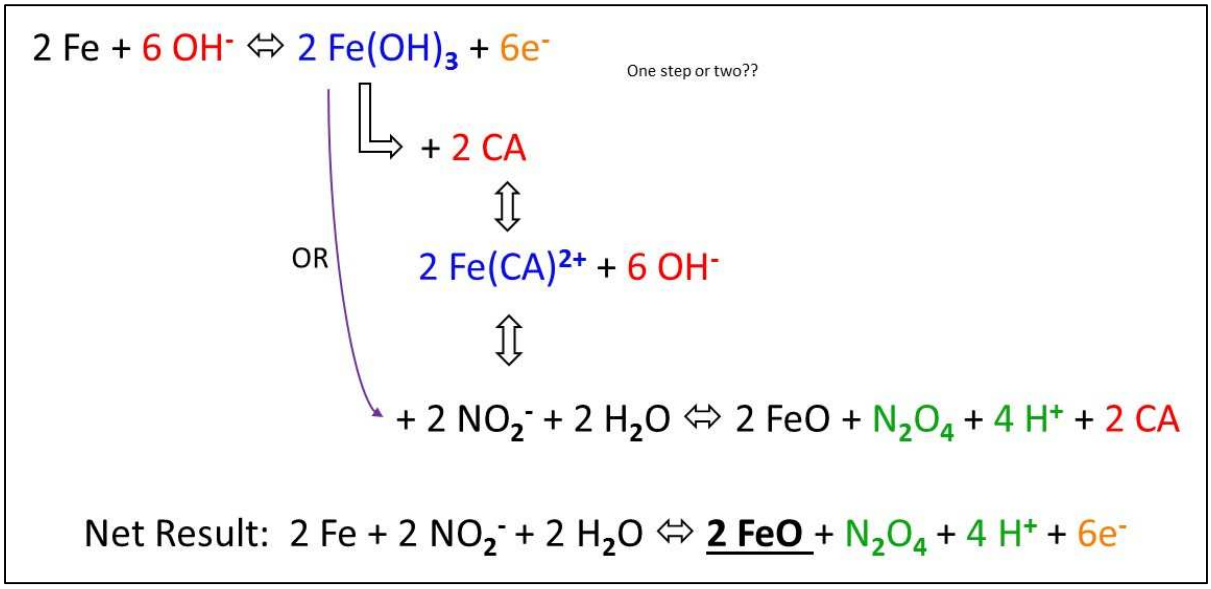

Scheme 6.1. Reactions forming FeO assuming free Fe^{3+} as the iron species. Transitional species are denoted in blue. Spectator ions are denoted in red. Electrons generated from the oxidation are denoted in yellow; these must be consumed in a reduction reaction elsewhere. Species that will further react are denoted in green. The purple arrow indicates the possible reaction if the complexing agent is not present.

The studies indicate the complexing agent may function in two possible ways. First, it may replace hydroxide and/or water molecules stabilizing Fe^{3+} in the solution, making it more readily available for reaction with nitrite. Second and more likely, even with the complexing agent present, the iron is probably not present as Fe^{3+} ion bound by the complexing agent, as noted. FeOOH species easily form polynuclear complexes with themselves which may have several FeOOH molecules present in the complex [22-24]. Iron (III) ion was also found to form tetrahedral structures in alkaline conditions [19]. Thus, 'O' may occupy one position, 'OH' a second, and complexing molecules the other two positions around the central iron atom. Several studies have found differences in the structures of the FeOOH and magnetite that are formed in the presence of different anions and complexing agents under alkaline conditions [25-28]. Thus, the complexing agent used in the bath is likely preventing formation of these polynuclear complexes that would make it more difficult for nitrite to react with and would also precipitate

from the bath as sludge. The passivating layer formed on the steel at higher potentials may be these polynuclear species of FeOOH, so preventing the formation of the polynuclear structures would also disrupt formation of the passive layer and maintain a more active surface. Scheme 6.2 is thus presented as an alternative scheme which incorporates FeOOH.

If Scheme 6.1 is correct, it is not known if $Fe(OH)_3$ actually forms, then the complexing agent forms the complex with iron in two discrete steps or if the complexing agent binds to the iron immediately after it is oxidized, in a single step. After releasing the Fe^{3+} ion, the complexing agent is recycled to complex another Fe^{3+} oxidized from the metal surface. Note the hydroxide ion is not altered so it appears as a "spectator" ion also. If Scheme 6.2 is correct, FeOOH would form first, then be complexed, in two steps. In both schemes, electrons are generated by the oxidation of iron which must be used to reduce other species to maintain charge neutrality; these possible reactions are dealt with in section 6.5.3.

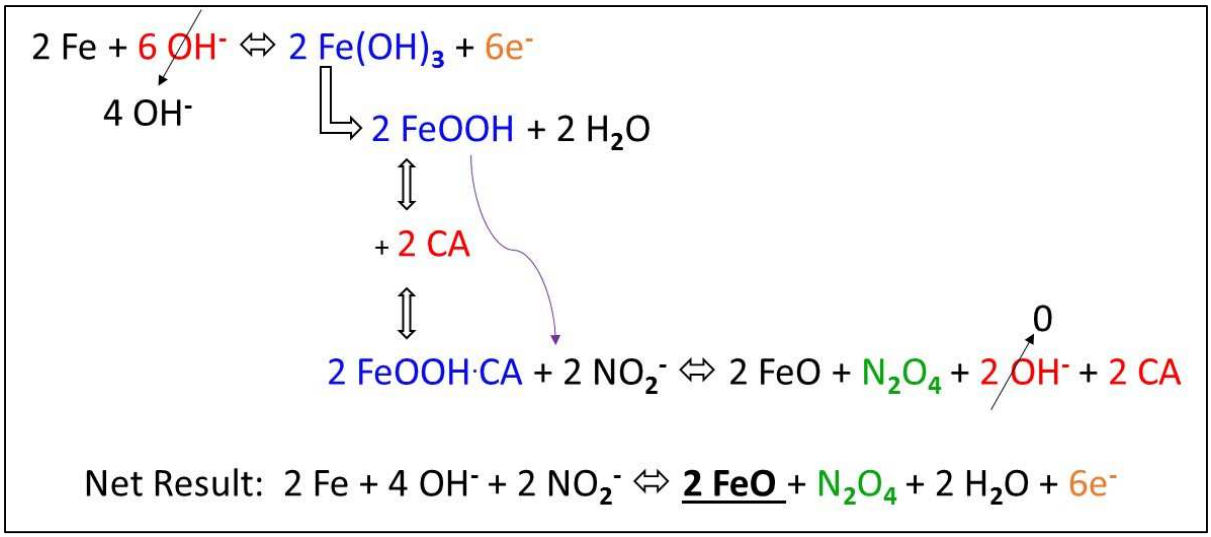

Scheme 6.2. Reactions forming FeO assuming FeOOH as the iron species. Color scheme is the same as Scheme 6.1.

In Scheme 6.1, two reaction products are denoted in green, species that will further react. Hydronium ion, H^+, is one. It must be noted that an oxygen source is needed to form FeO. At

this temperature and with all the salts present in the bath, it is unlikely much free oxygen would be present; the solubility of oxygen in water can be calculated by the following equation found in the CRC Handbook [29]:

$$\ln \chi_l = A + B/T^* + C \ln T^* \quad (6.1)$$

where $T^* = T/100K$; χ_l is the mole fraction solubility of the gas in the solution; and A, B, and C are correction factors generated through experimentation and curve smoothing. The correction factors are valid from 273.15K to 348.15K. The reference lists calculated mole fraction values for oxygen of 2.756×10^{-5} to 1.982×10^{-5} across the range of 288.15K to 308.15K, continually declining values with temperature increase. Continuing the trend, at 200°F (~368K), the calculated concentration of oxygen would be on the order of $10^{-5} – 10^{-6}$ mole fraction, which is quite small compared to the water and hydroxide concentrations present in the bath. Therefore, the necessary oxygen most likely comes from the bath components rather than atmospheric oxygen. In Scheme 6.1, water is included as the oxygen source with hydronium as the byproduct, which would be rapidly consumed at such high pH. In Scheme 6.2, hydroxide is the oxygen source; the latter scheme is perhaps the more provocative of the two because upon abstraction of a water molecule from $Fe(OH)_3$, the resulting formula is FeOOH and the necessary oxygen atom is then present with the iron. Upon gaining an electron from nitrite and reduction to Fe^{2+}, the negative charge of the hydroxide portion of the FeOOH molecule is no longer needed for charge balance and FeO results, with hydroxide as a byproduct. In Scheme 6.1, at high pH the 4 hydronium ions would quickly react with 4 hydroxide ions, thus, for both schemes, 4 hydroxide ions are consumed.

Nitrite in most situations will act as an oxidizing agent; it literally stated on the bottle used for the study, “oxidizer.” But as was observed, it acts as a reducing agent in this bath. The

appearance of the species, N_2O_4, is postulated to be the reason nitrite acts as a reducing agent in the bath. It is denoted in green because N_2O_4 is not stable at this temperature, and, if formed, would quickly decompose; this scenario is discussed in the section dealing with the electrons generated from iron oxidation, later. For the present discussion, the most direct, simple reaction for nitrite acting as reducing agent at high pH would be:

$$NO_2^- + 2\ OH^- \leftrightarrow NO_3^- + H_2O + 2e^- \quad (6.2)$$

with nitrate as the product and where the nitrogen atom changes from 3+ to 5+ oxidation state. At room temperature, this half reaction has a low electrochemical potential, -0.017V versus the standard hydrogen electrode (SHE) [30]; the potential will change somewhat with temperature increase but is very high versus the OCP observed for this system. Activity related to this transition would have the tendency to increase the observed OCP to more positive values; it was observed in Figure 4.8 how the addition of an extra oxidizing agent increased the OCP value. As before, an oxygen source is needed to form nitrate, in this case supplied by hydroxide. The fact the solution must be heated to 160^{o}F before the nitrite begins to display activity with Fe^{3+} suggests two possible explanations. First, there is simply an energy barrier that must be overcome to convert FeOOH to FeO which requires heating to high temperature to cause the reaction. Second, a different reaction mechanism is responsible and reaction 6.2 may not be the correct reaction involving nitrite.

The reaction producing N_2O_4 from nitrite is also quite simple and does not require hydroxide, water, or hydronium ions to balance the reaction:

$$2\ NO_2^- \leftrightarrow N_2O_4 + 2e^- \quad (6.3)$$

but has a potential of -0.867V [29] (-0.892V has also been reported [30]) at room temperature, meaning the reverse reaction is actually favored at low temperature. In the presence of a

sufficiently strong oxidant, however, the reaction could proceed as written. The reduction of $Fe^{3}+$ to Fe^{2+} is:

$$Fe^{3+} + e^{-} \leftrightarrow Fe^{2+} \quad (6.4)$$

with an electrochemical potential of 0.771V at room temperature, but this potential is for acidic conditions. Assuming for the moment this is the iron reduction reaction, at room temperature, the electrochemical potential of the reaction of nitrite and Fe^{3+} would be -0.096V (reactions 6.3 and 6.4 combined); electrochemically, it is not a favorable reaction at that temperature. At elevated temperature, however, it may turn to a positive value and proceed spontaneously. Activity related to reaction 6.3 would be observed at very high potential versus the OCP of the bath and would account for the positive shift of the OCP that was observed as the temperature increased in the presence of nitrite (Figure 6.11). No values were found for the reduction potential of FeOOH with FeO as the product so a similar calculation could not be performed; however, if Fe_2O_3 is forming at the same time so magnetite can form and help drive the reduction of FeOOH to FeO, the electrochemical potential of the FeOOH/FeO couple may be sufficient once the temperature is high enough to activate the nitrite.

6.5.2. The reaction forming Fe_2O_3

The preceding results have explained the roles of nitrite, as a reducing agent, and complexing agent, as well as one role of the high hydroxide content in the bath, that being formation of an iron (III) species which is reduced by nitrite, most likely goethite, FeOOH. The roles of nitrate and thiosulfate appear to factor into the second reaction, the formation of Fe_2O_3; both components appeared to affect the ability of nitrite to function as it did by itself when either or both was/were present with nitrite and hydroxide. The polarization results suggest the presence of $HFeO_2^{-}$, appearing as a peak at -0.89V (in Figure 6.3); this potential at this pH and

temperature was revealed to be in region of stability for $HFeO_2^-$ as predicted in the Pourbaix diagram (Figure 6.4). The peak was not present when thiosulfate was not in the bath with nitrite or nitrate alone, and possibly not when both were present; as noted earlier the peak in the region of $Fe^{3+}/HFeO_2^-$ was very broad at 200°F in nitrate/nitrite/hydroxide and $HFeO_2^-$ may not have distinguished itself as a separate peak. Thus, the thiosulfate appears to have some kind of stabilizing effect on $HFeO_2^-$.

The peak was also essentially absent when pure iron was measured, indicating formation of $HFeO_2^-$ is in some manner related to the presence of manganese. Activity was observed to increase in the vicinity of the manganese peak in the presence of nitrate, charge transfer agent, thiosulfate, or combinations of nitrate with the other two. Importantly, at 200°F in hydroxide with charge transfer agent, activity about the manganese was quite strong; in hydroxide only, this peak displayed little activity, most likely due to an increase in passivation of the manganese by a manganese hydroxide layer at the higher temperature, as noted earlier. The behavior suggests the charge transfer agent is preferentially adsorbing on the manganese, preventing the formation of manganese hydroxide, and allowing higher current flow at the manganese, thus increasing production of $HFeO_2^-$ in the vicinity of the manganese.

Thus, the reaction presented in Scheme 6.3 is postulated for the formation of Fe_2O_3, with nitrate oxidizing $HFeO_2^-$ to Fe_2O_3. The charge transfer agent is not displayed in the scheme as it simply acts as a charge mediator. Note that some of the hydroxide effectively acts as spectator ion but that some hydroxide is also consumed in this scheme. As in the earlier reaction forming FeO, electrons are generated from the oxidation of iron which will be discussed in a later section. And, importantly, nitrite is a byproduct, thus, nitrite is continually resupplied in the bath by this reaction.

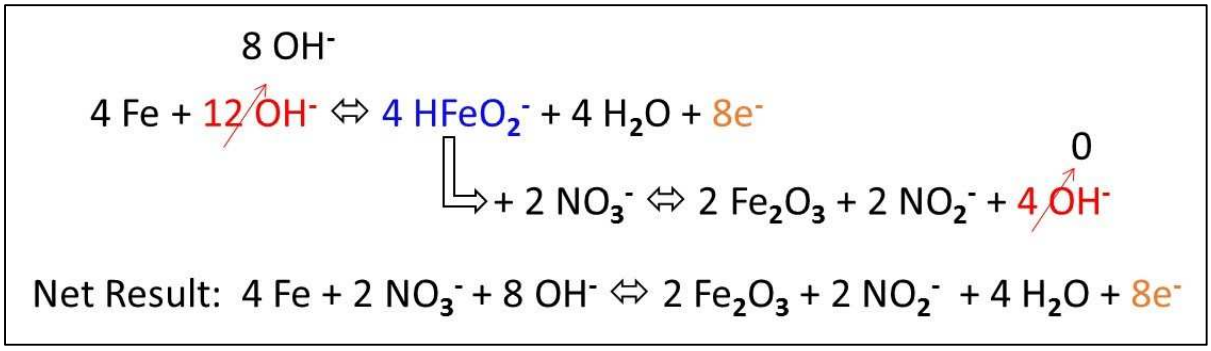

Scheme 6.3. Reactions forming Fe_2O_3. Colors as in Scheme 6.1.

Note that thiosulfate is not displayed in the scheme; these are straightforward reactions and it would not appear to be required in this case. However, since its presence is required to form magnetite in nitrate, nitrite, and hydroxide solution, another mechanism is suggested; one possibility is that the nitrate may over-oxidize $HFeO_2^-$ to other species when present alone. The thiosulfate may prevent this over-oxidation by donating electrons, for typically thiosulfate acts as a reducing agent. The most common half-reaction for thiosulfate is:

$$S_2O_3^{2-} + 6\ OH^- \leftrightarrow 2\ SO_3^{2-} + 3\ H_2O + 4\ e^- \quad (6.5)$$

The reaction is electrochemically favorable at room temperature (0.571V [29]) and may be even more so at 200°F. The electrons donated to prevent over-oxidation of $HFeO_2^-$ are observed on the right; hydroxide would also be consumed in the reaction. One reaction for nitrate oxidation of $HFeO_2^-$ is as presented in Scheme 6.3:

$$2\ HFeO_2^- + NO_3^- \leftrightarrow Fe_2O_3 + NO_2^- + 2\ OH^- \quad (6.6)$$

However, another possibility is:

$$HFeO_2^- + NO_3^- \leftrightarrow FeO_2 + NO_2^- + OH^- \quad (6.7)$$

where iron is in the 4+ oxidation state. At room temperature, this reaction would be favorable electrochemically with +0.70V potential (calculated from values in [29]). Several studies indicate that iron in 4+ oxidation state is possible but it is actually rather uncommon [31-34].

Also, no Pourbaix diagrams were found that considered FeO_2 as a possible species, thus it is not certain where the region of stability might lie. It would most likely lie at relatively positive potentials; FeO_4^{2-}, where iron is in 6+ oxidation state, is occasionally included in Pourbaix diagrams (Figure 4.10a, for example) and lies at more positive potentials than the Fe_2O_3 region, thus, iron in 4+ oxidation state would also be expected to appear at more positive potentials.

Pourbaix diagrams generated from an online application for iron also predict the formation of FeO_2^{2-} (iron in 2+ state) and FeO_2^-(iron in 3+ state) at very high pH levels (pH > 15) [35]. This Pourbaix diagram generator program, however, does not include a function to calculate the reactions at temperatures other than room temperature so it is not known where the boundaries would lie at higher temperatures; note those species were not considered in Figure 6.4 even though pH was considered up to 15. Another Pourbaix diagram generator program [36] allows for calculations at other temperatures but does not allow for consideration of those two species. Like $HFeO_2^-$, the region of stability may expand at higher temperatures. $FeO_2^-$is an intriguing species because it is generated by nearly the identical reaction displayed in reaction 6.5, with water as the byproduct rather than hydroxide:

$$2\ HFeO_2^- + NO_3^- \leftrightarrow 2\ FeO_2^- + NO_2^- + H_2O \qquad (6.8)$$

By Le Chatlier's Principle, reaction 6.8 may be favored: with all the hydroxide in the bath, reaction 6.6 may have a more difficult time proceeding to the right [12]. Nitrate is possibly generating FeO_2^-at such a rate as to prevent the detection of $HFeO_2^-$and $FeO_2^-$is the species responsible for the Fe^{3+} peak that is observed, rather than FeOOH. The thiosulfate slows or prevents reaction 6.8 so $HFeO_2^-$is detected. If $FeO_2^-$is the Fe^{3+} species getting generated, magnetite may not be formed from that species, thus, thiosulfate is necessary to prevent the formation of FeO_2^-.

6.5.3. Fate of electrons generated by iron oxidation

Using Schemes 6.1 - 6.3, if the assumption is made that the number of FeO molecules generated equals the number of Fe_2O_3 molecules generated, and reaction 6.1 describes the action of the nitrite molecule, a quandary results. Each two FeO molecules generated requires two nitrite molecules and yields two nitrate molecules; each two Fe_2O_3 molecules generated requires two nitrate molecules and yields two nitrite molecules. With these assumptions, the bath concentration for each component should never change, but they obviously do change for the chemicals must be replenished; this observation provides another reason the simple reaction, reaction 6.2, does not seem correct and that the formation of N_2O_4 provides an alternative reaction mechanism. It was also observed in Schemes 6.1 - 6.3 that electrons are generated from oxidation of iron by hydroxide. These electrons must be consumed somewhere in the bath; it is actually rather odd that nitrite, thiosulfate, and, as discussed in the following section, the tin compound are all necessary as reducing agents in the presence of all these free electrons.

Therefore, several additional reactions are proposed for the potential fate of these electrons. N_2O_4 has several routes to decompose. First:

$$N_2O_4 + 4\ OH^- \leftrightarrow 2\ NO_3^- + 2\ H_2O + 2\ e^- \qquad (6.9)$$

However, this reaction would add additional free electrons to the bath and would generate nitrate, leading to the same quandary as before. N_2O_4 could also easily decompose to 2 NO_2 (g) but NO_2 is a brown gas; no brown gas was ever detected in or leaving the bath. Most important, N_2O_4 can disproportionate through the reaction:

$$N_2O_4 + e^- \leftrightarrow NO + NO_3^- \qquad (6.10)$$

This reaction provides a route through which nitrite can be consumed at a greater rate than nitrate is reproduced and the bath components are eventually consumed. The reaction could also consume one of the free electrons. The NO produced could also further react:

$$2\ NO + H_2O + 2\ e^- \leftrightarrow N_2O + 2\ OH^- \quad (6.11)$$

This reaction could consume more free electrons. Several more reactions may occur in the bath which could be electrochemically favorable in these conditions:

$$NO_2^- + H_2O + e^- \leftrightarrow NO + 2\ OH^- \quad (6.12)$$

$$2\ NO_2^- + 2\ H_2O + 4\ e^- \leftrightarrow N_2^{2-} + 4\ OH^- \quad (6.13)$$

$$2\ NO_2^- + 3\ H_2O + 4\ e^- \leftrightarrow N_2O + 6\ OH^- \quad (6.14)$$

And the water reduction reaction:

$$2\ H_2O + 2\ e^- \leftrightarrow H_2 + 2\ OH^- \quad (6.15)$$

All need a source of electrons and, as noted earlier, very little gas appeared to be generated in the bath so the last reaction, while certainly possible, was not apparent; and, N_2O is quite soluble in water so reaction 6.14 may be favored [37-38]. Finally, the reverse of reaction 6.2 could easily occur where the nitrate is simply consuming free electrons and converting to resupply nitrite. In this manner, nitrate may aid in the oxidation of iron by hydroxide. Note also between Schemes 6.1 (or 6.2) and 6.3, 12 hydroxide ions are consumed; reactions 6.11 to 6.15 produce hydroxide which may maintain the hydroxide concentration near the levels of the new bath. Importantly, our client noted that when replenishing the bath, the solution used has the normal amount of hydroxide; the pH may be building up to levels which are actually too high, such that other species begin to be generated or one reaction, forming FeO or Fe_2O_3, is favored over the other. Also as noted, FeO_2^- is predicted by thermodynamics to be stable at very high pH; too much

hydroxide may actually begin to favor the over-oxidation of $HFeO_2^-$ by the nitrate to that species, making it increasingly difficult to form magnetite.

6.5.4. Role of the tin (Sn) compound

The reason for the addition of the tin compound to the bath was not made entirely clear to NDSU. Our client had the belief that its addition might improve the bath performance, and after some trial and error, this was revealed to be the case. Its activity in the bath did not lead to any new peaks, except for the occasions noted when the tin forced the OCP to more negative potential that was sufficiently low so as to force the deposition of the tin onto the substrate, then re-oxidize the tin once the potential was increased sufficiently positive. However, in those instances, the change of the OCP to more negative potentials is important; from a corrosion standpoint, substrates with more negative OCP values will corrode at a faster rate, thus, it may be essentially aiding the oxidation of the steel. In other instances, the current density of the passive region was observed to shift to more active levels, indicating the formation of the passive layer is disrupted.

Several observations were detected in the data which may help explain the behavior associated with tin. First, the lower OCP value lies much further into the region of stability for the $HFeO_2^-$ species (140mV lower than hydroxide only, at approximately 1.0V in the Pourbaix diagram of Figure 6.4). The low OCP may indicate higher production of $HFeO_2^-$ is achieved, possibly at the expense of Fe^{3+} species. The peak representing $HFeO_2^-$ in the tin/hydroxide combination is also stronger at all temperatures than in hydroxide alone. An unusual peak shape appeared in the vicinity of Fe^{3+}/$HFeO_2^-$ peaks when nitrate/tin/hydroxide were combined, Figure 6.19. There is a peak but it appears to represent $HFeO_2^-$ only; there is no indication from the figure that Fe^{3+} forms at all. In Figure 6.22, the results for thiosulfate/tin/ hydroxide were

presented. It was noted there the peak representing Fe^{3+} was very broad; the potential at the tip of that peak was at significantly more positive potential versus hydroxide-only. Thus, it may not represent the usual Fe^{3+} species at all, rather, the species that was indicated in Figure 6.33 by its absence after the OCP was allowed to increase before the scan was started – magnetite. In Figures 6.25 (tin/CTA/hydroxide) and 6.26 (thiosulfate/CTA/hydroxide), it was observed the width of the Fe^{3+} peak compared to the same peak in hydroxide-only was also broader; this may indicate the presence of more than one Fe^{3+} species when the peak is broader. Finally, the highest current density achieved in the passive region was when tin was combined with the complexing agent; the OCP was very low in that combination (Figure 6.28).

These results suggest the tin is active in some manner with $HFeO_2^-$, possibly enhancing the formation of $HFeO_2^-$, at the expense of Fe^{3+} generation. $HFeO_2^-$ was observed when tin was combined with nitrate and it appeared no current was detected for Fe^{3+}. But neither was magnetite detected where the top edge of the Fe^{3+} peak is normally located, which suggests tin may act in the same manner as thiosulfate by suppressing the formation of whatever species forms when nitrate over-oxidizes $HFeO_2^-$. Tin may actually perform this function better because the Fe^{3+} peak was observed when nitrate and thiosulfate were combined. Interestingly, Fe^{3+} was detected when tin was alone in hydroxide, the OCP was not different than hydroxide only, and the passive region was not observed to shift; this suggests, by itself, tin either has little activity, other than stabilizing the $HFeO_2^-$ that is formed, or the oxide layer formed by the hydroxide is a more powerful process. The assumption is reasonable when considering the large shift of the passive region in tin/hydroxide/complexing agent; the shift would be explained by the complexing agent stabilizing the Fe^{3+} species, as discussed earlier, and preventing it from

precipitating polynuclear iron oxide species on the steel. The activity of the tin in the passive region would then be detectable.

It is not known exactly how tin compound may act as a reducing agent in the bath but a plausible explanation can be found in the literature. Tin metal can be deposited on several metal substrates in electroless deposition processes from a high alkaline (~2M) tin solution at temperatures beginning around 60°C (140°F) [39-41]. A "brightening" aid can be added to the bath that will alter the crystal structure formed sufficiently such that the deposited tin reflects the light better and appears shiny [41]. However, all that is absolutely necessary is the tin, hydroxide, and increased temperature, conditions met by the present bath, albeit with extra components present. Tin has been determined to deposit through a disproportionation reaction, although exactly which species involved is not clear. The tin at high pH is present as $HSnO_2^-$ or $Sn(OH)_2$; one study determined that, thermodynamically, $HSnO_2^-$ would not disproportionate and the reaction likely involves $Sn(OH)_2$. The two disproportionation reactions would be:

$$2\ HSnO_2^- \rightarrow Sn + SnO_3^{2-} + H_2O \qquad (6.16)$$

$$2\ Sn(OH)_2 + 2\ OH^- \rightarrow Sn + SnO_3^{2-} + 3\ H_2O \qquad (6.17)$$

With the additional chemicals in the bath, however, the tin metal formed by either of these reactions could easily act as a reducing agent and re-form the tin (II) species. The half-cell potentials for tin metal in hydroxide forming oxy-tin species such as SnO_2, $HSnO_2^-$, and $Sn(OH)_3^-$ are all in the range of 0.9V, indicating the tin metal could indeed be a very strong reducing agent [29-30] and would be an even stronger reducing agent than thiosulfate (0.571V potential for reaction 6.5, as noted earlier).

The increased current in the passive region when tin compound was combined with complexing agent is reasonable in light of this model; as noted, the complexing agent would bind

Fe^{3+} or FeOOH species and prevent passivation by that species so the tin can be observed to be active on the surface. In this combination, the tin may actually be depositing as tin metal (testing for this was not part of the study). In addition, the OCP was observed to be a great deal more negative in this combination indicating the tin compound is having a detectable effect on the metal surface; recall when tin was in hydroxide alone, neither the OCP nor passive region were changed, suggesting passivation of the surface rendering the tin ineffective. In the nitrate/tin/hydroxide bath, the OCP was also much more negative. The tin acting in concert with the nitrate appeared to prevent the formation of Fe^{3+} species that would otherwise form the oxide layer, thus an oxidizing reaction was halted and the OCP would likely shift more negative. As noted in the discussion of Evans diagrams in Chapter 4, adding or removing an oxidizing reaction from the system would shift the OCP more positive or negative. The lower OCP was again observed in Figure 6.29 when tin, complexing agent, charge transfer agent, and nitrate were combined in the hydroxide, especially at 200°F. In Figure 6.30, as the concentration of hydroxide was increased but with the standard concentration of tin always present, the passive region was observed to continually shift to higher current also suggesting this mechanism may be viable; the hydroxide concentration had to attain a certain level for the tin metal to form. However, Molenaar and Coumans cited work in which too much hydroxide prevented the deposition of tin metal [39]; as noted earlier, the replenishing bath contains the standard amount of hydroxide in relation to the other ingredients, thus suggesting the hydroxide level may get too high and negate the effect of the tin.

6.5.5. Summary

A complex working model has been developed for a complex bath. The hypothesis is that two main reactions form FeO and Fe_2O_3 which precipitate together as Fe_3O_4. The model

suggests nitrite reduces FeOOH generated by hydroxide in the high temperature and pH conditions of the bath to FeO, while nitrate oxidizes $HFeO_2^-$ also generated under these bath conditions to Fe_2O_3. Thiosulfate and tin prevent the over-oxidation of $HFeO_2^-$ to unusable iron species while the complexing agent and charge transfer agent facilitate the overall process. Several possible reactions were presented to describe the fate of electrons generated by the oxidation of the steel substrate; further work is needed to determine which of the various products might be present in the bath, particular nitrogen oxide species. Overall, the working model fits the obtained data and should be useful in determining the direction of further studies.

6.6. Bath consumption and recovery

A few notes must be included about the possible causes of bath consumption because that process may provide additional clues into the inner workings of the bath. As noted, even with the addition of the replenishing bath, the bath will eventually stop functioning. One reason is it is very likely the concentration of Fe^{3+} species reaches levels that are too high and the reactions are no longer in their proper balance, with the reaction between nitrite and Fe^{3+} dominating the bath. This phenomenon was likely observed to an extent in Figure 6.2, the bath consumption results. It could be observed the peak at the top of the cathodic curl became stronger as the bath was used; with more Fe^{3+} floating free in the bath with use, more was available to react with nitrite at each step. The increase of iron could also be simply observed by the darkening of the bath as the iron reacted with the complexing agent.

Next, sulfite, the likely decomposition product of thiosulfate, has been determined to complex with Fe^{3+} at alkaline pH [42-43]. At neutral pH and in the presence of oxygen, iron is actually a catalyst to convert sulfite to sulfate, SO_4^{2-}. Our client reported some results from ion chromatography on bath samples which had been neutralized prior to measurement; sulfate, but

not sulfite, was detected, albeit not in large quantities. As the concentration builds over time, it is possible sulfite complexes the iron ions as they are generated at the surface when a new piece of steel is immersed in the bath, preventing them from forming other species such as FeOOH which would then further react to form the magnetite according to the working model.

Finally, it is not clear what the final decomposition product of the nitrate and nitrite species may be, so that must also be considered. The various possible nitrogen species generated in the bath might be able to complex with iron species and interfere with the formation of magnetite, although it is not known if this is the case for this bath.

To these ends, several attempts were made to recover the bath, with limited success. Phosphate is a strong complexing agent for Fe^{3+} [44]; therefore, to a completely consumed bath was added a solution of sodium phosphate and a white precipitate of iron phosphate was formed which was filtered out of the bath. Addition of a replenishing solution, however, did not recover the bath. Because the amount of iron in the bath is not known, it is very possible too much phosphate was used; when the replenishing solution was added and another piece of steel immersed, any phosphate present would complex the iron and interfere with magnetite formation. Secondly, no attempt was made to remove the sulfite from the bath, therefore, the sulfite may be immediately complexing any iron generated and the formation of magnetite is stopped.

The previous procedure was repeated using less phosphate, then followed by addition of potassium permanganate; a solid precipitate of manganese oxide, MnO_2, was generated in the bath and filtered off. The fact MnO_2 was formed is an indication permanganate oxidized some species in the bath, perhaps sulfite, $HFeO_2^-$, or any residual nitrite. Permanganate is a strong oxidizing agent and is capable of oxidizing the sulfite to sulfate even at high pH [45-46]. It is

unknown if elevated sulfate levels would cause problems but at the least it should not interfere with the free iron species by complexing with them as does the sulfite. When the replenishing bath was added and steel immersed in the bath, a limited amount of magnetite was formed on the surface, identifiable by the dark bluish-black color often observed with a thin magnetite layer. Nitrogen species may still have been present in the bath and interfering with magnetite formation; simply boiling the solution before addition of the replenishing bath may drive out any nitrous gases and the bath may then be recoverable. These results do suggest it may be possible to recover the bath if the right sequence of steps can be determined.

6.7. Conclusions

A complex chemical bath that forms magnetite on steel was studied by potentiodynamic polarization. The high alkalinity and high temperature necessary for the bath to function properly make it exceedingly difficult to study the system in its operational state by other methods of analysis, but electrochemical measurements can be made under these conditions. The individual components and combinations of the components in high alkaline conditions at a range of temperatures were measured to study synergistic and antagonistic behaviors between the bath components and determine what reactions may be occurring in the bath when steel is immersed in the solutions. The results suggested the formation of the magnetite in the bath proceeds by two simultaneous reactions, one forming FeO and one forming Fe_2O_3, resulting in the formation of $FeO{\cdot}Fe_2O_3$, i.e. Fe_3O_4. Extra chemicals are present in the bath that are not absolutely necessary to form magnetite; these were determined to interact in the bath as a complexing agent, charge transfer agent around manganese sites in the steel, and with a tin compound acting as an addition reducing agent that became more important as the initial layer of magnetite was deposited and covered the metal surface.

Possible reasons for the bath to stop functioning were presented and conclude that buildup of reaction byproducts of Fe^{3+} species of some form, sulfite, and possibly nitrogen oxide species create conditions in which the bath cannot function properly. The results also suggest too much hydroxide in the bath may also be detrimental to proper function; hydroxide may be a byproduct of several possible reactions and when a replenishing solution is added to the bath, the hydroxide levels may reach levels that are simply too high for the proper balance of the system.

6.8. References

[1] K. Subramanian, J. Mickalonis, Electrochimica Acta, 50 (2005) 2685-2691.

[2] D.A. Skoog, D.M. West, F.J. Holler, S.R. Crouch, Fundamentals of Analytical Chemistry, Edition 9, Cengage Learning, 2013.

[3] Figures 3.4 and 3.5 reprinted and adapted from Corrosion Science, 10 (5), H.E. Townsend, Jr., "Potential-pH diagrams at elevated temperature for the system Fe-H_2O," 343-358, 1970, with permission from Elsevier.

[4] John E. Bringas, Ed., Handbook of Comparative World Steel Standards, 4th Edition, ASTM International 2007.

[5] Figure 3.6 reproduced and adapted from Journal of Materials Chemistry, 19 (16), D. Portehault, S. Cassaignon, E. Baudrin, J.P. Jolivet, "Structural and morphological control of manganese oxide nanoparticles upon soft aqueous precipitation through MnO_4^-/Mn^{2+} reaction," 2407-2416, 2009, with permission of The Royal Society of Chemistry.

[6] D.A. Jones, Principles and Prevention of Corrosion, Prentice-Hall, Inc. 2005.

[7] W.S. Li, J.L. Luo, Corrosion Science, 44 (2002) 1695-1712.

[8] M.B. Valcarce, C. López, M. Vázquez, Journal of the Electrochemical Society, 159 (2012) C244-C251.

[9] K. Sayin, D. Karakaş, Corrosion Science, 77 (2013) 37-45.

[10] O. Girčienė, R. Ramanauskas, L. Gudavičiūtė, A. Martušienė, Corrosion, 67 (2011) 125001.

[11] M.B. Valcarce, M. Vázquez, Electrochimica Acta, 53 (2008) 5007-5015.

[12] W.L. Masterton, E.J. Slowinski, Chemical Principles, W.B. Saunders Co., Philadelphia, PA, 1969

[13] S.A. Park, J.G. Kim, J.B. Yoon, Corrosion, 70 (2014) 196-205.

[14] M.K. Nieuwoudt, J.D. Comins, I. Cukrowski, Journal of Raman Spectroscopy, 42 (2011) 1353-1365.

[15] J.C. Rubim, Journal of the Chemical Society-Faraday Transactions I, 85 (1989) 4247-4258.

[16] A. Hugot-Le Goff, J. Flis, N. Boucherit, S. Joiret, J. Wilinski, Journal of the Electrochemical Society, 137 (1990) 2684-2690.

[17] J. Dunnwald, A. Otto, Fresenius Zeitschrift fur analytische Chemie, 319 (1984) 738-742.

[18] S. Sun, H. Zeng, Journal of the American Chemical Society, 124 (2002) 8204-8205.

[19] P. Sipos, D. Zeller, E. Kuzmann, A. Vértes, Z. Homonnay, M. Walczak, S.E. Canton, Dalton Transactions, 41 (2008) 5603-5611.

[20] S. Krehula, S. Popović, S. Musić, Materials Letters, 54 (2002) 108-113.

[21] T. Misawa, K. Hashimoto, S. Shimodaira, Corrosion Science, 14 (1974) 131-149.

[22] A. Masion, J. Rose, J.-Y. Bottero, D. Tchoubar, P. Elmerich, Langmuir, 13 (1997) 3882-3885.

[23] J.-Y. Bottero, D. Tchoubar, M. Arnaud, P. Quienne, Langmuir, 7 (1991) 1365-1369.

[24] C.M. Flynn, Chemical Reviews, 84 (1984) 31-41.

[25] S.I. Pechenyuk, Y.P. Semushina, L.F. Kuz'mich, Russian Journal of Physical Chemistry A, 87 (2013) 490-496.

[26] D.-E. Zhang, X.-J. Zhang, X.-M. Ni, H.-G. Zheng, Materials Letters, 60 (2006) 1915-1917.

[27] H. Liu, L. Yang, M. Ma, P. Li, Y. Wei, Journal of Solid State Chemistry, 183 (2010) 542-546.

[28] H. Liu, H. Guo, P. Li, Y. Wei, Journal of Solid State Chemistry, 181 (2008) 2666-2671.

[29] CRC Handbook of Chemistry and Physics, D.R. Lide, Editor in Chief, 74th Edition, CRC Press, 1993.

[30] S.G. Bratsch, Journal of Physical and Chemical Reference Data, 18 (1989) 1-21.

[31] C.Y. Cummings, M.J. Bonné, K.J. Edler, M. Helton, A. McKee, F. Marken, Electrochemistry Communications, 10 (2008) 1773-1776.

[32] K. Shimizu, A. Lasia, J.-F. Boily, Langmuir, 28 (2012) 7914-7920.

[33] S.K. Dedushenko, Y.D. Perfiliev, L.A. Kulikov, Hyperfine Interactions, 218 (2013) 59-65.

[34] W. Cheng, J. He, Z. Sun, Y. Peng, T. Yao, Q. Liu, Y. Jiang, F. Hu, Z. Xie, B. He, S. Wei, Journal of Physical Chemistry C, 116 (2012) 24060-24067.

[35] https://materialsproject.org/, May, 2014.

[36] http://www.crct.polymtl.ca/ephweb.php, August 2004.

[37] Y. Kameoka, R.L. Pigford, Industrial and Engineering Chemistry Fundamentals, 16 (1977) 163-169.

[38] K.E. Johnson, D.T. Sawyer, Electroanalytical Chemistry and Interfacial Electrochemistry, 49 (1974) 95-103.

[39] A. Molenaar, J.J.C. Coumans, Surface Technology, 16 (1982) 265-275.

[40] A. Molenaar, J.W.G. de Bakker, Journal of the Electrochemical Society, 136 (1989) 378-382.

[41] R.L. Broggi, G.M. de Oliveira, L.L. Barbosa, E.M.J.A. Pallone, I.A. Carlos, Journal of Applied Electrochemistry, 36 (2006) 403-409.

[42] O.A. Travina, Y.N. Kozlov, A.P. Purmal', S.O. Travin, Kinetics and Catalysis, 38 (1997) 242-246.

[43] A.N. Ermakov, A.P. Purmal', Kinetics and Catalysis, 42 (2001) 531-542.

[44] S. Kotrly, L. Sucha, Handbook of Chemical Equilibria in Analytical Chemistry, Halsted Press, New York 1985.

[45] L.I. Simandi, M. Jaky, C.R. Savage, Z.A. Schelly, Journal of the American Chemical Society 107 (1985) 4220-4224.

[46] T. Ernst, M. Cyfert, M. Wilgocki, International Journal of Chemical Kinetics, 24 (1992) 903-908.

CHAPTER 7. SUMMARY

Electrochemical techniques are useful for the examination of coating systems and can add a great deal of information to other thermal and physical techniques typically employed to evaluate coatings. In this study, electrochemical impedance spectroscopy was used to study an epoxy-amine primer system containing monomers and oligomers of phenylenediamine (PDA). And potentiodynamic polarization measurements were employed to determine the reaction mechanism for the deposition of magnetite on steel in a high alkaline chemical bath. Both techniques provided useful information unobtainable by other means.

The EIS results were compared with the results from an earlier study of an organic-inorganic hybrid sol-gel system also cross-linked with phenylenediamine. Rather unusual EIS results were obtained with the sol-gel coatings that were replicated when oligomers of PDA were incorporated in the epoxy coatings but not when PDA monomers were incorporated. The main goal of the study was to demonstrate that the interesting EIS behavior was not necessarily the result of the sol-gel structure or the aluminum oxide layer as described in the literature; the aluminum oxide layer should be the same regardless whether PDA monomer or oligomer is present in the coating. Therefore, the EIS results suggest the interesting behavior is related to the coating structure. The study would seem to confirm the earlier conclusion that in-situ polymerization of the PDA monomers was responsible for the excellent corrosion protection by the sol-gel coating by both consuming oxygen in the electrolyte solution to form PDA oligomers and possibly by an osmotic effect of the coating trapping the salt ions by the newly formed PDA oligomers.

The study also determined that the level of cross-linking in the epoxy coatings affected the results. The lower cross-link density of the coating consisting of EPON 830,

xylylenediamine, and phenylenediamine oligomers appeared to provide sufficient space for salt ions to move through the coating to the substrate, even with the presence of the oligomers. The tri-functional epoxy THMTE and tri-functional amine TAEA imparted sufficient cross-link density to enable the coating to act as an osmotic membrane, most likely by adsorbing the ammonium and sulfate ions and thereby blocking pores and trapping the sodium and chloride ions; in a sodium chloride-only electrolyte, the sodium chloride appeared to easily penetrate the coatings. The results may stem from the apparent hydrophobic nature of the oligomers although this alone does not explain the different results between the three coatings containing equal amounts of oligomers of PDA, thus suggesting an effect of the cross-link density. The length of the oligomer chains added to the coating also appeared to affect the results with longer chains reducing the coating resistance, either by allowing more overlap of conductive fragments for improved electron movement within the coatings or altering the coating structure sufficiently to increase the pore space.

A working model for the deposition of magnetite on steel was developed based on the potentiodynamic polarization measurements obtained. Measurements were made of the complete bath across a range of temperatures to observed differences caused solely by temperature. It was determined that temperatures of 180^{o}F and 175^{o}F are required for nitrite and tin compound, respectively, to function properly, thus, the necessity to operate the bath at 200^{o}F. The complete bath was used until it was consumed, with periodic measurements, to observe how the results changed with use. To determine which chemicals were responsible for the observed results and displayed synergistic or antagonistic behaviors, the bath components were measured both individually and in various combinations. The working model suggests two forms of iron

species are first generated that then combine by reactions with other chemicals in the bath to form and precipitate magnetite.

The chemical bath will reach a point at which byproducts of the reactions build to a level that is too high for proper bath function, regardless whether additional chemicals are added to the bath; a potential method for bath recovery was presented. Results of the study also determined a simpler formulation of bath components formed magnetite; the resulting coating was thinner and formed at a slower rate than the full bath. The client company is pursuing further studies to determine if the simpler formulation suits their needs and whether it is a simpler formulation for their customers to work with, and, if not, whether the full bath can be recovered by the method proposed.

CHAPTER 8. FUTURE STUDIES

8.1. Epoxy-amine coatings and phenylenediamine

Further studies would be performed to fully characterize the phenylenediamine oligomers. A complete set of samples would be synthesized by the described method to include all combinations of metal catalysts with both fast and slow addition of hydrogen peroxide. The matrix would also include both m-PDA and p-PDA with the various metals. Iron did not appear to sufficiently oxidize m-PDA, yielding only a darker solution but no crystal formation; one of the other metal catalysts may accomplish the task. All products would be examined by ESI-TOF-MS for distribution of the molecular weights.

NMR results would ideally reveal the level of primary, secondary, and tertiary amine content of the oligomers to help determine their structure. The remaining primary amine content in less-oxidized oligomers may contribute to higher cross-link density and/or more rapid curing as was observed for the coating that incorporated oligomers synthesized with molybdenum as the catalyst, as described in section 5.3.5. Additionally, the NMR measurements might reveal whether there are structures in which addition of the next o-PDA ring is at the 3 and 4 positions rather than necessarily at the 4 and 5 positions as drawn in Figure 5.2. The resulting oligomers produced with molybdenum and manganese were very dark in color (as opposed to light to medium brown for the other catalysts) and were very dense, even though the yield and mass of crystals recovered was approximately the same as the other catalysts. These observations suggest something fundamentally different at the structural level.

For the epoxy-amine coatings with phenylenediamine isomers, a repeat of the experiment in which different lengths of oligomers are incorporated into the coatings may reveal more distinct differences if the oligomers could be separated into each individual molecular weight. It

was observed during the crystal drying process that the oligomers easily sublime; there was often a yellow discoloration around the drying container after a few days of drying that was easily cleaned with solvent. The oligomers may be separable by molecular weight by a simple sublimation and re-condensation process.

If free films of good quality can be obtained, further experiments may study whether ammonium sulfate and sodium chloride penetrate the membrane at different rates. The results described suggested the ammonium ions and sulfate ions may be adsorbed by the oligomers present within the coatings, whereas it appeared monomeric PDA incorporated into the coatings did not adsorb those ions. Recovery of the first aliquot of water to penetrate the coatings with addition of a small portion of copper salt would reveal the presence of ammonium by formation of a copper-ammonium complex detectable by UV-Vis spectroscopy.

8.2. Deposition of magnetite on steel

Further studies for the deposition of magnetite on steel is underway. The company is currently studying the simpler formula to determine if it can fit their needs. A simpler formula would permit cost savings for the company in terms of less chemical inputs. On the user side, the simpler formula may permit an easier system to work with and an extended bath lifetime if less iron species are generated and building up in the bath, with the need to treat and dispose of the exhausted bath less often.

If the simpler bath proves not useful and the bath composition remains as it is, further studies might include more experimentation with bath recovery. There was insufficient time to fully study the method described in section 6.6 to recover the bath. The addition of phosphate appeared capable of removing the excess iron in the bath; however, residual sulfite that was potentially forming complexes with that iron would have then been released freely in the bath

and may have formed complexes with the new iron generated during further attempts at deposition of magnetite. The addition of permanganate likely oxidized the sulfite to sulfate and the resultant MnO_2 was filtered out of the bath. As noted, limited deposition of magnetite did then occur after the addition of new bath chemicals.

To date, the company has not experimented with reducing the level of hydroxide in the replenishing solution while maintaining the levels of the other chemicals. The working model presented suggested much of the hydroxide consumed during the deposition process may actually be regenerated by other reactions; it is possible that the hydroxide level of replenished baths becomes too alkaline and the necessary balance of reaction rates becomes unbalanced. In the references citing the deposition of tin, it was noted that the pH could indeed become too alkaline for those systems to function properly. Additionally, nitrate may not be consumed at comparable rates to the other chemicals, therefore continual replenishment at the normal nitrate level may cause the total nitrate level to become out of balance, especially versus nitrite, a balance the client company said was rather crucial.

A major component of the hypothesis presented is that nitrogen oxide gases of some species are formed in the bath; as noted, no bubbles appeared to form in the solution so these gases, if generated, may remain dissolved in the bath. Therefore, a study of the headspace gases above the bath solution would be conducted to determine if nitrogen oxide gases are generated and their identities, if present.

The company is also studying whether a different charge transfer agent might produce improved results. The working model presented in this thesis suggests a better balance between the generation of the various iron species may result in less of the iron (III) species, most likely goethite, such that it would build up in the bath to a lesser degree and extend the bath lifetime. A

higher production rate of $HFeO_2^-$ might also aid coverage of the underlying steel by magnetite at more rapid pace such that the system ceases production of the iron (III) species at a shorter time interval and less is allowed to float freely in the solution. Several candidate charge transfer agents were suggested to the company.

A final study was alluded to during the discussion of tin, when present with complexing agent and hydroxide. If the complexing agent is preventing deposition of iron oxide polynuclear complexes on the substrate, the increased activity observed in the passive region may be revealing the deposition of tin. A simple study could be performed on the substrate to test for the deposition of tin metal, such as x-ray diffraction or energy dispersive spectroscopy. Such a study might help clarify the role of tin in the bath.